Unclassified
SECURITY CLASSIFICATION OF THIS PAGE

AD-A262 446

(2)

REPORT D

Form Approved
OMB No. 0704-0188

1a. REPORT SECURITY CLASSIFICATION Unclassified	1b. RESTRICTIVE MARKINGS
2a. SECURITY CLASSIFICATION AUTHORITY	3. DISTRIBUTION/AVAILABILITY OF REPORT Approved for public release Distribution unlimited
2b. DECLASSIFICATION/DOWNGRADING SCHEDULE	
4. PERFORMING ORGANIZATION REPORT NUMBER(S)	5. MONITORING ORGANIZATION REPORT NUMBER(S) AFOSR-TR- 3
6a. NAME OF PERFORMING ORGANIZATION University of Washington	6b. OFFICE SYMBOL (If applicable)
6c. ADDRESS (City, State, and ZIP Code) Dept. of Materials Science & Engineering Mail Stop FE-10 Seattle, WA 09195	7a. NAME OF MONITORING ORGANIZATION AFOSR 7b. ADDRESS (City, State, and ZIP Code) Bolling Air Force Base Washington, D.C. 20332-6448
8a. NAME OF FUNDING/SPONSORING ORGANIZATION AFOSR	8b. OFFICE SYMBOL (If applicable) NC
8c. ADDRESS (City, State, and ZIP Code) Bolling Air Force Base Washington, D.C. 20332-6448	9. PROCUREMENT INSTRUMENT IDENTIFICATION NUMBER F49620-89-C-0059
	10. SOURCE OF FUNDING NUMBERS

PROGRAM ELEMENT NO.	PROJECT NO.	TASK NO	WORK UNIT ACCESSION NO.
61102F	2303	BS	

11. TITLE (Include Security Classification)
TAILORED ORGANOMETALLIC POLYMERS (Unclassified)

12. PERSONAL AUTHOR(S)
R.M. Laine, C. Viney and R.J.P. Corriu (Addresses listed on following page)

13a. TYPE OF REPORT	13b. TIME COVERED	14. DATE OF REPORT (Year, Month, Day)	15. PAGE COUNT
Final	FROM 5/89 TO 10/92	93/01/31	131 (incl. this)

16. SUPPLEMENTARY NOTATION

17. COSATI CODES			18. SUBJECT TERMS (Continue on reverse if necessary and identify by block number)
FIELD	GROUP	SUB-GROUP	organometallic polymers, hypervalent silicon, high temperature, liquid crystalline, non-linear optical

19. ABSTRACT (Continue on reverse if necessary and identify by block number)

Molecular tailoring concepts were applied to the synthesis of novel inorganic and organometallic polymers, many of them starting from commonly available polymorphs of SiO_2 (beach sand). Liquid crystalline molecular order was identified in random co-oligomers and co-polymers of bis(catecholato)spirosiloxanes.
Factors affecting the nature and distribution of microstructural defects in liquid crystalline materials were identified, with a view to minimizing the scattering of light as it passes through such materials.

93 3 31 049

93-06611

20. DISTRIBUTION/AVAILABILITY OF ABSTRACT	21. ABSTRACT SECURITY CLASSIFICATION
☒ UNCLASSIFIED/UNLIMITED ☒ SAME AS RPT. ☐ DTIC USERS	Unclassified

22a. NAME OF RESPONSIBLE INDIVIDUAL	22b. TELEPHONE (Include Area Code)	22c. OFFICE SYMBOL
Dr Thomas E. Erstfeld	(202) 767-4963	

DD Form 1473, JUN 86 Previous editions are obsolete. SECURITY CLASSIFICATION OF THIS PAGE
Unclassified

20001101205

Tailored Organometallic Polymers

Richard M. Laine
Department of Materials Science and Engineering
University of Michigan
Ann Arbor, MI 48109-2136

Christopher Viney
Center for Bioengineering WD-12
University of Washington
Seattle, WA 98195

Robert J. P. Corriu
Laboratoire Unité Mixte de CNRS
Université de Montpellier II

Final Report, Project F49620-89-C-0059

to

The Air Force Office of Scientific Research
Bolling Air Force Base
Washington, D.C. 20332-6448

Attention: Captain (Dr.) Thomas E. Erstfeld

January 31, 1993

SUMMARY OF WORK

The research effort in these laboratories sought to apply the concept of molecular tailoring to the synthesis of novel, robust inorganic and organometallic polymers (IOPs). Polymers capable of forming a nematic liquid crystalline phase were sought, in order that the unique properties of nematic molecular order might be exploited when processing these materials.

Highlights of the research include:

- First synthesis of hexa-oxygenate silicate dianions without supporting aromatic ligands (Appendix 1). The synthesis proceeds from SiO_2 (beach sand) as the source of silicon. Previously, six-fold O-coordinated Si was known to exist only in the mineral stishovite, a polymorph of silica formed at high-pressures.

- The development of direct routes for synthesizing penta-alkoxy and penta-aryloxy silicon complexes, using common polymorphs of SiO_2 (Appendices 2-4). These synthetic pathways provide access to a wide variety of new silicon compounds for use as reagents in organic syntheses and the electronics industry, and as ceramic precursors. The new synthetic pathways sidestep the energy- and equipment-intensive carbothermal reduction step that typically precedes conventional silicon chemistry.

- Extrusion of preceramic fibers from THF solutions of organometallic precursors (yttrium, barium and copper carboxylates); the preceramic fibers can be pyrolytically converted into superconducting, flexible ceramic fibers. Working principles were developed for this process (Appendix 5). The organometallic precursors have excellent shelf life, sidestep the need to pre-form ceramic powders, and facilitate atomic-level mixing in what is necessarily a multi-component system.

- Synthesis of liquid crystalline random co-oligomers and co-polymers of bis(catecholato) spirosiloxanes, using a very simple synthetic route that requires three or four steps from SiO_2 (Appendix 6). These linear, rod-like molecules form nematic liquid crystalline phases over a wide temperature range, with the reversible clearing point for some compositions exceeding 400°C. Nematic liquid crystalline order in a fluid polymer leads to optimum processability. The random co-polymer primary structure of these molecules precludes intrachain periodicity and inhibits crystallization in the solid state. Amorphous molecular order in the solid state is desirable for optimizing optical transparency.

- Recognition that Rheinberg differential color contrast, previously applied only to the study of biological materials, provides an optimum combination of resolution and contrast for observing microstructural (and therefore optical) discontinuities in a liquid crystalline material (Appendix 7). In particular, for NLO materials, it is preferable to work with materials that are amorphous and that contain no microstructural light-scattering defects such as disclinations.

- Identification of molecular factors to which the scale of a liquid crystalline microstructure is sensitive (Appendix 8). The number of disclinations in a liquid crystalline microstructure is reduced if the molecules (1) have a large axial ratio, (2) are rigid, and (3) have low polydispersity.

- Observation that high strength disclinations (defects associated with a high degree of local microstructural distortion) may be present in a sheared liquid crystalline material, even though they are absent in quiescent material (Appendix 9). These defects will increase viscosity during processing, and would be effective light scattering centers if retained in a rapidly cooled product such as a thin fiber.

PUBLICATIONS RECOGNIZING SUPPORT FROM CONTRACT F49620-89-C-0059

R.M. Laine and C. Viney welcome requests for reprints of articles that they authored.

Papers

1. "Superconducting Fibers from Anhydrous Metal Carboxylates", R.M. Laine, K.A. Youngdahl, R.A. Kennish, M.L. Hoppe, Z.-F. Zhang and D.J. Ray, in Better Ceramics Through Chemistry IV, Mat. Res. Symp. Proc. Vol. **180** (C. J. Brinker, D. E. Clark, D. R. Ulrich, Eds), 1990, p.865.

2. "Chemical Processing of Ceramics", R.M. Laine in Sol-Gel Processing of Glasses, SPIE Proc. vol **1328** (J.D. Mackenzie, D.R. Ulrich, Eds), 1990, p.16.

3. "Factors Affecting Microstructural Scale in Liquid Crystalline Polymers", C.M. Dannels and C. Viney, in Electron Microscopy 1990, Proc. XII Internat. Congr. Electron. Micro. (L.D. Peachey, D.B. Williams, Eds), San Francisco Press, San Francisco, 1990, vol.4, p.220.

4. "Superconducting Fibers from Organometallic Precursors. 2. Chemistry and Processing", R.M. Laine, K.A. Youndahl, R.A. Kennish, M.L. Hoppe, Z.-F. Zhang, *J. Mat. Res.* (1991) **6**, 895.

5. "Characterizing the Scale of Liquid Crystalline Textures: Rheinberg Differential Color Contrast", C. Viney and C.M. Dannels, *Molec. Cryst. Liq. Cryst.* (1991) **196**, 133.

6. "Factors Affecting Microstructural Scale in Liquid Crystalline Materials", C.M. Dannels, C. Viney, R.J. Twieg, M.Y. Chang, *Molec. Cryst. Liq. Cryst.* (1991) **198**, 341.

7. "Chemicals, Polymers and Ceramics from the Beach (Silica)," C.R. Bickmore, M.L. Hoppe, R.M. Laine, K.A. Youngdahl, P. Nardi, T.R. Robinson and J. Uhm; in 5th Internat. Confer. on Ultrastructure Processing (L.L. Hench, J.K. West, D.R. Ulrich, Eds), John Wiley, 1991, in press.

8. "Synthesis of Novel Penta-alkoxy and Penta-aryloxy Silicates from Silica" K.A. Youngdahl Blohowiak, R.M. Laine, T.R. Robinson, M.L. Hoppe and J. Kampf, in Inorganic and Organometallic Polymers with Special Properties, NATO ASI Ser. E: Appl. Sci.-No. **206** (R. M. Laine, Ed.), Kluwer Publ., Dordrecht, 1992, p.99.

9. "How Light Microscopy Reveals Molecular Order in Liquid Crystalline Polymers", C.M. Dannels and C. Viney, *Polymer News* (1991) **16**, 293.

10. "SiO_2 as a Source of Si Containing Compounds / Polymers", D.J. Ray, R.M. Laine, C. Viney and T.R. Robinson, *ACS Polymer Preprints* (1991) **32**(3), 550.

11. "Polymers for Multifunctional Applications: Some General Considerations", C. Viney, in Inorganic and Organometallic Polymers with Special Properties, NATO ASI Ser. E: Appl. Sci.-No. **206** (R.M. Laine, Ed.), Kluwer Publ., Dordrecht, 1992, p.3.

12. "Characterizing the Microstructure of New Polymers", C. Viney, in Inorganic and Organometallic Polymers with Special Properties, NATO ASI Ser. E: Appl. Sci.-No. **206** (R.M. Laine, Ed.), Kluwer Publ., Dordrecht, 1992, p.395.

13. "Inorganic and Organometallic Polymers with Special Properties. Progress, Potential and Problems", R.M. Laine and C. Viney, in Inorganic and Organometallic Polymers with Special Properties, NATO ASI Ser. E: Appl. Sci.-No. **206**, (R.M. Laine. Ed.), Kluwer Publ., Dordrecht, 1992, p.413.

14. "Thermotropic and Lyotropic Copolymers of Bis(Dioxyphenyl) Silanes", D.J. Ray, R.M. Laine, T.R. Robinson and C. Viney, *Molecular Crystals and Liquid Crystals* (1993) **225**, 153.

15. "High Strength Disclinations in a Rigid Rod Nematic Polytolane", C. Viney, D.J. Brown, C.M. Dannels and R.J. Twieg, *Liquid Crystals* (1993) **13**, 95.

16. "Superconducting Fibers from Organometallic Precursors. 3. High Temperature Pyrolytic Processing", Z.-F. Zhang, R.A. Kennish, K.A. Youndahl Blohowiak, M.L. Hoppe and R.M. Laine, submitted to *Journal of Materials Research*, 1992.

17. "$BaSi(OCH_2CH_2O)_3$, a Hexa-Alkoxy Silicate Synthesized from SiO_2", M.L. Hoppe, R.M. Laine, J. Kampf, M.S. Gordon and L.W. Burggraf, *Angewandte Chemie*, 1993 in press.

Book

Inorganic and Organometallic Polymers with Special Properties, NATO ASI Ser. E: Appl. Sci.-No. **206** (R.M. Laine, Ed.), Kluwer Publ., Dordrecht, 1992.

Patent

"Silicon and Aluminum complexes", R.M. Laine, K.A. Youngdahl and P. Nardi, U.S. Patent #5,099,152, 24 March 1992.

AWARDS and HONORS

Election to French Academy of Science (R.J.P. Corriu)

NATO grant (900025) for a NATO Advanced Research Workshop on "Inorganic and Organometallic Polymers with Special Properties" (R. M. Laine with Dr. D. R. Ulrich).

NATO travel grant (867/91) for work on "Organometallic Oligomers and Polymers with Nonlinear Optical Properties" (R.M. Laine in collaboration with Dr. G.A. Balavoine of the University of Paris XI, Orsay).

"Creep Resistant Oxide Fibers" contract award to R. M. Laine and J. Halloran (start date Aug 22, 1991) from Wright Laboratory, Wright Patterson Air Force Base, based on discoveries made on Contract F49620-89-C-0059. Dr. Allan Katz of WPAFB is the technical monitor.

University of Washington Distinguished Teaching Award, 1992 (C. Viney). Awarded to 4 faculty out of >3000, campus-wide.

Invited Speaker, Materials Research Society Symposium on *Frontiers of Materials Science* (C. Viney, December 1992).

3M Nontenured Faculty Grant Award (C. Viney, July 1991 and May 1992).

APPENDIX 1

Angewante Chemie In Press, February, 1993

$BaSi(OCH_2CH_2O)_3$, a Hexa-Alkoxy Silicate Synthesized from SiO_2.

Martin L. Hoppe, Richard M. Laine,*,** Jeffrey Kampf, Mark S. Gordon and Larry W. Burggraf

Contribution from the Departments of Materials Science and Engineering, and Chemistry, University of Michigan, Ann Arbor, MI 48109-2136; Dept. of Chemistry, North Dakota State University, Fargo, ND:, and Air Force Office of Scientific Research, Bolling Air Force Base, W., D.C.

* Professor R. M. Laine
Department of Materials Science and Engineering
H. H. Dow Building, 2300 Hayward
University of Michigan
Ann Arbor, MI 48109-2136

M. L. Hoppe, Dept. of Materials Science and Engineering, University of Michigan
J. Kampf, Dept. of Chemistry, University of Michigan
M. S. Gordon, Dept. of Chemistry, North Dakota State University, Fargo, ND
L. W. Burggraf, Air Force Office of Scientific Research, W., DC

** This work was supported by the Air Force Office of Scientific Research. We would like to thank Professors Linda Nazar, Waterloo and Florence Babonneau, Paris for continuing successful collaborations, especially for running solid state NMR studies; and Professor R. J. P. Corriu for numerous very helpful discussions that have made this publication possible.

Introduction

Anionic (pentacoordinate) and dianionic (hexacoordinate) organosilicates were first reported more than 60 years ago.[1-4] Pentacoordinate Si complexes have recently received considerable attention because of: (1) the role they play in sol-gel processing of silicate glasses,[4-6] (2) their utility in organic synthesis and polymerization,[7-9] and (3) as precursors to organosilicon compounds.[10-12] Pentacoordinate silicates are easily prepared from tetrasubstituted Si centers containing alkoxy, alkyl-(aryl)alkoxy, hydridoalkoxy, -CN and halogen ligands.[10-22] Although polyhalogenato anionic silicates are relatively common, only perfluorinated derivatives are found to form hexacoordinate silicate dianions (e.g. SiF_6^{2-}).[23] Various salts of $Si(1,2\text{-}O_2C_6H_4)_3]^{2-}$, the triscatecholato dianion, first prepared in the early 30's, are the most common nonfluorinated hexacoordinate silicates.[2,3,10]

Surprisingly, the triscatecholato dianions are thermally and hydrolytically more stable than pentacoordinate, alkoxy silicates. Frye suggests that this enhanced stability arises because the aromatic rings provide charge delocalization.[1c] Corriu et al describe the synthesis of hexacoordinate dianionic germanium complexes, $M_2[Ge(1,2\text{-}O_2C_2Me_4)_3]$ (where M = K or Li and $1,2\text{-}O_2C_2Me_4$ = pinacolato) directly from GeO_2; however, these workers note that the silicon analog is still unknown.[24] Thomas et al, in recent work on polyhedral germanates observe both four, five and six fold O-coordination of Ge.[25] They suggest that the ability of Ge (but rarely Si) to exhibit six fold O-coordination is expected because it is a post transition metal element. They note that six fold O-coordinated Si is limited to the rare mineral stishovite, formed from a meteor impact.

It can be inferred from the above discussion that hexa-alkoxy silicates are not likely to form. This seems reasonable given that no examples have been described in the literature since the discovery of the triscatecholates in 1931. However, theoretical calculations suggest that simple hexa-oxygenate silicate dianions without supporting aromatic ligands should be stable.[26] We report here the first such example.

We recently reported the synthesis of the pentacoordinate $MSi(OCH_2CH_2O)_2(OCH_2CH_2OH)$ and $M_2Si_2(OCH_2CH_2O)_5$ (M = Li, Na, K, and Cs) silicates by direct reaction of one equivalent of MOH with one equivalent of SiO_2 (as silica gel, fused silica or sand) in excess ethylene glycol.[27] Efforts to delineate the scope of this reaction, led to studies of alkaline analogs, e.g. $MSi_2(OCH_2CH_2O)_5$ (M = Mg, Ca and Ba). The stoichiometry of these anticipated materials would be ideal for the preparation of aluminosilicates such as $CaO{\cdot}2SiO_2{\cdot}Al_2O_3$ (garnet). These studies provided rather unique and unexpected results. We report here the synthesis of the first example of the heretofore unknown hexa-alkoxy dianionic silicate directly from silica, ethylene glycol and barium oxide.

Thus, heating mixtures of BaO (85.2 g, 0.56 mol), SiO_2 (30.0 g, 0.5 mol) and glycol (500 mL) such that excess glycol and product H_2O distill off, leads to complete dissolution of the SiO_2 (2-4 h) On cooling the clear solution, white microcrystalline, methanol soluble product precipitates (≈ 90%

yield).[28] CaO and MgO can be used in place of BaO; although with MgO, low yields obtain due to the poor reactivity of MgO with $HOCH_2CH_2OH$. X-ray quality single crystals of the Ba complex can be grown by vapor infiltration of acetonitrile into a glycol solution of the Ba complex.

The structure, determined by single crystal X-ray diffraction (Figure 1),[29] reveals two crystallographically independent Ba^{2+}:$Si(OCH_2CH_2O)_3^{2-}$ ion pairs per asymmetric unit. ^{29}Si MAS solid state NMR data support these findings.[30] Each Si is in a slightly distorted octahedral coordination environment with three glycolates serving as bidentate ligands. There are 13 glycol lattice solvent molecules per unit cell. A number of coulombic Ba···O interactions as well as strong hydrogen bonding with the lattice glycols[31] likely account for the stability of the complex and also modify the stereo chemistry about each silicon. One Si exists in the Δ configuration with the 3 bidentate glycols adopting a ($\lambda\delta\delta$) configuration. The configuration about the other Si is $\Delta(\delta\delta\delta)$. The crystallographic inversion center also generates Si centers with $\Delta(\delta\lambda\lambda)$ and $\Delta(\lambda\lambda\lambda)$ stereochemistry.

There are no chemically significant differences in any of the Si-O or C bond distances or angles for the two molecules except for those imposed by stereochemistry. However, the Ba atoms occupy quite different environments in the crystal lattice. Each Ba has nine contacts <3.2 Å with O atoms. For Ba(1), two of these are with the Si(1)-trisglycolate complex (mean distances) (2.904(2)), two are with the Si(2)-trisglycolate complex (2.739(2)) and five are with lattice glycols (2.832(2)). For Ba(2), two contacts are with the Si(1)-trisglycolate complex (2.739(2)), three are with the Si(2)-trisglycolate complex (2.803(2)) and four are with lattice glycols (2.827(2)). Further, the Ba···Si distances are quite dissimilar. The Ba(1) to Si(1) and Si(2) distances are 3.874(1) and 3.768(1) Å respectively while the Ba(2) to Si(1) and Si(2) distances are 3.684(1) and 3.481(1) Å. The closest Ba···Ba distance is quite long at 4.750 (1) Å.

TGAs of $BaSi(OCH_2CH_2O)_3$ reveal the expected weight loss, calculated based on the chemical analysis[28] and lead, at >800°C, to the formation of phase pure $BaSiO_3$ (JCPDS File No. 26-1402). Details on the pyrolysis studies of the Mg, Ca and Ba complexes will be described elsewhere.[32]

Because no chemically significant differences in the Si-O bonds are observed in the crystal structure, despite the coloumbic interactions with Ba^{2+}, we reexamined the alkali metal reactions. Efforts to prepare alkali hexacoordinate silicates, using two equivalents of LiOH or KOH, gave the pentacoordinate species in lower yields.[27] The presence of a dication may be required to stabilize hexa-alkoxy dianionic silicates; however, this conclusion is not supported by preliminary theoretical studies.[26]

Preliminary minimal basis (STO-2G[33]) ab initio calculations were conducted on the free, isolated dianion, to determine if it has any inherent asymmetry. Geometry optimization, performed using analytical gradient routines in the electronic structure code GAMESS[34], was done with C_1 symmetry. The resulting structure (which has a positive definite hessian) predicts Si-O bond lengths that are within an 0.003Å range (1.805-1.807Å). The semi-empirical AM1[35] method predicts all six bond

lengths to be 1.794Å. Both of these results are remarkably close to the average experimental Si-O distance of 1.785Å in the presence of a Ba^{2+} counterion. Thus, within the accuracy for a molecule this size, these levels of theory predict that the isolated dianion exhibits no bond length distortion. Thus, the distortions seen in the x-ray structure probably arise as a result of crystal packing forces, H-bonding and Ba-O coulumbic interactions.

Future papers will detail the preparation of the monomers $MSi(OCH_2CH_2O)_3$ (M = Mg, Ca, and Ba) and tractable polymeric derivatives that offer access to novel silicon chemistries, including glasses and ceramics. Burlitch et al describe the use of $Mg(OR)_2/Si(OR)_4$ mixtures to form novel silicates.[36] Our work suggests that $MgSi(OR)_6$ may form as an intermediate. $MgSi(OCH_2CH_2O)_3$ prepared like the Ba analog can be used as a tractable cordierite precursor[37] and may also facilitate the Burlitch syntheses. The isolation of hexa-alkoxy silicates also provides support for recent work by Corriu et al,[38] wherein mechanistic evidence favors formation of hexacoordinate silicate anion intermediates in the nucleophilic reactions of pentacoordinated silicates. Finally, EXAFS studies of the hexacoordinate Ba complex indicate that the Si-O bond lengths, which range from 1.753 to 1.809Å, are essentially identical to those found for stishovite, 1.757 and 1.809Å[39].

References

[1] a) H. Meerwein, Justus Liebigs Ann. Chem. 1929, 476, 113; b) R. Müller, L. Heinrich, Chem. Ber. 1961, 94, 1943; c) C. L. Frye, J. Am. Chem. Soc. 1970, 92, 1205-1210.

[2] a) A. Rosenheim, B. Raibmann, G. Schendel, Z. Anorg. Chem. 1931, 196, 160; b) D. W. Barnum, Inorg. Chem. 1970, 9, 1942; c) D. W. Barnum, ibid. 1970, 11, 1424.

[3] a) C. L. Frye, J. Am. Chem. Soc. 1964, 86, 3170; b) J. J. Flynn , F. P. Boer, ibid. 1969, 91, 5756.

[4] a) R. J. P. Corriu, Pure and Appl. Chem. 1988, 60, 99-106; b) R. R. Holmes, Chem. Rev. 1990, 90, 17 (1990).

[5] C. J. Brinker, G. W. Scherer, Sol Gel Science 1990, Academic Press. Inc, Boston.

[6] R. M. Laine, in Sol-Gel Processing of Glasses, SPIE Proc. vol 1328, Mackenzie, J. D.; Ulrich, D. R.; eds. 1990, p16.

[7] a) S. K. Chopra, J. C. Martin, J. Am. Chem. Soc. 1990, 112, 5342-5343; b) M. Kira, K. Sato, H. Sakurai, Chem. Lett. 1987, 2243-2246.

[8] Y. Hatanaka, S. Fukushima, T. Hayama, Chem. Lett. 1989, 1711-1714.

[9] O. W. Webster, W. R. Hertler, D. Y. Sogah, W. B. Farnham, T. V. Rajan Babu, J. Am. Chem. Soc. 1983, 105, 5706-5708.

[10] A. Boudin, G. Cerveau, C. Chuit, R.J. P. Corriu, C. Reyé, Angew. Chem. 1986, 98, 473 ;

Angew. Chem. Int. Ed. Engl. 1986, 25, 473.
[11] R. J. P. Corriu, C. Guérin, B. J. L. Henner, W. W. C. Man, Organometallics 1988, 7, 237.
[12] A. Boudin, G. Cerveau, C. Chuit, R. J. P. Corriu, C. Reyé, Organometallics 1988, 7, 1165.
[13] C. Brelière, R. J. P. Corriu, G. Royo, W. W. C. Man, J. Zwecker, Organometallics 1990, 9, 2633-2635.
[14] R. Tacke, J. Sperlich, C. Strohman, G. Mattern, Chem. Ber. 1991, 124, 1491-1496.
[15] G. Cerveau, C. Chuit, R. J. P. Corriu, N. K. Nayyar, C. Reyé, J. Organmet. Chem 1990, 389, 159.
[16] R. Damrauer, B. O'Connell, S. E. Danahey, R. Simon, Organometallics 1989, 8, 1167-1171.
[17] D. A. Dixon, W. R. Hertler, D. B. Chase, W. B. Farnham, F. Davidson, Inorg. Chem. 1988, 27, 4012-4019.
[18] M. Kira, K. Sato, H. Sakurai; J. Am. Chem. Soc. 1988, 110, 4599-4602.
[19] D. Kummer, K.-E. Gaisser, T. Seshadri, Chem. Ber. 1977, 110, 1950-1962.
[20] R. R. Holmes, R. O. Day, J. S. Payne, Phos., Sulfur and Silicon 1989, 42, 1-13.
[21] R. R. Holmes, R. O. Day, J. J. Harland, J. M. Homes, Organometallics 1984, 3, 347-353.
[22] K. C. K. Swamy, V. Chandrasekhar, J. J. Harland, J. M. Homes, R. O. Day, R. R. Holmes, J. Am. Chem. Soc. 1990, 112, 2341-2348.
[23] S. N. Tandura, M. G. Voronkov, N. V. Alekseev, Top. in Curr. Chem. 1986, 131, 99-186.
[24] G. Cerveau, C. Chuit, R. J. P. Corriu and C. Reyé; Organometallics 1991, 10, 1510-1515.
[25] R. H. Jones, J. Chen, J. M. Thomas, A. George, M. B. Hursthouse, R. Xu, S. Li, Y. Lu, G. Yang.; Chem. Mater. 1992, 4, 808-812.
[26] L. W. Burggraf, L. P. Davis in Better Ceramics Through Chemistry II, Mat. Res. Soc. Symp. Proc. Vol 73, Mater. Res. Soc.; Pittsburgh, PA 1986, pp. 529-542.
[27] R. M. Laine, K. Y. Blohowiak, T. R. Robinson, M. L. Hoppe, P. Nardi, J. Kampf, J. Uhm, Nature 1991, 353, 642-644.
[28] Simple filtration followed by washing with dry ethanol and acetonitrile and then vacuum drying at 100°C for 2-6 h provides analytically pure samples. Chem. analysis of $BaSi(OCH_2CH_2O)_3 \cdot 3.25HOCH_2CH_2OH$[29] = $BaC_{12.5}H_{31.5}O_{12.5}Si$ (MW = 547.34)]: found (calc.) Ba = 25.10 (27.20), C = 27.44 (26.90), H = 5.80 (5.65), Si = 4.62 (5.13).
[29] Crystal data for **1**: [$BaSi(OCH_2CH_2O)_3 \cdot 3.25HOCH_2CH_2OH$], triclinic $P\bar{1}$, a = 10.151(8)Å, b = 13.865(5)Å, c = 15.709(6)Å, α = 102.90(3), β = 91.04(3), γ = 109.75(3), U = 2018(1), Z = 4, D_c = 1.70 g/cm^{-3}, μ (Mo-Kα) = 2.08 mm^{-1}, F(000) = 1080, colorless rectangular plate, 0.2 x 0.5 x 0.44 mm, 13038 data collected with $5° < 2\theta < 50$, 9298 unique reflections, R_{merge} = 0.0312, 8999 reflections with $F_o \geq 0.6\sigma(F)$ used in the refinement. Data were collected on a Siemens R3/v equipped with a LT-2 low temperature device at 175K and corrected for

absorption (psi scans) and secondary extinction. The structure was solved by direct methods and refined using Siemens SHELXTL PLUS. All non-H atoms were refined anisotropically, H atoms were located on a difference Fourier and allowed to refine isotropically. The O atom of one glycol of solvation is disordered over two positions at refined occupancies of 0.700(1) and 0.300(1). The related H atom was not placed. 745 parameters were refined with a weighting scheme [$w^{-1} = \sigma^2(F)+0.000382(F_o)^2$] to give a final convergence of R = 0.0282, Rw = 0.0374 and a final difference electron density max. of +0.80 e $Å^{-3}$, min. -0.82 e $Å^{-3}$. Further details of the crystal structure investigation are available on request from the Director of the Cambridge Crystallographic Centre, University Chemical Laboratory, Lensfield Road, GB-Cambridge CB21EW (UK), on quoting the full journal citation.

[30] Solid state ^{29}Si MAS NMR gives peaks at -143.3 and -145.5 ppm; M. Hoppe, L. Nazar, R. M. Laine, unpublished results.

[31] Significant H-bonding interactions for **1**: Distances (Å) are for the hydroxyl proton of a lattice glycol to the numbered oxygen of a coordinated glycol. Approximate errors are 0.04 Å. [a]O(11) 1.84, O(4) 1.97; [b]O(3) 1.60, O(6) 1.94; [c]O(7) 1.52, O(4) 1.91, O(13) 1.97; [d]O(11) 1.70, O(10) 1.87. Symmetry transformations a: x, y, z; b: 1+x, 1+y, z; c: 1-x, 1-y, -z; d: 2-x, 1-y, -z.

[32] P. Kansal, K. W. Chew; M. L. Hoppe, R. M. Laine, manuscript in preparation.

[33] W. J. Hehre, R. F. Stewart, J. A. Pople, J. Chem. Phys. 1969, 51, 2657.

[34] M. W. Schmidt, K. K. Baldridge, Boatz; J. H. Jensen, S. Koseki, M.S. Gordon, K. A. Nguyen, T.L. Windus, S. T. Elbert, QCPE Bulletin 1990, 10, 52.

[35] M.J.S. Dewar, E.G. Zoebisch, E. F. Healy, J. J. P. Stewart; J. Am. Chem. Soc. 1985, 107, 3902.

[36] a. J. M. Burlitch, M. L. Beeman, B. Riley, D. L Kohlstedt, Chem. Mater. 1991, 3, 692-698. b. F. D Duldulao, J. M. Burlitch, Chem. Mater. 1991, 3, 772-773.

[37] Z-F. Zhang, M. L. Hoppe, J. A. Rahn, S.-M. Koo, R. M. Laine, in "Synthesis and Processing of Ceramics: Scientific Issues," Mat. Res. Soc. Symp. Proc.; W. E. Rhine, T. M. Shaw, R. J. Gottschall, Y. Chen, 1992, vol 249, p. 81-86.

[38] R. J. P. Corriu, C. Guerin, B. J. L. Henner, Q. Wang, Organometallics 1991, 10, 3200.

[39] J. S. Tse, D. D. Klug, B. X. Yang, X. H. Feng, R. M. Laine, submitted for publication.

Figure Caption

Fig. 1. ORTEP drawing of the crystallographically independent $BaSi(OCH_2CH_2O)_3$ formula units with atoms represented as 50% thermal ellipsoids. Selected interatomic distances (Å): Si(2)-O(7) 1.835(2), Si(2)-O(8) 1.762(2), Si(2)-O(9) 1.753(2), Si(2)-O(10) 1.781(2), Si(2)-O(11) 1.809(2), Si(2)-O(12) 1.770(2), Ba(2)···O(7) 2.772(2), Ba(2)···O(10) 2.956(2), Ba(2)···O(12) 2.682(1), Ba(2)···Si(2) 3.481(1). Each Ba has a total of nine contacts of <3.2 Å with lattice solvent molecules and O's of the other molecule. Mean bond distances are typical Si-O 1.785(1), C-O 1.419(3), C-C 1.516(4).

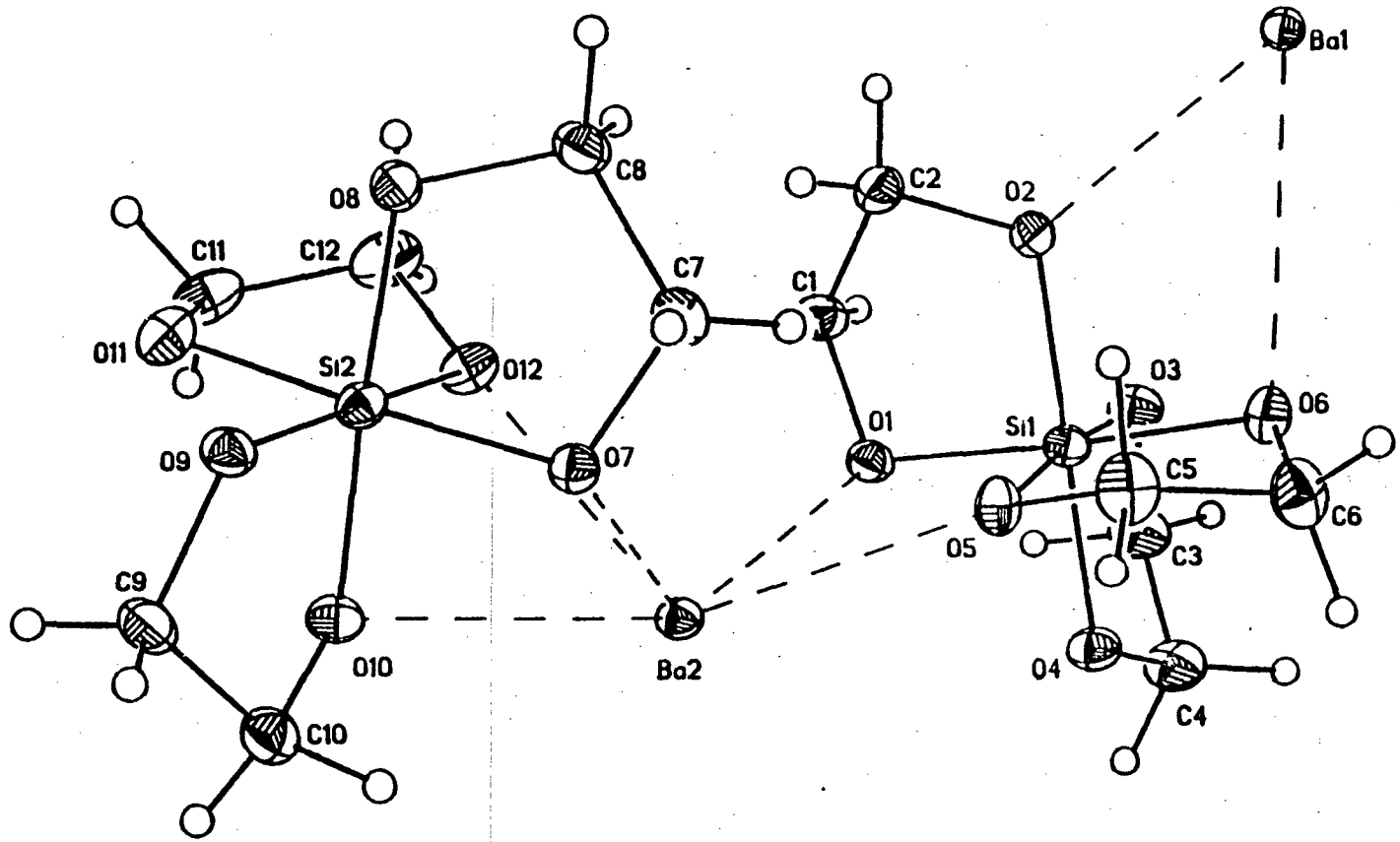
Ba1
C8
C2
O2
O8
C11
C12
C7
C1
O11
Si2
O12
O3
O6
O9
O7
O1
Si1
C5
C6
O5
C3
C9
O10
Ba2
O4
C4
C10

Barium Tris[ethanediolato(2-)]silicate, a Hexa-Alkoxy Silicate Synthesized from SiO_2.

By Martin L. Hoppe, Richard M. Laine,*,** Jeffrey Kampf, Mark S. Gordon and Larry W. Burggraf

Supplementary Material

Figure 2. Perspective ORTEP Drawing of one independent molecule of **1** showing the atom labeling scheme. Atoms are presented by 50% thermal ellipsoids.

Figure 3. Perspective ORTEP Drawing of second independent molecule of **1** showing the atom labeling scheme. Atoms are presented by 50% thermal ellipsoids.

Table 1. Structure Determination Summary

Bond distances

Bond angles

Unit Cell Packing Arrangements

Atomic Parameters

Thermal Parameters

Hydrogen Parameters

Observed and calculated structure factors

Nearest non-contact distances

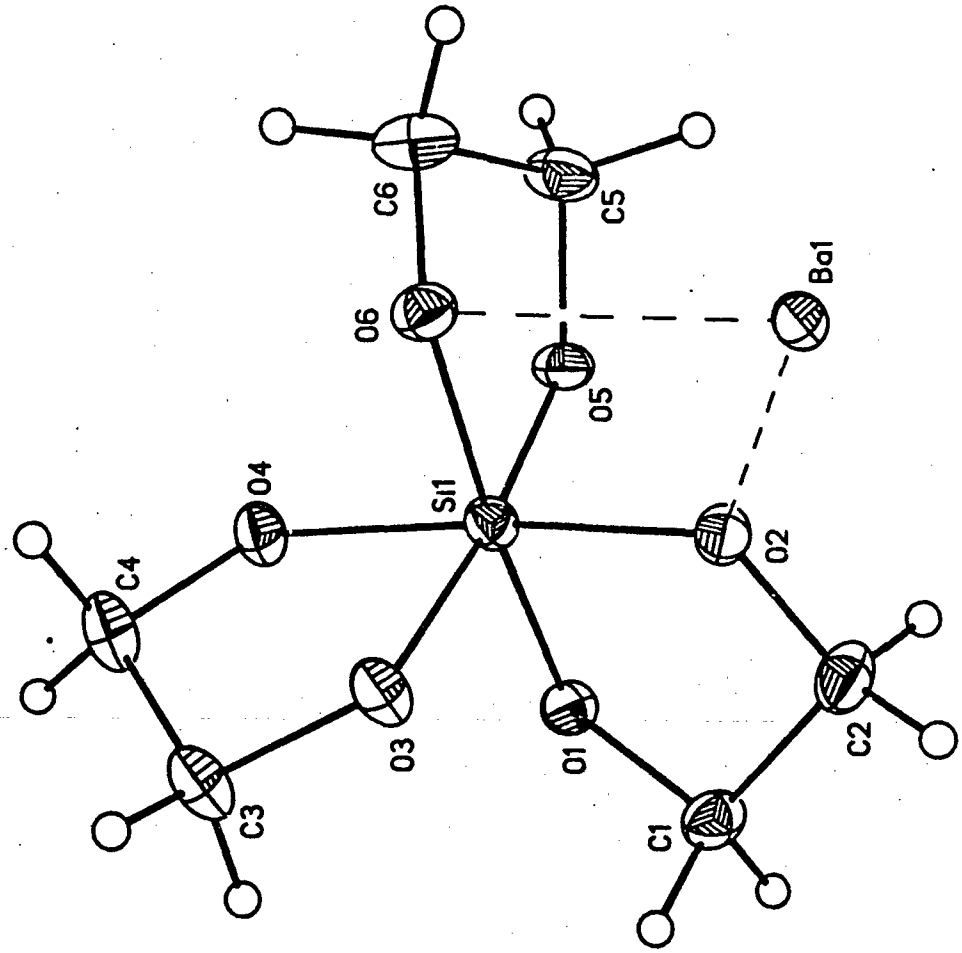
C6
C5
Ba1
O6
O5
O4
Si1
O2
C4
O3
O1
C2
C3
C1

APPENDIX 2

Synthesis of pentacoordinate silicon complexes from SiO_2

Richard M. Laine*†, Kay Youngdahl Blohowiak*, Timothy R. Robinson*, Martin L. Hoppe*, Paola Nardi*, Jeffrey Kampf† & Jackie Uhm*

* Department of Materials Science and Engineering, University of Washington, Seattle, Washington, USA
† Departments of Materials Science and Engineering, and Chemistry, University of Michigan, Ann Arbor, Michigan 48109-2136, USA

THE potential role of inorganic and organometallic silicon compounds in the development of new chemical reagents, polymers, glasses and ceramics[1] is limited at present by the paucity of simple silicon-containing starting materials. Whereas industrial carbon-based chemistry can draw on the diversity of compounds produced from crude oil, coal or other natural sources, silicon chemistry[2] relies almost exclusively on the carbothermal reduction of SiO_2 to silicon. This is then transformed into feedstock chemicals by reaction with HCl, or by routes such as the 'direct process' for making methylchlorosilanes[2], in which silicon is reacted with methyl chloride at 200–350 °C over a copper/tin catalyst. Organosilicon compounds are in demand in fields ranging from organic synthesis to ceramics to the electronics industry. New synthetic routes to these materials are therefore highly desirable, especially if they rely on low-cost SiO_2 and on processing methods that avoid the energy-intensive and equipment-intensive carbothermal reduction step which currently precedes almost all silicon

chemistry. Here we describe a direct process in which SiO_2 is reacted with ethylene glycol and an alkali base to produce highly reactive, pentacoordinate silicates which provide access to a wide variety of new silicon compounds.

Earlier investigations[3-5] have explored the chemical reactivity of the hexacoordinate silicon compound tris(catecholato) silicate, **1**, readily made by reaction of silica, sand or even quartz with catechol (1,2-dihydroxobenzene) in basic media (see scheme 1)[6-8]. Unfortunately, **1** is quite stable and can only be modified usefully by reaction with strong nucleophiles:

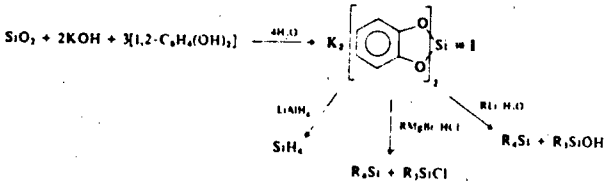

Scheme 1

The work of Kenney and Goodwin[9], which is complementary to the work in refs 3-5, demonstrates that protonation of mineral silicates followed by careful azeotropic removal of water provides up to 70% yields of the tetracoordinate silicon compound, $Si(OCH_2CH_3)_4$:

$$CaSiO_3 + 2HCl \xrightarrow[\text{(toluene/CH}_3\text{CH}_2\text{OH azeotrope)}]{-3H_2O} Si(OCH_2CH_3)_4 + CaCl_2 \quad (1)$$

We describe here a general method of synthesizing pentacoordinate, rather than hexa- or tetra-coordinate silicates, directly from SiO_2, ethylene glycol and base. The resulting glycolato silicates are very reactive, inexpensive and offer unique opportunities for the synthesis of a wide variety of silicon containing chemicals and polymers. Furthermore, they offer the opportunity to develop new routes to silicon-containing glasses, ceramics and zeolites.

A mixture of 60 g silica gel ($>600\ m^2\ g^{-1}$), fused silica (325 mesh, 0.5-0.8 $m^2\ g^{-1}$) or sand ($<0.2\ m^2\ g^{-1}$), 1.1 equivalents of a group 1 metal hydroxide (for example 44 g KOH) and an excess (2 l) of ethylene glycol (or other -1,2-diol, such as propane-1,2-diol) was heated under N_2 in a magnetically stirred, standard pyrex distillation setup so that the ethylene glycol was distilled off slowly (with removal of water), to result in the dissolution of the silica gel (1-2 h), fused silica (3-6 h) or sand (>200 h).

The products were isolated by cooling the much-reduced volume of the reaction solution to effect crystallization, or by precipitation with CH_3CN. Further washing with CH_3CN, followed by drying under vacuum (130 °C), provided white powders in >80% isolated yields (350 g where KOH was used). The reaction can be run using Li, Na, K or Cs hydroxide.

The products are essentially insoluble in all polar solvents except CH_3OH (but not in CH_3CH_2OH). Recrystallization is readily effected using CH_3OH/CH_3CN. The following results are from a typical elemental analysis for M = K (analysis carried out by Galbraith Laboratories, Inc., Knoxville) calc. (found) 27.53 (27.63)% C; 4.98 (4.64)% H; 13.60 (12.92)% Si; 17.84 (17.99)% K; 37.01 (36.81)% O (by difference). These results indicate a dimeric pentacoordinate species, labelled **2** in reaction (2) (refs 10, 11). In this scheme M is Li, Na or K. The Cs salt can be isolated as a monomer. Analysis gave typical values calculated (found) as 20.72 (21.06)% C; 3.63 (3.83)% H; 8.58 (8.21)% Si; 39.38 (38.84)% Cs; 27.32 (27.06)% O by difference. This indicates that a monomeric species, such as **3** in scheme 2 (below) was formed as

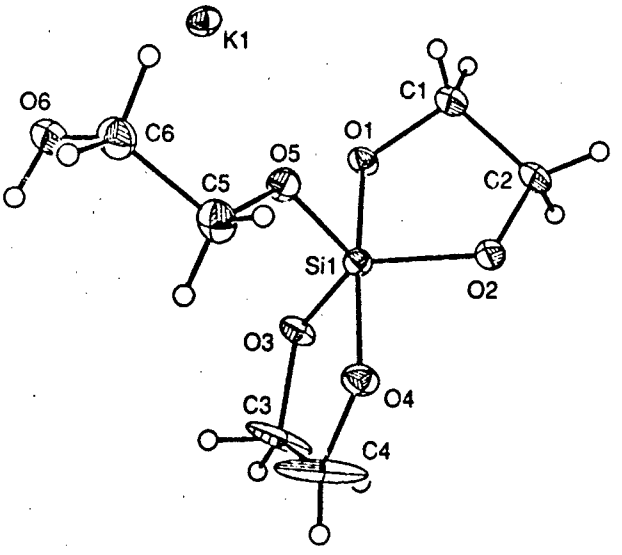

FIG. 1 X-ray single crystal structure of $KSi(OCH_2CH_2O)_2OCH_2CH_2OH$. Crystal grown from ethylene glycol/acetonitrile.

supported by the infrared (nujol) peak found for O-H at 3,300 cm^{-1} and the solubility in dimethylsulphoxide (DMSO).

NMR studies suggest that the products dissolve in CD_3OD through an exchange reaction. The ^{13}C spectra for all of the salts (Li, Na, K and Cs) show two peaks at 61.3 ± 0.3 and 64.3 ± 0.3 p.p.m. Similarly, a single peak appears in the ^{29}Si NMR at ~ −103.1 ± 0.3 p.p.m. The ^1H spectra all contain one broad singlet at ~3.4 p.p.m. The ^{13}C peak at 64.3 p.p.m. and the ^1H peak at 3.4 p.p.m. are consistent with free ethylene glycol, despite analytical results that indicate the materials are pure. The ^{29}Si NMR peaks are consistent with those previously reported for aliphatic, pentacoordinate silicates[11-14].

A plot of the ratio of the ^{13}C peak heights for free ethylene glycol to those for bound glycol, as a function of temperature for the dry K salt dissolved CD_3OD, shows a first-order increase in free ethylene glycol as the temperature is lowered to −50 °C. At −50 °C, the ratio of free to bound glycol is 0.85 (±0.05). Therefore, it appears that exchange proceeds beyond replacement of a bridging or monodentate glycol (in the Cs salt) with more than one CD_3O- group. The likely exchanges are shown in scheme 2.

The extent of the exchanges and the exact mechanism(s) whereby they occur must await more detailed kinetic studies.

Further support for the alcohol exchange process and for an intermediate monomeric species comes from the recrystallization of the dimer from ethylene glycol/acetonitrile which provides X-ray-quality crystals. The structure shown in Fig. 1 was refined to $R_w = 0.0492$. The structure is typical of an ionic solid in that the potassium contact distances between nearest neighbours are essentially identical. As is common for pentacoordinate, aliphatic silicate complexes, the ligand oxygens

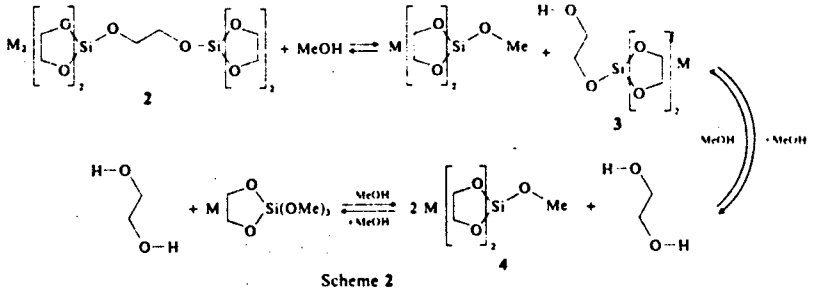

Scheme 2

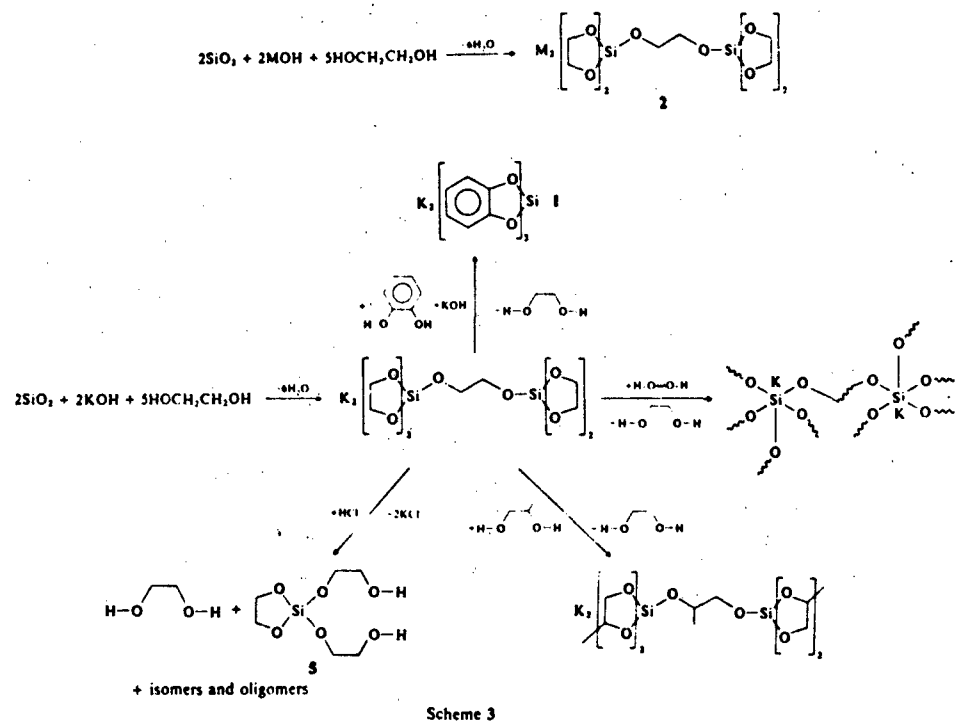

Scheme 3

occupy a trigonal bipyramidal geometry about the silicon[12-14].

The ready exchange of alkoxy ligands permits the synthesis of a wide variety of derivatives. Refluxing $M_2[Si_2(OCH_2CH_2O)_5]$ in an excess of a different 1,2-diol (for example, 1,2-propanediol or pinacol (2,3-dimethyl-2,3-butanediol)) followed by a removal by distillation of excess diol and free ethylene glycol (0.5–2 h at the reaction temperature) results in complete ligand exchange and the formation of new dimeric materials (following drying under vacuum at 130 °C), as illustrated in scheme 3. Pinacolate derivatives have been prepared previously[12-14]. Reaction of **2** with 6 equivalents of catechol and an additional equivalent of base provides the tris(catecholato)Si^{2-} species of scheme 1, in quantitative yield. With 4–5 equivalents and no additional base, the tris species is also isolated, but novel polymers are produced simultaneously (ref. 15, and R.M.L. and N. Budrys, unpublished results).

Exchange with other diols including 1,3-propanediol, $H(OCH_2CH_2)_4OH$ and hydroquinone produces polymer products with anionic silicon moieties in the polymer backbone (scheme 3). Detailed characterization of the polymers will be reported elsewhere, but the following example illustrates the simplicity of the process.

Heating a mixture of 9.9 g (24 mmol) of $Li_2[Si_2(OCH_2CH_2O)_5]$ and 30 g (124 mmol) of $H(OCH_2CH_2)_4OH$ under vacuum (~0.1 mm Hg) for ~3 h at 130 °C results in dissolution of the lithium salt and recovery of 8–12 ml of a clear liquid distillate (depending on total heating time) that consists of roughly equal molar amounts of $H(OCH_2CH_2)_4OH$ and $HOCH_2CH_2OH$ (determined by gas chromatography). The material remaining in the flask becomes increasingly viscous with time as bidentate glycol groups are replaced by monodentate, crosslinking $H(OCH_2CH_2)_4OH$. The new polymer is soluble in CH_3OH, CH_3CH_2OH and 1:1 $CH_3CH_2OH:CH_3CN$ and may be useful as an ion conductor for battery applications[16,17].

Finally, pyrolysis of the glycolato silicates leads directly to silicate glasses or glass ceramics[19]. The alkali complexes, when pyrolysed in air at 10 °C min^{-1} to temperatures above 300 °C for at least 2 h, provide the line compounds $M_2Si_2O_5$ (ref. 18). If excess base is used, then partially crystallized alkali-rich silicate glasses are formed preferentially.

The four-coordinate alkoxy silane complex, **5**, obtained by neutralization of **2** with HCl gas, can be used as a substitute for $Si(OCH_2CH_3)_4$ in sol-gel reactions. Unlike $Si(OCH_2CH_3)_4$, **5** is miscible with H_2O, offers rheologically useful properties for coating and fibre applications and can be used directly to form glass-polymer composites, 'ceramers'. It can also be mixed with the various alkali derivatives of **2** and heated to form alkali-poor silicate glasses (unpublished results, R.M.L. *et al.*). □

Received 19 March; accepted 27 August 1991.

1. *Inorganic and Organometallic Polymers with Special Properties* (ed. Laine, R. M.) *NATO ASI Series E: Appl. Sci.*, No. 30 (Kluwer, Dordrecht, 1991).
2. *Kirk-Othmer Encyclopedia of Chemical Technology*, *3rd Ed.*, Vol. 20, 750–880 (Wiley-Interscience, New York, 1979).
3. Boudin, A., Cerveau, G., Chuit, C., Corriu, R. J. P. & Reye, C. *Angew. Chem. Int. Ed.* **25**, 473–474 (1986).
4. Corriu, R. J. P., Perz, R. & Reye, C. *Tetrahedron* **39**, 999 (1983).
5. Boudin, A., Cerveau, G., Chuit, C., Corriu, R. J. P. & Reye, C. *Organomet.* **7**, 1165–1171 (1988).
6. Rosenheim, A., Raibmann, B. & Schendel, G. *Z. anorg. Chem.* **196**, 160 (1931).
7. Barnum, D. W. *Inorg. Chem.* **9**, 1942 (1970).
8. Barnum, D. W. *Inorg. Chem.* **11**, 1424 (1970).
9. Kenney, M. E. & Goodwin, G. B. *US Patent No.* 4,717,773 (January 1988).
10. Frye, C. L. *J. Am. chem. Soc.* **92**, 1205–1210 (1970).
11. Tandura, S. N., Voronkov, M. G. & Alekseev, N. V. *Topics Curr. Chem.* **131**, 99–186 (1986).
12. Swamy, K. C. K. *et al. J. Am. chem. Soc.* **112**, 2341–2348 (1990).
13. Holmes, R. R. *Chem. Rev.* **90**, 17 (1990).
14. Holmes, R. R., Day, R. O. & Payne, J. S. *Phos. Sulf. Silicon* **42**, 1–13 (1989).
15. Laine, R. M., Ray, D. J., Viney, C. & Robinson, T. R. *Am. chem. Soc. Polym. Preprints* **32**, No. 3, 550 (1991).
16. Fujita, M. & Honda, K. *Polymer Commun.* **30**, 200 (1989).
17. Spindler, R. & Shriver, D. F. *J. Am. chem. Soc.* **110**, 3036 (1988).
18. Levin, E. M., Robbins, C. R. & McMurdie, H. F. *Phase Diagrams for Ceramists*, 5th Printing (eds. Reser, M. K.) 87–92 (American Ceramic Society, 1985).
19. Bickmore, C. R. *et al. 5th Int. Conf. Ultrastructure Processing* (eds Hench, L. L., West, J. K. & Ulrich, D. R.) (Wiley, New York, in the press).

ACKNOWLEDGEMENTS. We thank J. Negrych and Minco, Inc. for discussions and gifts of fused silica and virgin sand. We also thank R. J. P. Corriu and P. Knochel for discussions and suggestions. We thank B. Posin for early contributions. We thank the Air Force Office of Scientific Research and the Office of Naval Research for support.

APPENDIX 3

Synthesis of Penta-alkoxy- and Penta-aryloxy Silicates Directly from SiO_2

K. A. YOUNGDAHL BLOHOWIAK,[b] R. M. LAINE,*[a,b] T. R. ROBINSON,[b] M. L. HOPPE,[a] and J. KAMPF.[a] Contribution from the Depts of Materials Science and Engineering, and Chemistry, [a]University of Michigan, Ann Arbor, MI 48109-2136 and, the [b]Dept of Materials Science and Engineering, University of Washington, Seattle, WA

ABSTRACT: It is likely that the utility of silicon chemistry would be greatly expanded, if new, general routes to organosilicon compounds could be developed. In particular, synthetic routes stemming from the use of silica (sand) would be particularly attractive because of the modest cost of pure starting material. To this end, we have developed novel chemistry that offers considerable opportunity as a general synthetic technique for the synthesis of unique hypervalent, penta-alkoxy and penta-aryloxy silicates. These species can be further elaborated to form novel compounds that exhibit a wide variety of properties including charge transfer from anionic silicon to cationic pyridinium counterions.

Introduction

Analogies are frequently drawn between the chemistries of silicon and carbon because both are group IV elements. However, efforts to establish correlations between their two chemistries have often challenged the creativity of synthetic chemists. For example, carbon readily forms cyclopropane rings; whereas, until relatively recently, similar compounds containing silicon were unknown[1-4]. Likewise, C-E (E = element) multiple bonds are common; however, Si-E double bonds have only been prepared rather recently[3]. Si-E triple bonds remain a challenge [4]. In these instances, the commonalities of their chemistries have been extended where it was not thought possible.

In other instances, the chemistry of silicon clearly diverges from that of carbon. For example, except for very special cases, there are no carbon analogs to penta and hexacoordinate Si [5-15]. Because the commonality does not hold in these areas, it becomes of interest to explore the extent to which there is divergence. It is in this exploration that totally new and unrelated chemistries may be developed. The purpose of the studies described here is to develop the chemistries of hypervalent Si. In particular, we focus on the synthesis of Si containing species from SiO_2, and the manipulation of these compounds to produce novel oligomers with electronic properties of potential value in the development of new NLO materials.

R. M. Laine (ed.), Inorganic and Organometallic Polymers with Special Properties, 99–111.

Background

Rosenheim and coworkers were the first group to describe the direct reaction of silica with a coordinating ligand [5]. They found that catechol could be used to transform a wide variety of metal oxides into catecholato complexes, as illustrated for SiO_2 in Scheme I:

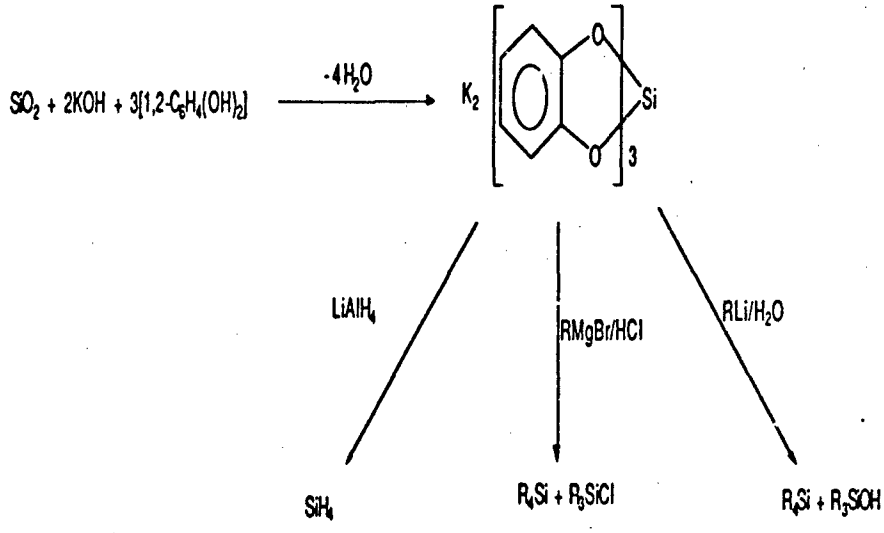

Scheme I

Corriu and coworkers [11-13], in pursuit of new synthetic routes to silicon containing compounds, have explored methods of transforming the resulting triscatecholato silicate into a wide variety of silicon containing compounds, as shown in Scheme I. Unfortunately, triscatecholato silicate is quite robust and reacts only under forcing conditions with strong nucleophiles. Consequently, it is only possible (except with very sterically hindered "R" groups) to generate tri- or tetrafunctionalized silicon species. Difunctional species would be most useful because they offer the opportunity to form polymers.

In our work, we have sought to escape the need for forcing conditions by identifying ligands that are more reactive than catecholate groups and/or through choice of different reactants. We have been successful in developing both approaches as we will discuss below.

Initial efforts to escape the stability of triscatecholato silicate, centered on the question: Will other 1,2 dihydroxy species (e.g. aliphatic diols) react with SiO_2, like catechol, to provide stable, isolable products? Ethylene glycol was particularly of interest because it is the prototypical 1,2-diol. In the late 60's, Frye reported that the preparation of spirosiloxanes from $Si(OEt)_4$ and 1,2 diols was quite facile, if the reaction is run in ethanol with a small amount of NaOMe as catalyst[7] as shown in Scheme II:

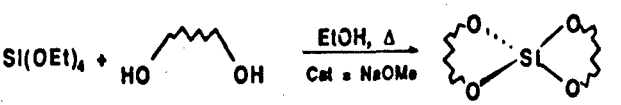

Diols: $HO\text{-}CMe_2CMe_2\text{-}OH$

$HO\text{-}CH_2CEt_2CH_2\text{-}OH$

$HO\text{-}CMe_2CH_2CMe_2\text{-}OH$

$HO\text{-}CH_2CH_2\text{-}OH$ (polymerization)

However, Frye found that with ethylene glycol, the product obtained was polymeric species. Fortuitously, he also discovered that in the presence of amine bases, novel penta-coordinate species will form [8]:

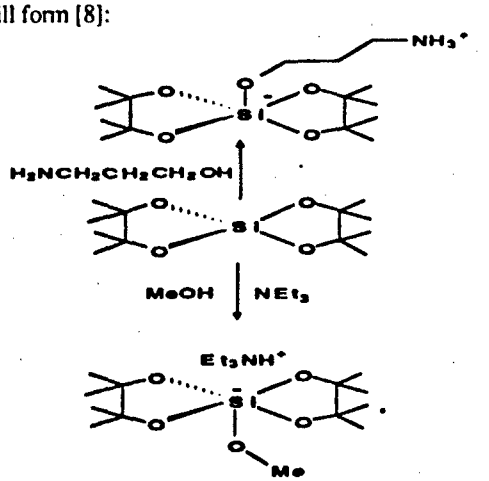

By coupling the diol exchange reaction with the formation of penta-alkoxy silicates, the same products can be isolated directly from the reaction of $Si(OEt)_4$ with 2.5 equivalents of diol and an amine:

$$Si(OEt)_4 + 2.5\ HOCH_2CH_2OH + Et_3N \xrightarrow{-EtOH} Et_3NH^+[Si(OCH_2CH_2O)_2OCH_2CH_2OH]^- \quad (1)$$

In this instance, even ethylene glycol provides a monomeric, penta-alkoxy silicate containing one monodentate and two bidentate glycols. No dimers are observed despite the clear opportunity to form.

Penta-alkoxy Silicates

These latter results prompted us to explore the feasibility of dissolving silica in ethylene glycol, in the presence of base, as illustrated in reaction (2). It was expected that removal of H_2O would be necessary to drive the reaction. Therefore, the reaction was run so that excess ethylene glycol and any product H_2O would be removed by distillation. Based on Frye's work and Corriu and coworkers efforts, the expected reaction should be:

$$SiO_2 + x's\ HOCH_2CH_2OH + MOH \xrightarrow{-3H_2O} M^+[Si(OCH_2CH_2O)_2OCH_2CH_2OH]^- \quad (2)$$

When reaction (2) is run with Li, Na, K or Cs hydroxide, the silica slowly dissolves with continuous distillation. As excess glycol is removed, the solution becomes increasingly viscous. After approximately 70% of the excess ethylene glycol has been removed, the reaction is allowed to cool and the product precipitates out. The resulting product, when washed with acetonitrile and vacuum dried with mild heating, gives a fine, free flowing powder.

Initial efforts to recrystallize this powder were thwarted by its insolubility in a wide variety of solvents including: THF, acetone, N-methylpyrrolidone, DMSO and DMF. It was only through good fortune that it was found to be soluble in MeOH (but not EtOH). Thus, the material can be purified by recrystallization, with difficulty, from $MeOH/CH_3CN$.

Chemical analysis of the potassium salt recrystallized from MeOH gives: calc. (found) %C, 27.53 (27.63); %H, 4.98 (4.64); %Si, 13.60 (12.92); %K 17.84 (17.99); %O by difference, 37.01 (36.81); which suggests a dimeric pentacoordinate species, $M_2^{2+}[Si(OCH_2CH_2O)_2OCH_2CH_2OSi^-(OCH_2CH_2O)_2]$ rather than the monomer expected based on Frye's studies.

The last of the series to be made, the Cs glycolato silicate, exhibited solubility properties quite different from the other complexes. For example, it is soluble in EtOH and DMSO. However, attempts to obtain NMR spectra in DMSO-d_6 were thwarted by the rapid precipitation of an insoluble material and the observation of free ethylene glycol in the ^1H NMR spectrum. Elemental analysis of the Cs glycolato silicate: calc. (found) %C, 20.72 (21.06); %H, 3.63 (3.83); %Si, 8.58 (8.21); %Cs 39.38 (38.84); %O by difference, 27.32 (27.06); indicates formulation as $Cs^+[Si(OCH_2CH_2O)_2OCH_2CH_2OH]^-$, a monomeric structure, as originally expected in reaction (2).

NMR studies in CD_3OD suggest that all of the glycolato silicates dissolve in CD_3OD via an exchange reaction. The ^{13}C spectra for all of the glycolato silicates (Li, Na, K, Na, Cs) exhibit two peaks at 61.3±0.3 and 64.3±0.3 ppm. Similarly, a single peak appears in the ^{29}Si NMR at -103.1±0.3 ppm. The ^1H spectra all contain one broad singlet at ≈ 3.4 ppm. The ^{13}C peak at 64.3 ppm and the ^1H peak at 3.4 ppm are consistent with free ethy-

lene glycol, despite analytical results that indicate the materials are pure. The ^{13}C peaks for free and bound ethylene glycol give height ratios (at low temperatures, to -70°C) that suggest more than one glycol is exchanged. The ^{29}Si NMR peaks are consistent with those previously reported for aliphatic, pentacoordinate silicates [9,10]. The fact that the Cs glycolato silicate gives the same set of spectra are consistent with an exchange reaction as suggested by Scheme II:

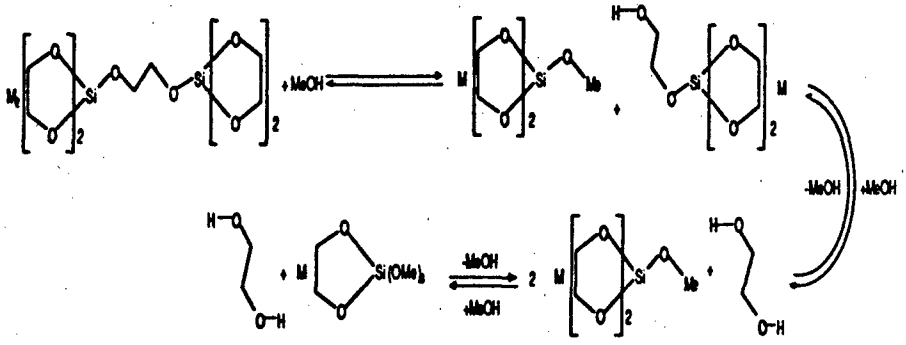

Scheme II

The exact mechanisms and the extent of exchange will require detailed kinetic and mechanistic analyses that will be addressed at a later date. Further support for the proposed exchange process comes from recrystallization of the dimer from glycol/acetonitrile. The excess glycol drives exchange and permits isolation of x-ray quality crystals of the monomeric product shown at the far right of Scheme II:

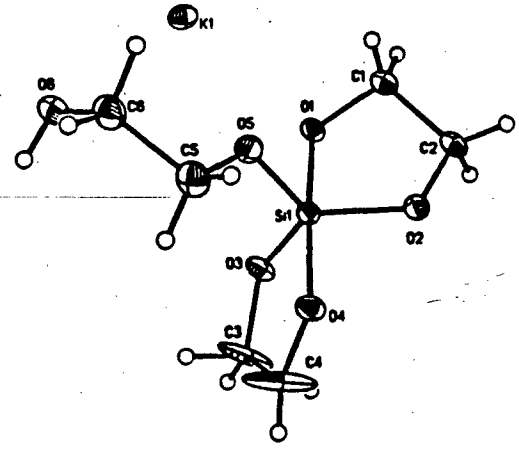

The crystal structure (R_f = 4.92%) for $K^+[Si(OCH_2CH_2O)_2OCH_2CH_2OH]^-$ indicates that the glycols form a nearly regular trigonal bipyramid, as is common for

penta-alkoxy silicates. The potassium is equidistant from its nearest neighbors, indicating that the complex is ionic in nature.

The most important feature of the glycolato silicates is that, unlike the triscatecholato silicate, the glycol groups are easily exchanged. The rate of exchange is sufficient to permit ready replacement of the glycol ligands with other diols. Thus, refluxing the potassium silicate in excess 1,2 propanediol, pinacol (2,3 dimethylbutane-2,3 diol) or catechol (with an equivalent of base) gives quantitative yields of the new diol complex. A related pinacolate was previously isolated by Holmes et al. The catechol exchange reaction provides a cleaner route to triscatecholato silicate than the original route which is hampered by the ready oxidation of free catechol anion. Also of interest is the fact that if 1,3 or larger "bite" diols (e.g. polyethylene glycols) are used in place of 1,2-diols, then it is possible to prepare ionic polymers containing penta-alkoxy silicate centers. In this instance, it is necessary to distill out the displaced glycol to force the reaction to go. Scheme III summarizes some of the reactions found to occur for $M_2[Si(OCH_2CH_2O)_2OCH_2CH_2OSi(OCH_2CH_2O)_2]$:

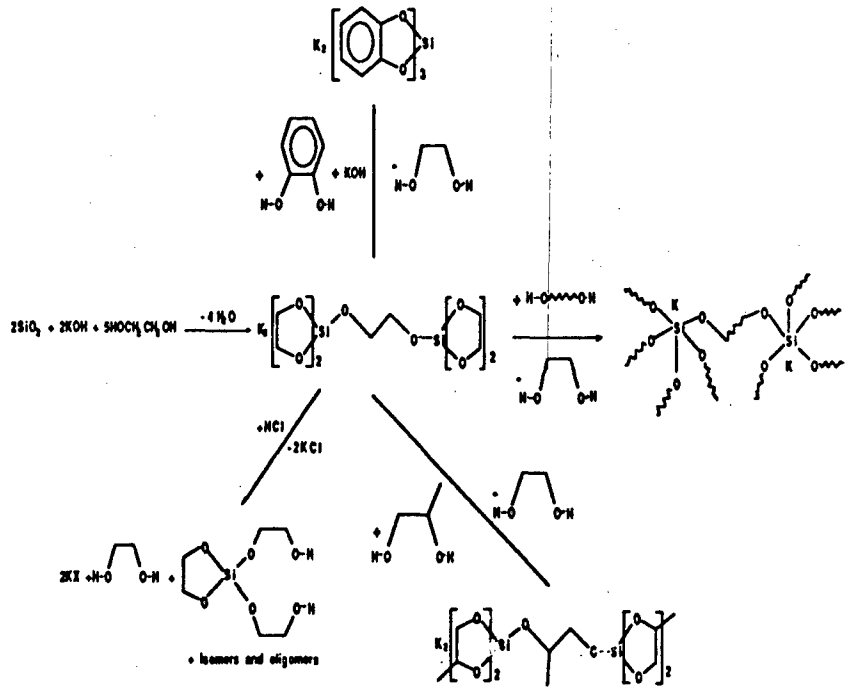

Scheme III

Penta-aryloxy Silicates

The reactions shown in Scheme III most likely represent only crude beginnings to what the authors hope will be a new, rich area of silicon chemistry. Indeed, the above results with penta-alkoxy silicates suggested that further attempts be made to elaborate triscatecholato silicate by using electrophiles instead of nucleophiles as chosen by Corriu et al[13-15].

To this end, we describe here two simple reactions of triscatecholato silicate with acetyl chloride and dry HCl. In the first case, we find that reaction of solvent free triscatecholato silicate with one equivalent of acetyl chloride in THF at temperatures below -40°C leads to a simple acetylation product as shown in Scheme IV. The structure of the monoacetylated material appears to be so sterically hindered that an attempt to displace the acetylated ligand with hydroquinone in refluxing THF

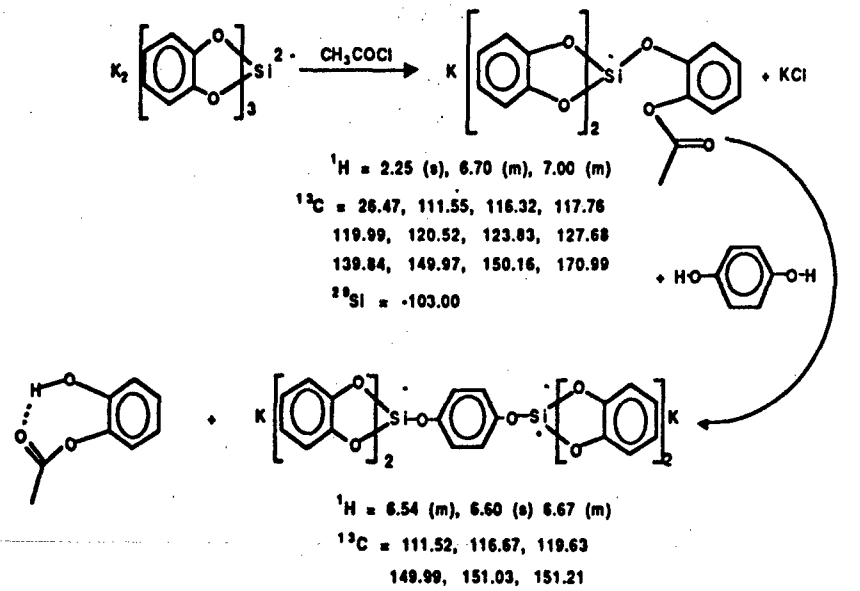

Scheme IV

was rewarded with the precipitation of the dimeric hydroquinone bridged species, I-K, shown above. Complex I-K is the penta-aryloxy analog of the glycolato complex. It is quite robust by comparison.

The bridging hydroquinone ligand is of interest because it may permit the anionic silicon centers to communicate electronically. Consequently, we sought an alternate synthetic route that might allow the preparation of a wide variety of penta-aryloxy silicates including unsymmetrical dimeric complexes with the intent of exploring

the electronic properties of pentacoordinate silicon centers. This interest led us to develop the dry HCl reaction shown in Scheme V:

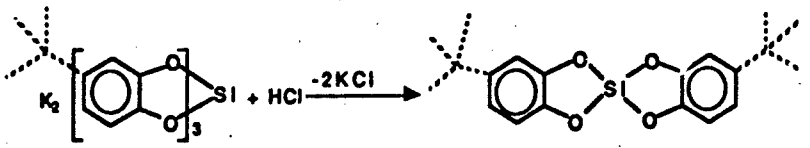

R = H, ^{1}H NMR = 6.89 br, 6.84m, 6.98m ppm

R = t-Bu, ^{1}H NMR = 1.15s, 1.28s, 6.89b ppm

R = H, ^{13}C NMR = 121.22, 123.71, 143.01 ppm

R = t-Bu, ^{13}C NMR = 32.54, 35.29, 114.21 ppm
116.23, 117.77, 144.52, 145.90

Scheme V

This reaction provides the biscatecholato silicon complex in approximately 30% unoptimized yield. As suggested in Scheme V, it can also be used to prepare the bis(4-t-butylcatecholato) silicate or spirosiloxane in essentially the same unoptimized yield. The pentane soluble bis(catechol) complex exhibits NMR and IR spectra identical to those reported by Allcock et al.[16] for the same complex prepared by reaction of catechol with $SiCl_4$.

We find that the bis complexes, when reacted with alkali hydroquinonates, provide a facile route to penta-aryloxy dimers:

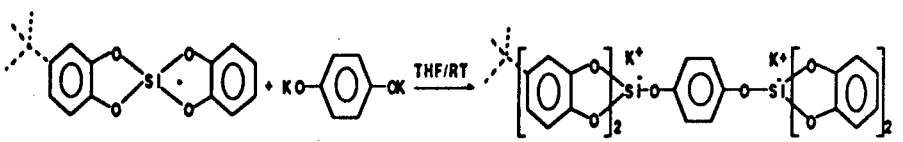

Scheme VI

In Scheme VI, the presence of the t-butyl group is meant to indicate that the reaction works well with that derivative; however, it should not be misconstrued to indicate that unsymmetrical complexes can be made. Efforts in this direction have been unsuccessful for a variety of reasons.

The reactions shown in Scheme VI also work when hydroquinone and pyridine are used in place of an alkali hydroquinonate. In this case the dimer forms with pyridinium, $C_5H_5NH^+$, counterions. Unlike I-K or I-Li, which are colorless, compound I-C_5H_5NH is yellow. Two other groups have observed the formation of yellow, pentacoordinate silicates where pyridinium counterions are used. Holmes et al [12] have described the crystal structure of yellow pyridinium phenylbis(1,2-naphthaquinonato) silicate shown on the next page and Flynn and Boer [17] have described the crystal structure of yellow dipyridinium triscatecholato silicate:

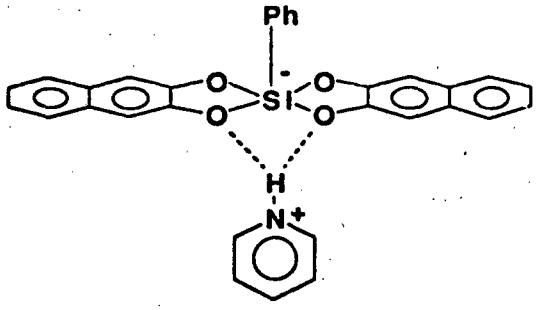

pyridinium phenylbis(1,2-naphthaquinonato) silicate

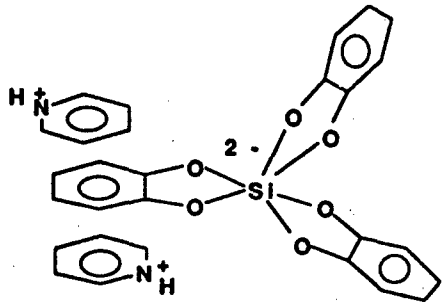

dipyridinium triscatecholato silicate

Flynn and Boer suggest that the yellow color arises as a consequence of charge transfer interactions between the pyridinium cations and the silicate anion. This observation suggested an opportunity to develop a series of organometallic compounds, with high dipole moments, potentially of value in the development of novel NLO materials. Because the Si-O bond (130 kcal/mol) is much stronger than a typical C-C bond (85-90 kcal/mol), the opportunity exists to develop silicon based materials that offer not only NLO properties but also exceptional stability to high laser fluences and the resultant temperatures[18].

Unfortunately, the Flynn and Boer crystal structure indicates that both pyridiniums stack above and below only one of the catecholate groups. This could suggest that any charge transfer transitions that exists may occur between a "masked" catechol dianion and the two pyridiniums cations rather than between a silicon dianion and the pyridinium complex. In contrast, the Holmes structure, wherein the pyridinium is hydrogen bound to two oxygens of two separate naphthoquinonate groups, does not seem to offer an opportune physical interaction that would readily permit charge transfer (CT) between the pyridinium and the naphthoquinonate groups. Indeed,the limited number of compounds studied provides insufficient proof to warrant discussion about whether or not C-T interactions are at

all involved.

The facilty with which the penta-aryloxy silicates can be synthesized, based on the reactions shown in Schemes IV-VI, provides the opportunity to verify the existence of silicon based CT interactions. This constitutes an additional motivation to develop the chemistry of penta-aryloxy silicates. Using the chemistries shown in Schemes IV-VI, as discussed in detail elsewhere. We have now prepared both the pyridinium ($C_5H_5NH^+$) and methyl-pyridinium ($C_5H_5NCH_3^+$) derivatives of **I** and the bis(4-t-butyl) hydroquinonate dimer, **II**. The $C_5H_5NCH_3^+$ derivatives were prepared by metathesis of the **I**-K and **II**-K compounds with $C_5H_5NCH_3^+I^-$.

Our initial work with these compounds has focussed on efforts to resolve the question of the origin of the visible aborption that results in the yellow coloration. One of the simplest tests that can be used to identify electronic transitions of CT origin is to explore the effects of changes in absorption energy and molar absorbance as a function of solvent polarity. It is well known that solvents with higher polarities will stabilize higher polarity CT excited states. The result will be a decrease in the energy required to populate the CT state. This corresponds to a decrease in λ max. Moreover, there will be a coincident increase in the molar absorbtivity. The converse may also be true. If CT occurs from a more polar ground state to a less polar excited state, the reverse solvent effect may be obtained.

We have determined the λ max and the molar extinction coeffient, ε for sets of **I** and **II** for two solvents, EtOH and $CHCl_3$ as recorded in Table 1. As a baseline, the UV-Vis data for both the N-methyl-pyridinium compound and **I**-K are listed.

The questions of whether or not these absorptions are: CT; π-π^*; localized on the pyridinium; localized on the catechol or hydroquinone ligands; associated with CT from "masked" catecholato (or hydroquinonate) anions to pyridinium or CT from silicate anions to pyridinium, must all be answered. Fortunately, most of these questions can be answered by inspection of the Table 1 results. For example, it can be seen that neither N-methylpyridinium iodide or **I**-K exhibit absorptions in the visible region. Thus, the visible absorptions that appear only when a pyridinium silicate complex is formed must be ascribed to an interaction between the two ions. Thus, localized π-π^* transitions can be ruled out.

The evidence then suggests a CT interaction. In complex **I**-$C_5H_5NCH_3^+$, λ max in EtOH is at ≈ 345 nm with a molar extinction coeffient $\varepsilon \approx 3200$. On changing solvent to $CHCl_3$, we find a significant red shift to a λ max ≈ 400 nm with a molar extinction coeffient $\varepsilon \approx 3500$. One typically finds that a shift to a less polar solvent should destabilize a more polar excited state in CT, which is exactly opposite to what is encountered here. This change can be readily explained by recalling that if the cation is more effectively solvated in EtOH than in $CHCl_3$, then its average distance from the anion will be greater. Moreover, the opportunity for effective electron transfer will be less. Therefore, in a more polar solvent more energy will be required to obtain charge transfer (shorter λ max) and the effi-

Compound	Solvent	λ_{max}	ε_{max} CT	λ_{max} π-π^*
		(nm)	(nm)	(nm)
$C_5H_5NCH_3^+ \cdot I^-$	EtOH	--	--	228 259 288
	$CHCl_3$	insoluble		
$I\text{-}K^+$	EtOH	--	--	240 276
	$CHCl_3$	insoluble		
$I\text{-}C_5H_5NCH_3^+$	EtOH	345	3200	231 256 284
	$CHCl_3$	400	3500	256 266 305
$II\text{-}C_5H_5NCH_3^+$	EtOH	Hidden in π-π^* transitions		231 258 284
	$CHCl_3$	361	920	249 286
$C_5H_5NCH_3^+$ Glycolate	EtOH	343	1300	257 290
	$CHCl_3$	375	4300	248 306

Table 1. Solvato-Chromatic Shifts of Selected Penta-aryloxy Silicates and Methylpyridinium Glycolato Silicate.

ciency will be less (lower ε). This is what is seen on moving from EtOH to $CHCl_3$; un less, we are destabilizing the ground state with respect to the excited state.

The $II\text{-}C_5H_5NCH_3^+$ data are not what could be expeced based on the $I\text{-}C_5H_5NCH_3^+$ results. For $II\text{-}C_5H_5NCH_3^+$; λ max in EtOH is < 300 nm and in $CHCl_3$ λ

max is ≈ 361 nm with a molar extinction coeffient ε ≈ 920 in. These results provide further evidence for CT. They also hold for our above explanation, but only if the presence of the very bulky t-butyl groups prevent close contact (and good overlap) of the pyridinium ion with the silicon center. This last point emphasizes the most important question. Is the apparent CT, a transfer of electron density from silicate to pyridinium or from anionic -like catechol (or hydroquinone) to pyridinium.

The true test of this difference was to make the glycolato N-methylpyridinium complex. In this species there no aryloxy groups are bound to the anionic silicate center. Metathesis of $C_5H_5NCH_3^+I^-$ with $K_2[Si(OCH_2CH_2O)_2OCH_2CH_2OSi^-(OCH_2CH_2O)_2]$ provides the N-methylpyridinium glycolate. As can be seen at the bottom of Table 1 and in Figure I, for this compound in EtOH λ max ≈ 343 nm with ε ≈ 1300. On changing solvent to $CHCl_3$ we again find a significant red shift to a λ max ≈ 375 nm with a molar extinction coeffient ε ≈ 4300.

Thus, CT must occur between the anionic silicon center and the pyridinium π system. Indeed, in both $I\text{-}C_5H_5NCH_3^+$ and N-methylpyridinium glycolate, the lowest energy π-π* band in the pyridinium undergoes a red shift to ≈ 305 nm from 286 nm. This indicates an increase in electron density corresponding to a partial transfer of charge.

The shifts in λ max for both $I\text{-}C_5H_5NCH_3^+$ and N-methylpyridinium glycolate on changing from polar EtOH to $CHCl_3$ offer significant potential for NLO activity providing the correct conditions (e.g. non-centrosymmetric space group for χ^2) can be met. These properties are currently being evaluated.

In conclusion, the chemistries of hypervalent Si appear to offer tremendous opportunities for the development of new materials and new challenges for the synthetic chemist.

Acknowledgements

We would like to thank the Office of Naval Research for generous support of the penta-alkoxy studies through ONR Contract No. NOOO14-88-K-0305. and the Air Force Office of Scientific Research for generous support of the penta-aryloxy work through AFOSR Contract No. F49620-89-C-0059.. We would also like to thank Professors R. J. P. Corriu and P. Knochel for very useful discussions and suggestions. We thank Professor Barry Posin for early contributions to these studies.

References

1. D. Seyferth, D. C. Annarelli, J. Am. Chem. Soc. (1975) **97**, 7162.
2. W. Ando, M. Fujita, H. Yoshida, A. Sekiguchi, J. Am. Chem. Soc. (1988) **110**, 3310.
3. D.-H. Pae, M. Xiao, M. Y. Chiang, and P. P. Gaspar, J. Am. Chem. Soc. (1991) **113**, 1281. and references therein.
4. B. T. Colegrove and H. F. Schaefer III, J. Am. Chem. Soc. (1991) **113**, 1557.
5. A. Rosenheim, B. Raibmann, and J. Schemdel, Z. Anorg. Allgem. Chem. (1931) **196**, 160.
6. D. Kummer, K-E. Gaisser and T. Seshadri, Chem. Ber. (1977) **110**, 1951.
7. C. L. Frye, J. Org. Chem.(1969) **34**, 2496.
8. C. L. Frye, J. Am. Chem. Soc. (1970) **92**, 1205.
9. K. C. K. Swamy, V. Chandrasekhar, J. J. Harland, J. M. Holmes, R. O. Day, and R. R. Holmes, J. Am. Chem. Soc. (1990) **112**, 2341.
10. R. R. Holmes, R. O. Day, and J. S. Payne, Phos., Sulfur and Silicon (1989) **42**, 1.
11. S. N. Tandura, M. G. Voronkov, and N. V. Alekseev, Top. Curr. Chem., (1986) **131**, 99.
12. R. R. Holmes, R. O. Day, J. J. Harland, A. C. Sau, and J. M. Holmes, Organomet. (1984) **3**, 347.
13. A. Boudin, G. Cerveau, C. Chuit, R. J. P. Corriu and C. Reye, Organomet. (1988) **7**, 1165.
14. R. J. P. Corriu, Pure and Appl. Chem. (1988) **60**, 99.
15. R. Corriu, C. Guérin, B. Henner, and Q. Wang, J. Orgmet. Chem. (1989) **365**, C7.
16. H. R. Allcock, T. A. Nugent, and L. A. Smeltz, Syn. Inorg. and Metal-Org. Chem. (1972) **2**, 97
17. J. J. Flyn and F. P.Boer, J. Am. Chem. (1969) **91**, 5756.
18. see for example, J. A. Bandy, H. E. Bunting, M. H. Garcia, M. L. H. Green, S. R. Marder, and M. E. Thomson, "Special Publication of the Royal Society of Chemistry (1989) **69**, 225 and references therein.

APPENDIX 4

US005099052A

United States Patent [19]

Laine et al.

[11] Patent Number: 5,099,052

[45] Date of Patent: Mar. 24, 1992

[54] SILICON AND ALUMINUM COMPLEXES

[75] Inventors: Richard M. Laine, Seattle; Kay A. Youngdahl, Issaquah; Paola Nardi, Seattle, all of Wash.

[73] Assignee: Washington Research Foundation, Seattle, Wash.

[21] Appl. No.: 509,022

[22] Filed: Apr. 13, 1990

[51] Int. Cl.[5] C07F 7/18; C07F 7/04

[52] U.S. Cl. 556/443; 556/464; 556/482; 546/14; 544/181; 544/229; 549/4; 549/6

[58] Field of Search 556/443, 464, 482; 546/14; 544/229, 181; 549/4, 6

[56] References Cited

U.S. PATENT DOCUMENTS

3,455,980	7/1969	Frye	260/448.8
4,447,628	5/1984	Farnham	556/415
4,577,003	3/1986	Farnham	556/464
4,632,967	12/1986	Farnham	526/194

OTHER PUBLICATIONS

Perozzi et al., J. Am. Chem. Soc., vol. 106, pp. 1591-1593 (1979).

Farnham et al., J. Am. Chem. Soc., vol. 103, pp. 4608-4610 (1981).

Frye et al., J. Am. Chem. Soc., vol. 93, No. 25, pp. 6805-6811 (1971).

Cecil L. Frye, J. Am. Chem. Soc., vol. 92, No. 2, pp. 1205-1210 (1970).

Youngdahl, K. A. and R. M. Laine, "Synthesis of Soluble Siliconates and Siloxanes from Silica" (abstract No. 421), Spring Newsletter, Jan. 1989, Division of Inorganic Chemistry, American Chemical Society.

Holmes, R. R. et al., "Cyclic Pentaoxy Siliconates", *Phosphorus, Sulfur, and Silicon*, 1989, vol. 42, pp. 1-13.

Boudin, A. et al., "Reaction of Grignard Reagents with Dianionic Hexacoordinated Silicon Complexes: Organosilicon Compounds from Silica Gel", *Angew. Chem. Int. Ed. Engl.* 25 (1986) No. 5.

03 above in German.

Barnum, D. W., "Reaction of Catechol with Colloidal Silica and Silicic Acid in Aqueous Ammonium", *Inorganic Chemistry*, vol. 11, No. 6, 1972.

Primary Examiner—Jose G. Dees

Assistant Examiner—Porfirio Nazario

Attorney, Agent, or Firm—Christensen, O'Connor, Johnson & Kindness

[57] ABSTRACT

Silicon and aluminum complexes having the following formula:

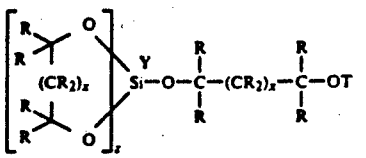

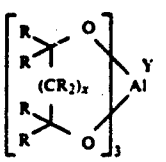

wherein x is 0 or 1, T is H or

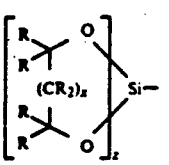

each R is independently selected from the group consisting of H, OH, C_{1-6} alkyl, C_{1-6} alkoxy, C_{2-6} alkene, C_{6-12} aryl, C_{1-6} hydroxyalkyl, C_{1-6} thioalkyl, C_{2-12} alkoxyalkyl, C_{3-20} heteroaromatic, and combinations thereof, wherein R may further contain one or more atoms of a non-carbon element such as Si, Ge, Sn, P, and the like; and Y is a cation, are prepared by reacting silica or alumina with a diol, in the presence of a base, while removing water formed during the reaction. Methods for producing such complexes starting with silica or alumina, and methods for converting such complexes into other silicon or aluminum-containing compounds, are disclosed.

7 Claims, No Drawings

SILICON AND ALUMINUM COMPLEXES

This invention was made in part with Government support under Contract N00014-88K-0305 awarded by the Department of the Navy and F49620-89-C-0059 awarded by the Department of the Air Force. The Government has certain rights in this invention.

FIELD OF THE INVENTION

The present invention relates to complexes containing at least one silicon or aluminum atom, to the preparation of such complexes starting with silica or alumina (in various chemical and mineral forms), and to the use of these complexes to prepare other silicon or aluminum-containing compounds.

BACKGROUND OF THE INVENTION

Silicon-based chemicals are used in a wide variety of applications, such as in biocides, stain- and dirt-resistant polymers for carpets, advanced ceramics for aerospace applications and electronic components. The market for silica and other silicon-containing materials amounts to several billion dollars per year.

One important aspect of this market, not immediately evident even to a first-hand observer, is the fact that all silicon-based materials beyond sand are produced by primitive ceramics processing technologies that: (1) add considerable cost to the typical product: (2) limit the scope of applications, and (3) offer limited opportunity for growth because of the maturity of the process.

Silicon products may be derived from the carbothermal reduction of silica to silicon metal:

$$SiO_2 + 2C \xrightarrow{\sim 1200^\circ C} Si + CO + CO_2 \quad (1)$$

The resulting metallurgical grade silicon (90–98% purity) must then undergo further processing to make other products. For example, to make many of the industrially useful (high purity) forms of silica (e.g., fumed or electronics grade silica), it is necessary to first react the Si metal produced in reaction (1) with Cl_2 or HCl to make $SiCl_4$ which can then be burned (e.g., reaction 4):

$$Si + 2Cl_2 \rightarrow SiCl_4 \quad (2)$$

$$Si + HCl \rightarrow HSiCl_3 + SiCl_4 \quad (3)$$

$$SiCl_4 + H_2O + O_2 \rightarrow SiO_2 + HCl + HClO_x \quad (4)$$

Carbothermal reduction requires high heat and specialized equipment. The result is an energy and equipment intensive process. Reaction of silicon with chlorine or HCl also requires specialized, expensive equipment to deal with toxic and corrosive materials. Despite these considerable drawbacks, because the basic technology was developed late in the last century and early in this century, all of the processing problems have been worked out. This, coupled with economies of scale, makes this approach to the production of fumed and electronics grade silica commercially successful.

Similar problems pervade the alumina and aluminum chemicals technologies. Indeed, these technologies are even more expensive and complex because of the need to electrolytically reduce molten alumina/cryolite melts to form aluminum, the source of most aluminum chemicals and many aluminum containing ceramics.

The production of silicon-based chemicals follows somewhat similar chemistry. Most silicone polymers derive from the "Direct Process":

$$RCl + Si \xrightarrow{Cu/Zn/250\text{-}500^\circ C} RSiCl_3 + R_2SiCl_2 + R_3SiCl + \ldots \quad (5)$$

This simple reaction only works well when RCl is MeCl or PhCl. When it is MeCl, the major product is Me_2SiCl_2, which is hydrolyzed and polymerized to give polydimethylsiloxane, the basic silicone polymer:

$$Me_2SiCl_2 + H_2O \rightarrow [Me_2SiO]_n + HO-[Me_2SiO]_x-H \quad (6)$$

low MW oligomers

wherein n is 3-5 and $x < 100$

$$[Me_2SiO]_{3,4} \xrightarrow{Me_3SiOK} Me_3SiO-[Me_2SiO]_m-H \quad (7)$$

The above reactions, when coupled with standard organic chemistry reactions, some special derivatives and processing procedures, provide the basis for the major portion of the silicone and silicon chemicals industry. It is surprising that there are few, if any, alternate methods for producing silicon-based polymers. If there were, and these new methods provided commercially competitive materials even a fraction as successful as the silicone polymers, the rewards would be exceptional. Preferably, these new methods should also involve an inexpensive and readily available starting material. In view of this, silica is an attractive starting material for producing silicon-containing species, such as those described above.

Silica, SiO_2, is the most common material found in nature. As sand, it is a basic ingredient in building materials, the manufacture of low-tech glass products and ceramics. In purer forms, it is used as an abrasive (e.g., toothpaste) and as a drying and texturizing agent in food and food-related products. It is also used in the manufacture of electronic materials and optical products.

Silica is a feedstock material used for the manufacture of silicon-based chemicals. Synthetic routes stemming from the use of silica gel offer the important attribute of being very inexpensive (research grade silica sells for ~$15/kg or less). Additionally, silica gel is very easy to handle due to its relative nonreactivity. Industrial fused silica sells for less than $1/kg, and can be used here.

On the other hand, because of its low reactivity, there are few simple, low-temperature methods of chemically modifying silica. One such method is dissolution in base to give sodium silicate:

$$NaOH + SiO_2 \rightarrow Na_4SiO_4 \quad (8)$$

Unfortunately, this reaction has limited application for the formation of useful feedstock chemicals. The recent work of Kenny and Goodwin [*Inorganic and Organometallic Polymers*, N. Zeldin et al., ACS Symposium Series 360,238, (1987)] on silicic acid esterification provides one successful transformation:

$$Na_4SiO_4 + HCl \longrightarrow NaCl + "Si(OH)_4" \quad (9)$$

$$"Si(OH)_4" + EtOH \xrightarrow[\text{azeotrope}]{\text{toluene}} H_2O + Si(OEt)_4 \quad (10)$$

$Si(OEt)_4$, currently produced by reaction of EtOH with $SiCl_4$, reaction (11), is used commercially to form fumed and electronics grade silica.

$$SiCl_4 + EtOH \xrightarrow[\text{azeotrope}]{\text{toluene}} 4HCl + Si(OEt)_4 \quad (11)$$

It is also used to form optical glasses and boules for spinning fiber optics.

It has been reported that soluble complexes of silicon can be prepared from silica gel and catechol in water. These reports teach that the reactions of silica with 1,2 aromatic diols lead to the formation of hexacoordinate, monomeric silicon complexes:

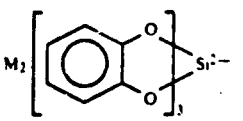

M = Na, K, etc.

This approach was modified and refined by Corriu and co-workers by using basic methanol solutions under anhydrous conditions. A. Boudin, et. al., *Angew. Chem. Int. Ed. Engl*, 25 (5):474–475 (1986). These stable salts could then be alklyated by strong nucleophiles, such as Grignard reagents, to form three (and frequently four) new silicon-carbon bonds:

$$K_2Si(OC_6H_4O)_3 + 3\ EtMgBr \longrightarrow \xrightarrow{H_3O^+} \quad (12)$$

$Et_3SiOC_6H_4(OH)$

The problem with this approach is that the catechol complex, tris(1,2-dihydroxobenzoato) siliconate, is relatively expensive and can only be modified under forcing conditions using expensive reagents such as $LiAlH_4$, RMgBr, or RLi and the products are limited to tri or tetrasubstituted silicon. Consequently, its large scale utility is limited. Furthermore, formation of mono-and dialkyl derivatives was not possible.

The invention described herein resulted from an exploration into methods of making more reactive complexes of silica using aliphatic 1,2 or 1,3 diols, such as ethylene glycol, instead of catechol. Thus, one aspect of the present invention described in greater detail hereinbelow, involves certail novel silicon complexes that may be formed by a reaction between silica and 1,2 or 1,3 aliphatic diols. These complexes have been determined to contain one or more anionic pentacoordinate silicon atoms.

Previously, pentacoordinate silicon species have been reported. For example, U.S. Pat. No. 3,455,980 discloses pentacoordinate silicon complexes of vicinal aliphatic diols, including ethylene glycol. The disclosure in this patent differs from the present invention, however, in that these prior complexes were not formed from silica but, rather, from a compound of the formula $(R'O)_4Si$ in the presence of excess aliphatic diol and an amine. Also, the structures of the pentacoordinate silicon species disclosed in this patent are different from the structures of those disclosed herein.

U.S. Pat. Nos. 4,632,967, 4,577,003, and 4,447,628 are also directed to pentacoordinate silicates, all of which have structures that are different from those of the present invention.

Generally, the prior art has taught that only monomeric, pentacoordinate silicon complexes derive from monomeric tetracoordinate silicon complexes and only dimeric complexes from dimeric starting materials (always bridged by polyalkyl siloxanes). This is despite forming monomeric pentacoordinate silicon under conditions where sufficient diol is added to form dimeric species.

In an article entitled "Pentacoordinate Silicon Derivatives. IV.[1] Alkyl-ammonium Siliconate Salts Derived from Aliphatic 1,2-Diols" [C. L. Frye, *J. Am. Chem. Soc.* 92:5, 1204–1210 (1970)], there are disclosed silicon-based compounds that are similar to, but structurally different from, those of the present invention.

Some additional publications that may be relevant to the background of the present invention are the following: "Cyclic Pentaoxy Siliconates," R. R. Holmes et al., *Phosphorus Sulfur and Silicon and the Related Elements* 42:1-13 (1989); "Reaction of Grignard Reagents With Dianionic Hexacoordinated Silicon Complexes: Organosilicon Compounds from Silica Gel," A. Boudin, et. al., *Angew. Chem. Int. Ed. Engl*, 25 (5):474–475 (1986); "Reaction of Catechol with Colloidal Silica and Silicic Acid in Aqueous Ammonia," D. W. Barnum, *Inorganic Chemistry* 11 (6):1424–1429 (1972); and "Pentacoordinate Silicon Compounds. V.[1a] Novel Silatrane Chemistry," C. L. Frye, et al., *J. Am. Chem. Soc.* 93(25):6805–6811 (1971).

In spite of previous work involving functionalization of silica and other work involving preparation of pentacoordinate silicon complexes, there has remained a need for new and improved ways of producing useful silicon compounds. The present invention provides novel pentacoordinate silicon complexes, methods of preparing them from silica, and processes for converting silica into a variety of useful silicon compounds via these complexes.

In a similar fashion, we find that alumina (Al_2O_3) can also be converted to soluble chemical complexes by reaction with base in the presence of diols.

SUMMARY OF THE INVENTION

An object of the present invention is to enable preparation of useful silicon-containing compounds using silica as a starting material.

It is another object of the present invention to obtain silicon-containing compounds that may be further reacted to produce a variety of useful silicon compounds.

It is yet another object of the present invention to provide a method for making soluble silicon products starting with silica and using simple and inexpensive reactions.

It is yet another object of the invention to demonstrate that this approach can be applied to another metal oxide, alumina.

The above and other objects of the present invention, as will hereinafter become more readily apparent, have been achieved by the discovery that silica or aluminum can be made to react with aliphatic diols in the presence

of a base and with removal of water during the reaction, to produce pentacoordinate silicon complexes or aluminum complexes. These complexes may be relatively easily functionalized by way of further chemical reactions to produce a variety of valuable silicon and aluminum containing compounds. Through purification and hydrolysis, these compounds can be used directly to form high purity silica or alumina. Alternatively, when heated they can serve as precursors to a wide variety of glasses and ceramics.

The initial product of the reaction between the aliphatic glycol and silica or alumina may also be transformed into other products by way of ligand exchange reactions employing different ligands or cation exchange reactions employing different cations.

In general, the reactions of the present invention to produce silicon or aluminum complexes may be depicted as shown in the following scheme:

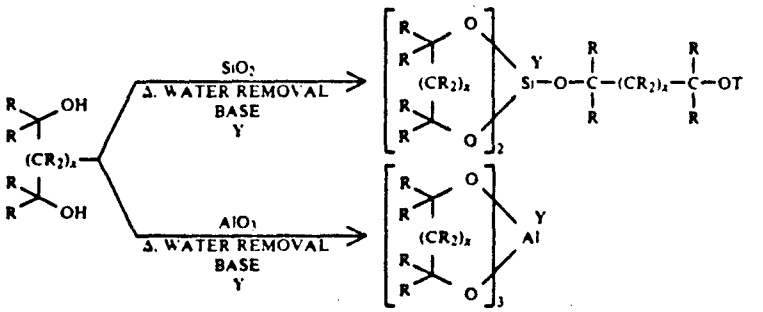

wherein x is 0 or 1, each R is independently selected from H, OH, C_{1-6} alkyl, O-C_{1-6} alkyl, C_{2-6} alkene, C_{6-12} aryl, C_{1-6} hydroxyalkyl, C_{1-6} thioalkyl, C_{2-12} alkoxyalkyl, C_{3-20} heteroaromatic, and combinations thereof, wherein the R groups may also contain other, non-carbon elements such as Si, Sn, Ge, P, and the like; T is H or

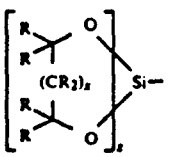

Y is cationic, most commonly mono or dicationic, but can be a cation of higher charge that binds dimers together to form clusters.

The product of the above reaction is a monomeric (T=H) or dimeric (T=other than H) silicon complex or an aluminum complex. As noted above, the product may subsequently be reacted with another ligand or another cationic species to result in a ligand or cation exchanged product. The product of the above reaction may also be converted into other useful silicon or aluminum-containing compounds or ceramics, e.g., via standard methodologies.

DETAILED DESCRIPTION OF THE INVENTION

The present invention is based on a discovery that silica or alumina can be converted into silicon or aluminum complexes under relatively mild reaction conditions by causing the silica or alumina to react with an aliphatic diol in the presence of a base, while removing water that is formed during the reaction. The reaction produces silicon complexes or aluminum complexes, often in high yield.

The following scheme depicts an exemplary reaction starting with silica to form a complex of the present invention and several secondary reactions that lead to a variety of useful silicon-containing products:

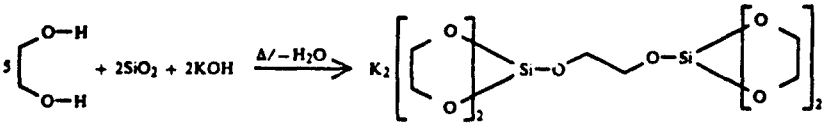

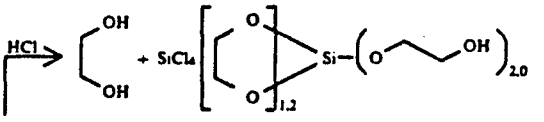

-continued

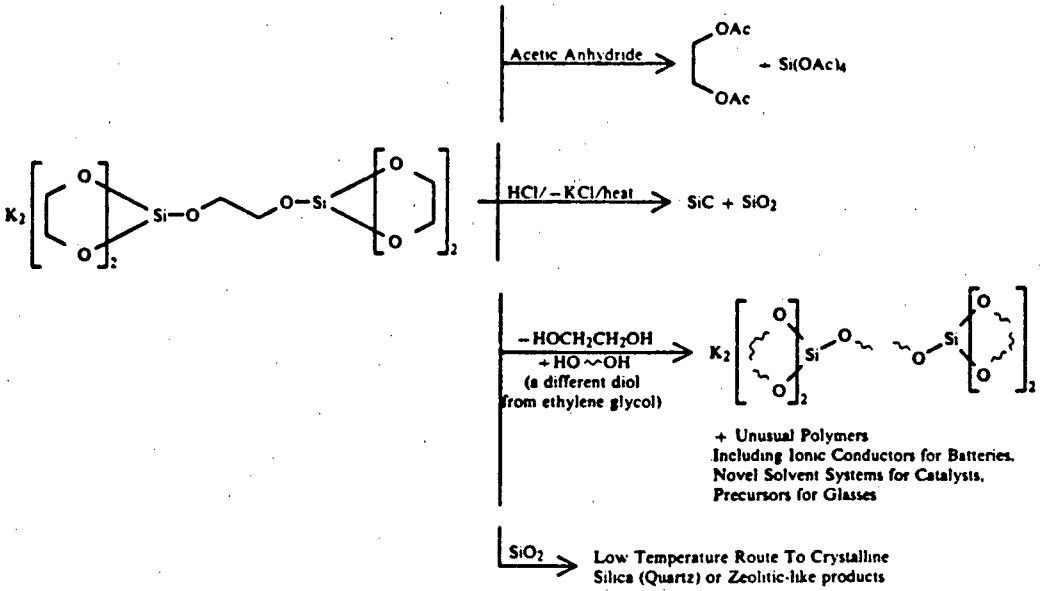

The starting materials, an aliphatic glycol, silica or alumina, and a base, may be obtained from commercial sources, such as the Sigma Chemical Company and the Aldrich Chemical Company, or may be synthesized using available starting materials and known reactions.

Generally speaking, a molar excess of an aliphatic diol is added to silica or alumina and a base, a suitable solvent is added, and the mixture is allowed to react. It is possible to run the reaction in excess reactant as solvent. The molar ratio of diol:silica:base is typically 3-5:1-3:1-3 and of diol:alumina:base it is typically 3-7:-1-3:3-9.

The base used in the reaction is most preferably an alkali metal hydroxide or oxide, such as lithium hydroxide, sodium hydroxide, potassium hydroxide, or cesium hydroxide. The base will generally provide the cation, Y, in the final product.

In general, the cation that is present in the final product is relatively unimportant in the context of the present invention. As far as the inventors are aware, there are no specific requirements to be imposed on the cation, and a chemist will readily be able to select any of a variety of cations that will work for purposes of the present invention. However, many transition metal cations will be reduced if conditions are not suitable and care in choice of reaction conditions should be exercised with this in mind. It is preferred that the cation be derived from an alkali metal or alkaline earth metal, but it may also be derived from other chemical species.

An example of another chemical species that may serve as a cation in the silicon complexes is a quaternary salt. Suitable quaternary salts have the general structure:

$$R'_4EX$$

wherein E is N, P, or Sb; each R' is independently C_{1-4} alkyl, and X is an anion such as hydroxide or some species that generates OH^- on reaction with water.

Exemplary divalent cations are: Mg^{2+}, Ca^{2+}, Ba^{2+}, Ni^{2+}, and Co^{2+}.

The diol that is employed may be any one having the formula:

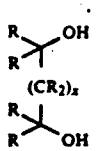

wherein x is 0 or 1, and each R is independently selected from H, OH, C_{1-6} alkyl, C_{1-6} alkoxy, C_{2-6} alkene, C_{6-12} aryl, C_{1-6} hydroxyalkyl, C_{1-6} thioalkyl, C_{2-12} alkoxyalkyl, C_{3-20} heteroaromatic, and combinations thereof, wherein R may have one or more (preferably 1-3) non-carbon elements, such as Si, Sn, Ge, and P.

The alkyl moieties may be straight chain, branched, and/or cyclic. Exemplary nonlimiting alkyl moieties are: methyl, ethyl, propyl, i-propyl, cyclopentyl, 2-methylbutyl, and the like.

The alkene moieties may be straight chain, branched and/or cyclic. Nonlimiting examples are the mono, di, and polyunsaturated analogues (where possible) of the above-listed alkyl groups having greater than two carbon atoms.

The aryl groups are generally aromatic hydrocarbon moieties that have 6 to 12 carbon atoms. The aryl groups may be attached directly to the diol or be attached by way of an intervening alkyl moiety. Nonlimiting examples of the aryl groups are: benzyl, phenyl, and the like.

The hydroxyalkyl groups may be any straight chain, branched, and/or cyclic C_{1-6} alkyl group substituted with one or more (preferably 1-3) hydroxyl groups. Nonlimiting examples are 1-hydroxyethyl, 2-hydroxyethyl, 1-hydroxypropyl, and the like.

The thioalkyl groups may be any straight chain, branched, and/or cyclic C_{1-6} alkyl attached to the diol by way of a sulfur atom. Nonlimiting examples are any of the alkyl moieties described above attached by a sulfur atom to the diol.

The alkoxyalkyl groups may be any ether moiety containing 2 to 12 carbon atoms. Nonlimiting examples are methoxymethyl, ethoxymethyl, methoxyethyl, and the like.

The heteroaromatic groups may be any C_{3-20} group (preferably C_{3-8}) containing one or more (preferably 1 or 2) heteroatoms (preferably O, N, and/or S). Nonlimiting examples are groups derived from pyridine, thiophene, pyrazine, triazine, etc.

Preferably, the diol is unsubstituted or is independently substituted by 1-3 nonhydrogen substituents. Also, the preferred substituents are C_{1-6} alkyl or C_{2-6} alkenyl. Further, the substituents are preferably located on different carbon atoms of the complex.

Some combinations of substituents will not be desirable due to incompatibility, steric crowding, and/or instability under reaction conditions. One of oridinary skill will be able to determine these combinations based on standard synthetic considerations and/or routine experimentation.

Optically active diols are also contemplated; these diols may be resolved before use in the reaction, or may be used as a mixture of racemates. Similarly, the final products formed by using a diol with an optically carbon atom may be resolved during purification or may be used as a mixture of stereoisomers.

Vicinal diols are preferred as the diols herein. However, under some circumstances, the hydroxyl groups may have a 1, 3 orientation on the diol, depending upon the flexibility of the diol ligand, etc.

Any grade or form of silica may be employed in the reactions. A preferred silica is 10–400 mesh with minimal organic impurities. However, each beach sand can be used.

Any grade or form of alumina may be used in the reaction. A preferred alumina is 10–400 mesh.

The basic reaction starting with silica or alumina that is described above may be conducted in a variety of solvents. Preferred solvents are higher boiling alcohols such as ethylene glycol, 2-aminoethanol, amyl alcohol, 2-ethoxyethanol, and the like. However, other solvents are also possible, such as DMSO, sulfolane, N-methyl pyrrolidone.

The reaction will generally be conducted at from ambient temperature to higher temperatures. Conveniently, the reaction may be conducted at the boiling point of the solvent that is employed. For most purposes, the upper limit of the temperature range will be approximately 200° C. Preferably, the temperature range will be from about 30°-170° C. Most preferably, the temperature will range from about 80° C. to 150° C.

It is important that substantially all water that is formed during the reaction be removed as it is formed. It has been found that it the water is not removed, the products described herein are not obtained, as shown by Example 9, below. Conveniently, the water may be removed by azeotropic distillation; the precise temperature at which water can be azeotropically removed will depend upon the solvents which are used and other conditions, as will be readily understood by a synthetic chemist. The water may also be removed by known water-scavenging species or by any standard membrane transport protocol.

The reaction will typically be carried out for a time period of from a few minutes (e.g., twenty minutes) up to 2–4 days, as necessary.

The final product will often separate out of the reaction mixture as a precipitat on cooling; however, it may also remain dissolved in the reaction mixture and must be precipitated by addition of a nonsolvent such as acetonitrile. The product may be isolated and purified by any of a variety of standard methodologies. For example, the product may be taken up in a solvent, filtered, concentrated, and then crystallized. The crystallized product may then be recrystallized from a suitable solvent system. In some situations, it may be necessary to carry out column chromatography or another purification procedure to aid in the purification of the desired product.

In a preferred embodiment, ethylene glycol is reacted with silica in the presence of an alkali metal hydroxide or oxide to produce a dimeric pentacoordinate silicon complex, as depicted below:

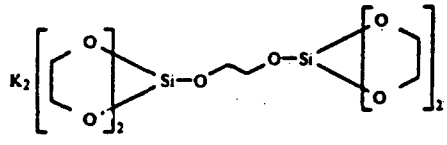

Other preferred reactants, etc., are summarized in the following Table:

Diol	Base	Solvent	Reaction Temp (°C.)	Product
1,2-ethanediol	MOH M = Li, Na, K, Cs	$HOCH_2CH_2OH$	100-200	$K_2Si_2(OCH_2CH_2O)_5$
1,2-ethanediol	$M(OH)_2$ M = Mg, Ca, Sr, Ba	$HOCH_2CH_2OH$	100-200	$MSi_2(OCH_2CH_2O)_5$
1,2-ethanediol	$Ca(OH)_2$	$H_2NCH_2CH_2OH$	100-200	$CaSi_2(OCH_2CH_2O)_5$
1,2-ethanediol	$Ca(OH)_2$	$HSCH_2CH_2OH$	100-200	$CaSi_2(OCH_2CH_2O)_5$
1,2-ethanediol	$Ca(OH)_2$	Eu—OCH_2CH_2OH	100-200	$CaSi_2(OCH_2CH_2O)_5$
1,2-ethanediol	$Ca(OH)_2$	$H(OCH_2CH_2)_2OH$	100-200	$CaSi_2(OCH_2CH_2O)_5$
1,2-ethanediol	$Ca(OH)_2$	$HN(CH_2CH_2OH)_2$	100-200	$CaSi_2(OCH_2CH_2O)_5$
1,2-ethanediol	$Ca(OH)_2$	$O(CH_2CH_2OH)_2$	100-200	$CaSi_2(OCH_2CH_2O)_5$
Pinacol	MOH M = Li, Na, K, Cs	$HOCH_2CH_2OH$	100-200	$M_2Si_2(OCMe_2CMe_2O)_5$
Glycerol	MOH M = Li, Na, K, Cs	$HOCH_2CH_2OH$	100-200	$M_2Si_2(OCH_2CH(CH_2OH)O)_5$
1,2-propanediol	MOH M = Li, Na, K, Cs	$HOCH_2CH_2OH$	100-200	$M_2Si_2(OCH_2CH(CH_3)O)_5$

-continued

Diol	Base	Solvent	Reaction Temp (°C.)	Product
1,3-propanediol	MOH M = Li, Na, K, Cs	$HOCH_2CH_2OH$	100–200	$M_2Si_2(OCH_2CH_2CH_2O)_5$
1-amino-2,3 propanediol	MOH M = Li, Na, K, Cs	$HOCH_2CH_2OH$	100–200	$M_2Si_2((OCH_2CH(CH_2NH_2)O)_5$
cyclohexane (Cyc) 1,2-diol	$Ca(OH)_2$	$HOCH_2CH_2OH$	100–200	$CaSi_2[1,2\text{-}(O)_2Cyc]_5$
1,2-diphenyl-ethane 1,2-diol (dip)	$Ca(OH)_2$	$HOCH_2CH_2OH$	100–200	$CaSi_2[1,2\text{-}(O)_2Dip]_5$

Additional details on the basic reaction parameters as applied to specific reactants are provided in the Examples section hereinbelow.

After the product is formed in the above reaction, it may either be purified as described above or may be converted in situ into other products, as desired. The silicon or aluminum complexes may be treated with a variety of reactants, including HCl, acetic anhydride, acetyl chloride, additional silica or alumina, and the like. These treatments will produce, in a staightforward manner, various functionalized aluminum- or silicon-containing species. Examples of silicon species that may be obtained in this manner are: $Si(OCH_2CH_2O)_2$, $SiCl_4$, $Si(OAC)_4$, SiC (produced by heating), crystalline silicon containing species (e.g., quartz), zeolitic-like products, neutral silicon-containing polymers, and the like. Examples of aluminum species are alkaline earth aluminate glasses and ceramics, etc.

The ionic polymers produced by exchange, e.g., Example 6, can be used as coatable ion conductors for making clear electrodes for electronic displays, nonlinear optical applications and for battery applications.

In addition to the above-described reactions starting with the silicon and aluminum complexes, exchange reactions may also be carried out. In a ligand exchange reaction, the complex is treated with an excess amount of a ligand that is different from the diol used to form the complex. During the reaction, the new ligand will take the place of the originally used diol in the complex.

Alternatively or concurrently, the silicon or aluminum complex may be subjected to a cation exchange reaction by contacting the complex with an excess amount of a cationic species that is different from the starting cationic species. For example, if potassium hydroxide were used in the initial reaction, producing a potassium salt of a pentacoordinate silicon complex, an exchange reaction with an ammonium salt could be used to substitute an ammonium cation for the potassium cation. However, care should be taken in carrying out such a reaction to avoid conditions, particularly acid conditions, in which the cyclic dioxy moiety in the complex is cleaved. Examples of exchange reactions are also described in the Examples section below.

Analogous processes and approaches can be used when Al_2O_3 rather than silica is used as the metal oxide reactant.

The invention now being generally described, the same will be better understood by reference to certain specific examples which are included herein for illustrative purposes only, and are not intended to be limiting of the present invention.

EXAMPLES

A. General

1. Procedures

All operations were carried out with the careful exclusion of extraneous moisture. Air-sensitive materials were manipulated using standard Schlenk and glovebox techniques. ^1H, ^{13}C and ^{29}Si spectra NMR spectra were taken in CD_3OD and referenced to TMS. All chemicals were purchased from standard vendors and used as received, except the diols, which were distilled under nitrogen before use.

2. Equipment

Infrared spectra were recorded on an IBM FTIR-44 spectrophotometer. Nuclear magnetic resonance data were collected on a Varian 300 MHz spectrometer. Elemental analyses were performed by Galbraith Laboratories in Knoxville, Tenn.

B. Materials

1. Preparation of $K_2Si_2(OCH_2CH_2O)_5$

13.8 grams of 400 mesh silica gel (0.23 mol) and 14.8 grams (0.26 mol) of potassium hydroxide (85%) were weighed into a 500 mL round bottom flask. 125 mL of freshly distilled (from Mg/MgI_2) EtOH and 250 mL of distilled ethylene glycol were added to the flask and the mixture was heated to boiling. The ethanol fraction was distilled off to remove (by azeotrope) any water formed during the reaction. The mixture was then heated further until the solution appeared homogeneous. Partial dissolution of the silica occurred during this period. Distillation was continued to remove the major fraction of the excess ethylene glycol and water formed during reaction. During distillation, most of the silica dissolved. Upon cooling, the remaining colorless liquid turned to a sticky white solid mass. This mass was taken up in 350 mL of freshly distilled methanol and filtered through a Celite-covered frit. The filtrate was concentrated in vacuo to ~20 mL after which portions of dry acetonitrile were added slowly to precipitate out a fine white powder. The precipitate was then collected on a glass frit and washed with 3×200 mL of acetonitrile. Recrystallization from methanol and acetonitrile/ether resulted in a pure white powder which was vacuum-dried. This resulted in 90 g (0.21 mol) of product or 90% yield. NMR: ^1H, 3.4 ppm (under solvent peak); ^{13}C, 61.1, 64.3 ppm; ^{29}Si, −103.0 ppm. Elemental analysis, calc. (found) % C, 27.53 (27.63); % H, 4.98 (4.64); % Si, 13.60 (12.92); % K 17.84 (17.99); % O by difference, 37.01 (36.81).

2. Production of Functionalized Silicon-Containing Species

When $K_2Si_2(OCH_2CH_2O)_5$ is added slowly to neat anhydride and heated, initially, KOAc can be filtered off after the reaction is cooled. Acetyl chloride can also be used. Removal of excess anhydride and 1,2-ethanediacetate under vacuum leads to a white solid which can be characterized as $Si(O_2CCH_3)_4$.

Treatment with two equivalents of HCl, followed by filtration of the KCl leads to the isolation of a neutral tetracoordinate, polymeric silicon compound with the empirical formula $Si(OCH_2CH_2O)_2$, which is in equilibrium with the excess ethylene glycol formed during neutralization to form ring opened diols, e.g., $Si(OCH_2CH_2O)_2(OCH_2CH_2OH)_2$, that can be used in place of $Si(OEt)_4$ for sol-gel processing of silica containing glasses. At higher concentrations, the $Si(OCH_2CH_2O)_2(OCH_2CH_2OH)_2$ species are in equilibrium with oligomeric/polymeric forms whose rheology can be controlled by removal of excess ethylene glycol or solvent addition to form coatable or spinnable materials that can serve as precursors to silicon-containing ceramics. These neutral four coordinate silicon-containing species can be used as precursors to other silicon containing species using techniques common to the polysiloxane synthetic chemist.

3. Preparation of $Li_2Si_2(OCH_2CH_2O)_5$

A procedure similar to that used for the potassium derivative was employed using 5.00 g (0.083 mol) of silica and 1.98 g (0.083 mol) of LiOH. When the "polymeric" portion of the product, that portion which is not immediately soluble, was left stirring for 1-2 days in methanol, it dissolved quantitatively. The resulting methanol-soluble material was recrystallized from methanol and acetonitrile/ether and vacuum-dried. This resulted in 26.2 g (71 mmol) of product or 85% yield. ^{13}C, 61.2, 64.4 ppm; ^{29}Si, −102.9 ppm.

4. Preparation of $Na_2Si_2(OCH_2CH_2O)_5$

Procedures identical to those described for the preparation of the potassium salt were used except 3.33 g (83 mmol) of NaOH were used. Again, stirring for 1-2 days in methanol resulted in complete dissolution. The methanol-soluble material could be recrystallized as above and dried in vacuum. This resulted in 26 g (75 mmol) of product or 90% yield. NMR (CD_3OD): ^1H, 3.36 ppm; ^{13}C, 63.2 ppm; ^{29}Si, −103.3 ppm.

5. Preparation of $CsSi(OCH_2CH_2O)_2(OCH_2CH_2OH)$

Procedures identical to those described for the preparation of the potassium salt were used except 8.74 g (83 mmol) of CsOH were used. The product in this instance was entirely soluble in ethanol. The product was precipitated out by addition of acetonitrile. Although almost all of the silica dissolved, the isolated yield was only 53%. NMR (CD_3OD): ^1H, 3.4 ppm (under solvent peak); ^{13}C, 63.2 ppm; ^{29}Si, −103.1 ppm. Elemental analysis, calc. (found) % C, 20.72 (21.06); % H, 3.63 (3.83); % Si, 8.58 (8.21); % Cs 39.38 (38.84); % O by difference, 27.32 (27.06). IR (nujol) ν O—H = 3300.

6. Exchange of Pinacol for Ethylene Glycol

1.5 g (3.46 mmol) of $K_2Si_2(OCH_2CH_2O)_5$ were mixed with 80 mL of freshly distilled pinacol (added as a solvent). The reaction mixture was then heated under N_2. The mixture melted, the siliconate dissolved and heating was continued until 65 mL of a mixture of ethylene glycol and pinacol were distilled off. On cooling, the remaining liquid became a white solid. Excess pinacol was washed away using 2 × 50 mL of acetonitrile. The remaining white material was then dissolved in methanol and recrystallized as above. The yield was essentially quantitative. The product is expected to be $K_2Si_2(OCMe_2CMe_2O)_5$. NMR (CD_3OD): ^1H, 3.4 ppm (under solvent peak); ^{13}C, 75.8, 26.5, 25.9 ppm; ^{29}Si, −109 ppm.

7. Exchange of 1,3-Propanediol for Ethylene Glycol

5.0 g (11.5 mol) of $K_2Si_2(OCH_2CH_2O)_5$ were mixed with 50 mL of freshly distilled 1,3-propanediol (added as a solvent). The reaction mixture was then heated under N_2. The siliconate dissolved and heating was continued until a 35 mL mixture of ethylene glycol and propanediol was distilled off. The remaining solution was syringed into 50 mL of cold diethyl ether. The product collected as an oil at the bottom of the flask. The oil was cannulated into a 50 mL Schlenk flask and dried in vacuo to a clear glassy solid. This solid was dissolved in 15 mL of MeOH and syringed into 70 mL of acetonitrile to give a precipitate which was filtered off on a medium frit. NMR (CD_3OD): ^1H 1.75 quintet, 1.74 quintet, 3.35 s, 3.66 triplet, 3.67 triplet, 5.13 s ppm; ^{13}C, 60.0 and 36.3 ppm; ^{29}Si, −107.2 ppm. The product can be partially polymeric.

8. Exchange of PEG_4 for Ethylene Glycol

5.0 g (13.5 mmol) of $Li_2Si_2(OCH_2CH_2O)_5$ were mixed with 50 mL of ethylene glycol. The stirred solution was heated under N_2 until all of the lithium salt dissolved. 40 mL freshly distilled PEG_4 (tetraethylene glycol) were then added. The execess ethylene glycol was distilled off to give a clear yellow solution. 20 mL of PEG_4 were removed by distillation at reduced pressure. 40 mL of EtOH were then added and acetonitrile was added to precipitate a crude glassy polymeric product which was filtered and dried in vacuo. The crude material was characterized by ^{13}C NMR (CD_3OD): ^{13}C, 73.6, 71.3, 64.3 and 62.1. The latter two peaks may indicate some ethylene glycol remains. The structure may be polymeric.

9. Attempt to Synthesize $Ba[Si_2(OCH_2CH_2O)_5]$

The following reaction was attempted:

$$BaO + 2\,SiO_2 + 5\,HOCH_2CH_2OH \xrightarrow{EtOH} Ba[Si_2(OCH_2CH_2O)_5] + H_2O$$

6.38 g (4.16 10^{-2} mol) of BaO were dissolved in 250 ml of EtOH, at room temperature, in a 500 ml Schlenk flask. Then 5.00 g (8.32 10^{-2} mol) of 400 mesh SiO_2 11.6 ml (d = 1.114 g/ml; 0.208 mol) of ethylene glycol were added to the solution.

Approximately 150 ml of ethanol were distilled out to form $Ba(OCH_2CH_2O)$, then 100 ml of ethanol were added, and the suspension was allowed to reflux for 16 hours. Most of the ethanol was then distilled out, leaving a white, viscous suspension. The rest of the solvent was removed under vacuum. The white residue was treated with 250 ml of methanol, and the system was allowed to stir for one hour; part of the initial residue proved to be insoluble. This latter was collected by filtration through a fritted filter, washed with methanol

and vaccum dried. It resulted in essentially quantitative recovery (4.9 g) of unreacted silica. The solvent from the methanolic solution was removed under vacuum, leaving a very thick liquid as residue. This latter was dissolved in the minimal amount of ethanol (~20 ml) and treated with 60 ml of acetonitrile: a white fine product precipitated out (8.99 g). The amount of recovered product is in accordance with the formation of [Ba-(OCH_2CH_2O)]. The ^1H and ^{13}C nmr spectra (CD_3OD) show the following peaks: ^1H nmr; 3.62 ppm; 5.35 ppm; ^{13}C nmr: 64.80 ppm.

10. Synthesis of the Aluminum Glycolate

5 g (0.049 mol) of Al_2O_3 and 7.03 g (0.294 mol) of lithium hydroxide were weighed in a 500 ml round bottom flask. Then 250 ml of ethylene glycol and 60 ml of ethanol were added. The mixture was allowed to heat, and first the ethanol/water azeotrope was distilled off. Then most of the ethylene glycol was removed by distillation. The system was cooled and left under nitrogen overnight; after 12 hours there was a white solid mass, which was treated with methanol; and solid went almost entirely in solution (there was only a slight cloudiness, which was eliminated by filtration through celite). The volume of the solution was reduced under vacuum until a white solid started to percipitate out; the precipitation was completed by adding acetonitrile, and then the product was filtered and dried under vacuum. The yield was quantitative. NMR (CD_3OD): ^1H, 3.58 ppm and 5.11 ppm; ^{13}C, 64.32 ppm.

The invention now being fully described, it will be apparent to one of ordinary skill in the art that many changes and modifications can be made thereto, without departing from the spirit or scope of the invention as set forth herein.

The embodiments of the invention in which an exclusive property or privilege is claimed are defined as follows:

1. A complex having the formula

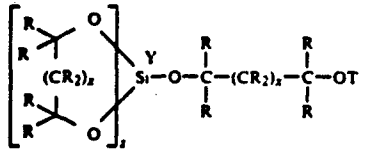

wherein x is 0 or 1; each R is independently selected from the group consisting of H, OH, C_{1-6} alkyl, C_{1-6} alkoxyl, C_{2-6} alkene, C_{6-12} aryl, C_{1-6} hydroxyalkyl, C_{1-6} thioalkyl, C_{2-12} alkoxyalkyl, C_{3-20} heteroaromatic, and combinations thereof, and wherein each said R group may further contain one or more atoms of elements selected from the group consisting of Si, Ge, Sn and P;

T is H or

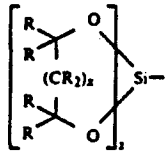

and Y is an alkali metal cation.

2. A complex according to claim 1, wherein each R is independently a methyl group or H.

3. A complex according to claim 1, wherein every R is H.

4. A complex according to claim 1, wherein T is

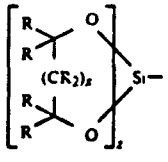

5. A silicon complex according to claim 1, wherein Y is Cs^+ and T is H.

6. A silicon complex according to claim 1, wherein Y is $2Na^+$, $2Li^+$, or $2K^+$ and T is

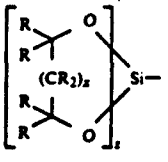

7. A silicon complex selected from the group consisting of $K_2Si_2(OCH_2CH_2O)_5$, $Li_2Si_2(OCH_2CH_2O)_5$, and $Na_2Si_2(OCH_2CH_2O)_5$[, $BaSi_2(OCH_2CH_2O)_5$, and $CaSi_2(OCH_2CH_2O)_5$].

* * * * *

APPENDIX 5

Submitted to *Journal of Materials Research*

Superconducting Fibers From Organometallic Precursors. Part III: High Temperature Pyrolytic Processing[1,2]

Zhi-Fan Zhang,[#,a] Richard A. Kennish,[a] Kay A. Youngdahl Blohowiak,[a,b] Martin L. Hoppe [a] and Richard M. Laine.[*, #,a] Contribution from the [a]Polymeric Materials Laboratory of the Washington Technology Center and the Department of Materials Science and Engineering. University of Washington, Seattle, WA 98195. [b]Boeing Corporation, Seattle, WA.

Abstract:

60-70 μm diameter preceramic fibers, extruded from THF solutions containing 1:2:3 stoichiometric mixtures of yttrium, barium and copper carboxylates, were pyrolytically transformed into ceramic fibers using controlled heating schedules and reactive atmospheres. The objectives of the work reported here were to identify appropriate processing conditions such that during pyrolysis the preceramic fibers would: (1) eliminate the organic ligands without pore or void formation; (2) reach full density with a controlled grain size; and (3) form single orthorhombic phase, 123 fibers with reasonable mechanical properties. The mechanisms of organic ligand decomposition and loss were examined using mass spectral fragmentation, DRIFT spectra, and TGA. Microstructural and phase evolution were correlated with heating schedules, and atmospheres, using XRD, DTA, SEM and limited flux exclusion studies.

The mechanisms of decomposition of the spinnable mixtures suggest intermolecular rather than intramolecular decomposition pathways. Different pyrolysis atmospheres were also examined to explore methods of controlling the degradation process. Slow pyrolysis in air followed by oxygen anneals appears to give superior fibers.

The pyrolyzed fibers exhibit the appropriate orthorhombic phase according to x-ray powder diffractometry. Preliminary flux exclusion measurements demonstrate that the fibers are superconducting although the measured ΔT_c is not exceptional. Future work on the low temperature pyrolysis program is required to obtain better fiber integrity and to improve ceramic fiber mechanical and superconducting properties.

Now with the Department of Materials Science and Engineering, University of Michigan, Ann Arbor, MI 48109-2136

* To whom correspondence should be addressed at the Department of Materials Science and Engineering, University of Michigan, Ann Arbor, MI 48109-2136.

Key Words: Superconducting fibers, preceramic polymers, metal carboxylates, precursor fiber pyrolysis.

Introduction:

The optimal ceramic superconducting fiber must be dense, thin, flexible, and single phase. Commercial ceramic fibers that meet the "flexible" criterion are typically less than 20 μm in diameter.[3]

The current methods of producing superconducting "wires", with few exceptions, provide filaments (50-100 μm) rather than flexible fiber. These methods include powder-in-tube ,[4] melt process,[5] laser-heated pedestal growth[6] techniques, and suspension spinning.[7a]

The processes presently used to fabricate thin ceramic fibers (< 20 μm) include suspension spinning,[7] sol-gel,[8] and preceramic (organometallic) polymer processing.[9] However, only sol-gel and preceramic polymer processing can be used industrially to fabricate ceramic fibers without the preformation of ceramic powders. Clearly, there are opportunities to develop improved processing methods to produce superconducting fibers with properties similar to ceramic fibers currently produced commercially.

Of the two approaches, organometallic processing has some advantages over sol-gel processing. First, atomic mixing and rheological properties in sol-gel processing are controlled by hydrolysis/condensation reactions. Second, close control of sol-gel reaction time and reaction conditions is necessary to obtain the rheological properties required for further processing. In contrast, these properties in preceramic polymer processing are controlled by the polymer architecture, ligand structure, solvent content and solvent type. Thus, as discussed in the previous paper in this series,[2] it is possible to obtain more effective atomic mixing, especially for multi-component (multimetallic) systems, and easier control of rheological properties. Organometallic polymer precursor solutions generally have excellent "shelf life" and are not prone to forming intractable gels.

However, preceramic polymer processing suffers from its own unique problems such as effective removal of carbon containing ligands and large volume-density change during heat-treatment. The latter problem derives from the fact that molecular precursors commonly have densities that are much lower than those of the final ceramic products, because of the organic ligands required to ensure processability. The volume-density changes require exceptional control of fiber processing conditions to minimize stress induced fiber fracture and/or shape distortion.

Based on criteria discussed in a previous paper,[2] we have chosen to use metal carboxylates as polymer precursors to process ceramic superconducting fibers. The chemistry and low temperature fiber processing methods described earlier provide the basis for the work presented here, which focuses on the thermolytic transformation of the precursor fibers into ceramic fibers. Limited efforts to understand how these processing conditions affect superconducting properties are also presented; although, these will be the subject of a later paper.

Background

Solutions formed by mixing metal carboxylates have been used extensively to prepare superconducting thin films.[10-22] However, whether or not they can be used to process superconducting fibers is still open to question, because (unlike thin films) the resulting precursor fibers have to be self-supporting.

Three general processing domains must be optimized to obtain intact ceramic superconducting

fibers from organometallic precursors -- preparation and processing of polymers to form the precursor fiber, conversion of precursor fiber to ceramic fiber, and optimization of the ceramic fiber properties. The first domain involves the syntheses of potentially processable precursors, selection of a suitable precursor system with a correct elemental stoichiometry, and formation of spinnable solutions from which self-supporting precursor fibers can be drawn or extruded. The molecular architecture of precursor systems, choice of solvent and the solvent content provide a set of variables that permit optimization of rheological properties.

We have evaluated these processing variables for selected metal carboxylates[2] and find that THF solutions containing a 1:1:3:1 molar mixture of yttrium isobutyrate [$Y(O_2CCHMe_2)_3$], barium isobutyrate [$Ba(O_2CCHMe_2)_2$], copper isobutyrate [$Cu(O_2CCHMe_2)_2$] and barium 2-ethylhexanoate [$Ba[O_2CCH(Et)(CH_2)_3Me]_2$ can be used to spin preceramic fibers with diameters of 60-70 μm .

The focus of this paper is the second domain, the pyrolytic conversion of the preceramic fibers to ceramic fibers with concomitant retention of fiber integrity. The pyrolysis conditions must also lead to the correct phase and desired microstructure. Three problem areas were considered: (1) curing to ensure precursor infusibility , (2) volume change/densification, and (3) final microstructure and phase. Scheme I illustrates these areas and the important variables requiring control.

Insert Scheme 1

To thermally transform a precursor fiber into a ceramic fiber, one must prevent melting or creep during the heating process. To do this, one must render the precursor fiber infusible. Infusibility is enhanced by reactions that provide extensive crosslinking of the organic ligands (e.g. by polymerization or redistribution) before or during pyrolysis. However, the resulting crosslinked organic ligands must eventually be removed during the transformation to a ceramic product. Therefore, the initial crosslinking process must be followed by depolymerization and/or oxidative degradation of the organics retain in the now infusible fiber.

Oxidative removal of the retained organics (as CO/CO_2) is the method of choice. However, several potential complications can be anticipated. For example, if the rate of oxidation is too rapid then the gaseous products formed may induce formation of pores or voids in the final ceramic product, inhibit densification and/or generate mechanical stresses that will cause fiber cracking.

Alternatively, if the organics retained are highly crosslinked then it is likely that carbon will be retained in the final ceramic product. Thus, it may be necessary to use more vigorous oxidizing conditions to ensure against this possibility. There is an obvious balance between this requirement and the one above. Thus, control of the pyrolysis atmosphere is essential during the degradation process.

Processable precursor systems containing minimal amounts of carbon are desirable in view of the above problems, but also because they offer maximum precursor fiber density and high ceramic yield. The latter attributes minimize the volume change that will occur during transformation to ceramic fiber.

Finally, control of the final microstructure and phase will rely on the proper choice of final heating parameters. In turn, control of these properties will play an important role in the post-pyrolysis heat-

treatments necessary to optimize the properties of the final ceramic fiber, the third domain. For example, heating and soaking fibers in oxygen may improve the superconductivity.[23]
The work presented here focuses primarily on the second processing domain, the pyrolytic conversion of precursor fibers to superconducting ceramic fibers. Some preliminary work on post-pyrolysis processing is also presented as a check to determine whether the efforts in the second domain will permit work in the third domain.

Experimental Techniques:

Precursor Fiber Formation:

Metal carboxylate syntheses were described in our previous paper.[2] THF solutions of metal isobutyrate/metal 2-ethylhexanoate mixtures offer good spinnability (rheological properties). Two systems were examined. The molar ratio of the metal carboxylates in the two systems is:

System 1: $Y(O_2CCHMe_2)_3 : Ba(O_2CCHMe_2)_2 : Ba[O_2CCH(Et)(CH_2)_3Me]_2 : Cu(O_2CCHMe_2) = 1 : 1 : 1 : 3.$

System 2: $Y(O_2CCHMe_2)_3 : Ba(O_2CCHMe_2)_2 : Ba[O_2CCH(Et)(CH_2)_3Me]_2 : Cu(O_2CCHMe_2)_2 = 1 : 1 : 1 : 3.$

Systems 1 and 2 are quite similar. They differ only in that System 1 uses a Cu(I) isobutyrate derivative whereas System 2 employs the analogous Cu(II) isobutyrate derivative. The solids content for spinnable solutions of both systems can be as high as 1.25g/ml. Precursor fibers can be hand drawn for both systems. System 1 solution has to be handled in an inert atmosphere because of the oxygen and moisture sensitivity of the Cu(I) component. Therefore, our efforts have focused on System 2. Green-blue precursor fibers with diameters of 60-70 μm can be extruded from System 2 solutions.[2]

Curing and Pyrolysis:

Decomposition of both the individual carboxylates (in bulk) and extruded 123 precursor fibers was examined. Prior to pyrolysis, precursor fiber samples were dried at room temperature for times varying from several hours to days. Various heating schedules and atmospheres were used to cure and pyrolyze the precursor fibers. The pyrolyses were conducted either in a Thermolyne burnout furnace (type 6000) equipped with a Eurotherm temperature controller (Model 812), or a Lindberg tube furnace (model No. 58114) equipped with a Eurotherm temperature controller (Model No. 818S). All experiments not conducted in stagnant air were run in the tube furnace which allows for careful control of the atmosphere. In all cases, the samples were placed on polycrystalline MgO substrates.

Bulk carboxylate samples were pyrolyzed in N_2, air, and O_2 atmospheres to identify primary and secondary decomposition products. The heating schedules for the bulk decomposition trials were 5°C/min to 950 °C. The results of these studies are shown in Tables I and II.

Chemical analyses

Chemical analyses (see Table I) for selected metal carboxylates were performed by Galbraith

Laboratories of Knoxville, TN.

Thermogravimetric Analyses (TGA):

TGA studies were carried out using a Perkin Elmer TGA-7 Thermogravimetric Analyzer. Sample sizes of approximate 15 to 30 mg were loaded and heated in dry O_2, air, or N_2, at a flow rate of 50 mL/min. A typical heating schedule was 5°C/min to 900-925°C, but variations of this schedule were used to obtain different details.

Differential thermal analyses (DTA):

DTA experiments were conducted on a Perkin Elmer DTA 1700 Differential Thermal Analyzer. Sample sizes of approximately 10-20 mg were loaded and heated in dry O_2, air, or N_2, at a flow rate of 50 mL/min. The reference material used in the DTA was aluminum oxide. It should be noted that this particular DTA instrument shows a consistent 40-50 °C higher onset temperature for the same event as observed in TGA corresponding studies. Therefore, when comparing TGA and DTA data in this study, this offset should be taken into account. The DTA temperatures correlate with literature temperatures.

Mass Spectroscopy:

A VG 70SEQ tandem hybrid mass spectrometer was used to obtain the mass spectral data. The multiplier was 1000. The source temperature was 200 °C, the acceleration voltage was 4 KeV (except as noted), and a temperature programmable, direct insert sample probe was used for data acquisition. Several drops from a 1 mg/mL solution of sample were applied to the direct probe. The probe was then inserted into the instrument and heated at 30 °C/min. Spectra were collected sequentially so as to correlate with temperature changes.

Diffuse Reflectance Infrared Fourier Transform (DRIFT):

DRIFT spectra were recorded on a Nicolet 5DBX spectrophotometer. Sample sizes were approximately 5 mg. Samples were mixed intimately with 250 mg of dried KBr and ball milled using a model 3110-3A WIG-L-BUG amalgamator purchased from Crescent Dental Manufacturing. Once pulverized, the samples were quickly transferred to a sample holder in air. The spectrometer sample chamber was purged with N_2 until the absorbance due to CO_2 was no longer present (≈ 15 minutes).

X-ray Diffraction (XRD):

XRD patterns were obtained using a Philips XRG-3100 automated powder diffractometer to identify crystal phases. The working voltage and current were 45 kV and 40 mA respectively. Cu Kα (λ = 1.54 Å) radiation with a Ni filter was used. The scanning angle was 20 - 60 degrees 2θ with a step scan of 1/4° 2θ per 1/4 second. Fiber samples were crushed to a powder in air prior to XRD analysis.

Scanning Electron Microscopy (SEM):

SEM studies were performed using a JEOL 840A microscope. SEM samples were mounted on a silver paste covered aluminum stub. After drying under vacuum, samples were sputter coated with a

300 Å layer of Au/Pd to enhance their conductivity. Secondary electron image micrographs were recorded to establish the microstructures.

Flux Exclusion:

Flux exclusion was used to measure the superconductivity of the materials produced. The flux exclusion curves were obtained using a Keithly 220 programmable current source, an EG&G Model 5209 lock-in amplifier, a Hewlett Packard HP3478A Multimeter, a Wavetek 11 MHz stabilized sweep generator (Model 22), and a Hewlett Packard 1201B oscilloscope connected to a Compaq 286 Computer. A sample size of 5-20 mg of pyrolyzed fiber segments was embedded in a Duco glue plug and dried until hard. The plug was lowered into a chamber containing two identical, but oppositely balanced copper coils, a third coil was wound around these coils. The chamber was cooled in liquid N_2 to 77K and then warmed at 1K/min to 105K. The magnetic susceptibility was recorded as a function of temperature in this range. Measurements were conducted in a self field of 0.32 Gauss.

Results and Discussion:

Bulk Materials Pyrolysis Studies

A. Macroscopic Decomposition Processes. The decomposition (mass loss) temperature ranges for selected individual metal carboxylates heated in different pyrolysis atmospheres at 1 atm were determined by TGA. The results of these studies are listed in Tables I and II. Coincidentally, mass spectral (MS) analyses of the volatile fragments that derive from decomposition of the carboxylates were conducted to support the TGA results (see below).

Insert Tables I and II

The TGA patterns of Y isobutyrate heated in O_2, air, and N_2 are shown in Figure 1. Most of the TGA analyses of the complexes shown above exhibit behavior similar to that of Y isobutyrate heated in air and N_2 Two exceptions are found for the Y isobutyrate, and the Cu isobutyrates heated in O_2. The unusual curve seen for yttrium isobutyrate heated in O_2 illustrates ignition rather than simple oxidative degradation.

Insert Figure 1

The Cu(I) and Cu(II) derivatives decompose at lower temperatures than the other metal carboxylates, when heated in air or O_2. Both derivatives exhibit an initial weight loss followed by a sizable weight gain (see Figures 2 and 3). This behavior is indicative of initial reduction to copper metal, despite decomposition in air, followed by reoxidation to CuO or Cu_2O.

Insert Figures 2 and 3

The Cu(I) isobutyrate is intriguing because there is an initial weight gain from 100 to 104% at 100-120 °C during heating in an air or O_2. This weight gain can be explained, if the first reaction observed is oxidation of Cu(I) to Cu(II) by formation of a bridging peroxide [Cu(II)-O-O-Cu(II)]. The mass

change calculated for bridging peroxide formation would be 105%. The final ceramic yield in air is 51% which is reasonable for the formation of CuO (calculated at 52.2%). These results contrast with the Cu(II) isobutyrate results.

The calculated weight loss for Cu(II) isobutyrate decomposition is 73.3% for formation of Cu metal, 69.9% for formation of Cu_2O, and 66.6% for CuO. The TGA results (in air) indicate that weight loss is 72.9% at ≈ 240 °C. At temperatures >600 °C, it is only 70.5%. This would be acceptable if the final product were Cu_2O. However, this is unlikely for thermodynamic reasons and the fact that two exotherms are observed in the DTA (Figure 4) which suggest oxidation of Cu first to Cu_2O and then to CuO.

Insert Figure 4

Furthermore, if the spinnable mixture is heated to 120-150°C in a sealed flask in N_2, a film of Cu metal is observed to form on the upper inside surfaces of the flask. A portion of the copper volatilizes during the decomposition process. Therefore, the 27.1% weight loss found at ≈ 240 °C is probably a consequence of three separate chemical processes; ligand degradation, copper volatilization and partial oxidation. Copper volatilization is potentially harmful to processing phase pure 123 because it will lead to off-stoichiometry ceramic products.

Fortunately, volatile Cu species are not observed when the preceramic mixtures are pyrolyzed in air. As seen in Figure 5, the found ceramic yields for System 2 (37.3%) matches the theoretical value. The likely reason for minimized volatilization is that decomposition proceeds via intermolecular, intermetallic pathways rather than decomposition of the individual carboxylates. During dissolution and/or pyrolysis, the Cu carboxylates appear to interact with either the Y or Ba carboxylates (or both) to form polymetallic clusters[2] and therefore Cu volatilization can be avoided (see below).

Insert Figure 5

The formation of Cu metal is also consistent with the XRD results for pyrolysis of System 2 in N_2 as shown in Figure 6. In this case, insufficient oxygen is available for reoxidation. Cu metal therefore appears at 300 °C (see below).

Insert Figure 6

The weight loss observed for the Cu (II) precursor due to volatilization is not observed for the Cu (I) isobutyrate. The oxide bridge that may form initially in the Cu (I) system should limit volatilization since the formation of Cu oxide is enhanced relative to the Cu(II) system. In addition, the Cu (I) precursor may be polymeric,[2,24] which will also reduce the likelihood of volatilization.

The DTA curves of all the metal carboxylates selected in this study did not show any exothermic transitions when samples were pyrolyzed in N_2, but exothermic events were observed when they were pyrolyzed in air or O_2.

B. Molecular Decomposition Processes. The Cu (II) mass spectral fragmentation patterns (see Table III) are in accord with the literature on the decomposition of copper carboxylates. The fragmentation

patterns for the other metal carboxylates (Table III) differ from the Cu patterns but exhibit strong similarities. Two reasonable decomposition pathways can be suggested (Scheme II). The first pathway is initiated by cleavage of a C-O bond resulting in $RCO_2M\text{-}O\cdot$ plus a $C_4H_7O\cdot^+$ (m/e = 71) fragment which is most probably an acylium ($Me_2CHC{=}O\cdot^+$) ion. The acylium ion fragments readily to CO and the isopropyl species ($Me_2CH\cdot^+$, m/e = 43) which in turn can lose H· to form propene ($CH_3CH{=}CH_2$, m/e = 42). $RCO_2M\text{-}O\cdot$ can abstract hydrogen from some R-H species (e.g. m/e = 43) to form $RCO_2M\text{-}OH$. This can rearrange with loss of free acid to form M=O. Alternately, two M-OH can react to generate H_2O (m/e = 18) and RM-O-MR.

Insert Table III

The fragmentation pattern of the free acid appears in most spectra, superimposed on the other fragmentation processes. The fact that it only appears at temperatures above 130 °C in the MS vacuum indicates that it derives from the decomposition process, not from impurities retained during synthesis. Free isobutyric acid fragments by loss of a methyl group to form an m/e = 73 species which then can lose CO_2 to form an m/e = 29 species. These fragmentation patterns are suggested, based on published data.[25]

The second decomposition pathway begins with expulsion of CO_2 (m/e = 44), or decarboxylation, with coincident formation of M· (zerovalent metal) and again the m/e = 43 species. The m/e = 43 species is abundant in all the fragmentation spectra. Decomposition by decarboxylation is common for copper carboxylates. Some literature references describe the formation of copper aryl and alkyl compounds from copper carboxylates by loss of CO_2.[26] This process can be used to explain copper volatilization, if we assume that CO_2 loss coincides with formation of a volatile copper alkyl complex, e.g. $Cu(CHMe_2)_2$. An unidentified, volatile copper species is also obtained during the decomposition of $Cu(O_2CCF_3)_2$.[27]

The complexity of the metal 2-ethylhexanoate fragmentation pattern is deconvoluted by analogy to the isobutyrate results. Thus, two possible pathways result from cleavage of a C-O bond or decarboxylation. The first path leads to fragments of $CH_3(CH_2)_3CH(Et)CO\cdot$ (m/e = 127 small) which further fragments. The second path leads to formation of an acylium fragment [$CH_3(CH_2)_3CH(Et)CO\cdot^+$, m/e = 101] and further fragmentation products similar to those found for the isobutyrate ligand. In addition, the free acid is also produced, but only after the probe has been heated to 130°C.

C. Decomposition of Carboxylate Mixtures. The TGA for System 2 (Figure 5) suggests that an unexpected intermediate forms in the mixed carboxylate system that cannot be predicted based on the TGAs of the individual carboxylates. The Table II data for air pyrolyses show that the individual carboxylates fully decompose either to metal oxides or metal carbonate at temperatures less than 340°C; yet, the TGA for System 2 shows that the last, primary stage of decomposition in air occurs at ≈ 340-380 °C. In a similar system, Hamdi et al.[28] also report two major decomposition steps in Y, Ba, and Cu neodecanoate mixture, showing considerably more structure than the TGAs obtained from the individual components. These results suggest that the components of the mixture actually form very strong chemical interactions which alter the chemical behavior of the system with respect to the individ-

ual metal carboxylates. In our previous paper,[2] we presented the optical microscopy data obtained from System 2 solutions, that also suggest the formation of multimetallic carboxylate clusters in the precursor system. Other examples of multimetallic carboxylate clusters have been reported in the literature.[29]

Pyrolysis of a bulk sample of System 2 in N_2 leads to excessive segregation, even at 300°C, as evidenced by the strong absorption lines for copper metal in the XRD (Figure 6). This segregation is clearly maintained even after soaking at 500°C or heating to 925°C for 1 h . At these temperatures, the XRD patterns still show copper metal and the presence of $BaCO_3$, which would remain stable to 925°C only if extensive segregation had occurred at lower temperatures. These results are supported by the DRIFT spectra (Figure 7) which show a C=O stretch at $\nu_{C=O}$ = ~ 1700 cm^{-1}, indicating that significant amounts of carbonate remain at 925°C.

Insert Figure 7

In comparison, System 2 heated in air exhibits XRD patterns (Figure 8) that show no sign of copper metal at any temperature studied, nor is there any evidence of extraneous carbonate phases after heating to temperatures of 900 °C. The corresponding DRIFT spectrum (Figure 9) is free of $\nu_{C=O}$ absorption, although the $\nu_{C=O}$ of carbonate is seen at lower temperatures.

Insert Figures 8 and 9

Fiber Pyrolysis Studies

The main intent of the work presented in this section is to demonstrate the feasibility of transforming System 2 precursor fibers to 123 ceramic fibers. Even though System 1, the Cu(I) derivative system, is spinnable, it was abandoned due to its air sensitivity.

A SEM image of the unheated precursor fiber from System 2 (Figure 10) shows smooth amorphous surfaces.

Insert Figure 10

Control of fiber integrity is critical. The weight loss and density increase for System 2 precursor fibers during heat-treatment results in an exceptional volume decrease (>90%).[2] Most shape distortion and fiber fracture occurs below 400°C where most of the organics are lost (see Figure 5). It is likely that mass transport of gases into and out of the fiber during degradation of the organic ligands is more critical than later densification at higher temperatures.

In early studies, the precursor fibers were heated at 130-160 °C for several days to promote crosslinking and infusibility. However, it was found that identical results could be obtained using a continuous heating schedule. Thus, a very slow heating rate (< 0.5 °C/min, in air) to 400°C was chosen to optimize crosslinking and limit the rate of evolution of volatile organics.

The third, conversion stage (above 400°C), was designed to promote crystallization in the resultant ceramic fibers. Heating rates of less than 2°C/min and an oxidizing atmosphere were chosen to promote smooth densification coincident with complete crystallization.

A. Decomposition in Nitrogen and Conversion in Air. Because the Y isobutyrate ignites on heating in pure O_2, fiber pyrolysis studies in a pure O_2 atmosphere were avoided. Decomposition studies (<500 °C) were initially run in an N_2 atmosphere followed by treatment in an air atmosphere at higher temperatures to facilitate removal of residual carbon impurities, typically carbonates, and to obtain the desired microstructure and phase. A typical heating schedule was: 0.2°C/min to 500°C in N_2, 1°C/min to 900°C in air followed by a 2 h hold at 900°C.

Less fiber fracture occurs upon heating in N_2 to 500 °C than on heating in air (see below). This can be explained by assuming that any exothermic, gas producing reactions are reduced or eliminated in N_2. The DTA experiments run for the individual compounds and System 2 do not show any exothermic events during pyrolysis under N_2. However, fiber pyrolysis in N_2 still leads to fibers that exhibit high porosity (at < 500°C) and signs of melting as seen in the SEM images shown in Figures 11 and 12. Furthermore, the XRD data (Figure 6) indicate significant segregation and as mentioned above we observe Cu volatilization in N_2. Thus, an oxidizing atmosphere is essential to all stages of fiber pyrolysis.

Insert Figures 11 and 12

B. Decomposition and Conversion in Air. A heating schedule consisting of heating in air at 100°C for 4 d, 150°C for 4 d, 200°C for 4 d, 275°C for 4 d, 350°C and 500°C each for 1 d, and then 1°C/min to 930°C was chosen first. Loss of fiber integrity started at 175 °C as evidenced by cracking of precursor fibers. After a 7 day hold at 175°C, most of the fibers exhibited severe cracking. The remaining fibers continued to fracture as the temperature was raised to 300°C. Thus, long term curing did not provide a smooth, continuous transition process.

Heating schedules of 0.2°C/min to 500°C, then 1-2°C/min to 900-950°C followed by holds of 0.25-8 h in air or O_2 were then examined. Although slow, these heating schedules are still much faster than initial curing schedule, and are continuous processes. Cracking and shape distortion are still a problem; however, optimal ceramic fibers with diameters of 15-25 μm and lengths up to 4 cm can be recovered.

SEM images of the fibers were taken at selected points during heating schedules to examine microstructural development. Fibers heated up to 500°C (Figure 13) appear dense without visible microstructure, but exhibit irregular surfaces. However, heating to 900 °C gives dense fibers with average diameters ≈ 15-25 μm and grain sizes < 1 μm (Figure 14). Longer hold times (e.g. several hours) at 900°C leads to larger grain sizes. Fibers heated to temperatures of 930-950 °C (Figures 15, 16) display excessive grain growth and porosity.

Insert Figures 13-16

Because the SEM images show that fibers pyrolyzed with a hold at 900-910°C (for less than 2 hours) exhibit the best microstructure (grain sizes ≤ 1 μm and fairly dense), XRD studies were conducted to identify the phase(s) formed. According to the X-ray diffraction pattern, pyrolysis to 900°C gives materials partially converted to the orthorhombic 123 superconducting phase. The XRD patterns also show that holding at 900°C for a longer time gives better conversion to the orthorhombic phase as

deduced from increases in peak splitting at 32.5° 2θ. The XRD taken of the precursor powder heated to 950 °C displayed a standard splitting at 32.5° 2θ (Figure 17), indicating good conversion to the orthorhombic, superconducting phase. However, as seen in Figures 15 and 16 these fibers exhibit excessive grain growth and some porosity. Therefore, they cannot offer useful mechanical properties.

Insert Figure 17

Furthermore, because XRD data cannot reveal the presence of small amounts (<5%) of extraneous phases or amorphous material, the above results do not provide sufficient proof of superconducting behavior. Flux exclusion and conductivity measurements provide more accurate measurements of the extent of the superconducting phase. Conductivity measurements can also be deceiving if conduction is filamentary. Thus, flux exclusion tests for superconductivity; albeit on a qualitative basis, will give useful information.

Good superconducting behavior and therefore high phase purity are typified by a high T_c and a narrow ΔT_c. Flux exclusion measurements demonstrate that fiber samples processed without an oxygen heat treatment do not display superconductivity, even for fibers heated in air to 950 °C. A post-pyrolysis heat-treatment was found to be necessary. Therefore a heating schedule was adopted wherein fibers were heated at 0.2°C/min to 400°C in air, then 1°C/min to 910°C for 1-8 h in air, followed by a 450°C soak in O_2 for 24 h. After soaking in O_2, the 910°C pyrolyzed fibers display some superconductivity with a T_c onset of 90K and ΔT_c of 15K (Figure 18).

Enhancing the oxygen content proved very helpful; therefore, a heating schedule of 0.2°C/min to 400°C in air, then 1°C/min to 910°C in O_2, followed a 450°C, 5 h soak in O_2 was then implemented. The first sample treated in O_2 for 2 hours at 910°C gave superconducting behavior similar to that obtained for a sample soaked in O_2 for 24 h at 450°C. However, the second sample, treated in O_2 for 8 hours at 910°C, gave much improved flux exclusion (Figure 19).

Insert Figures 18 and 19

The degree of flux exclusion (the change in the inductance) is used here in a qualitative fashion only, to assess the extent of superconductivity in a given sample. In both the above cases, sample sizes were about the same (~15 mg). The first sample showed a change in inductance of about 6 μV, whereas the change in the second sample was about 45 μV. This indicates significantly greater superconductivity in the second sample than in the first. This makes sense, given the longer O_2 soak time at the higher temperatures. However, both flux exclusion curves are broad, with ΔT_cs of ≈ 15K.

The broad ΔT_c is likely due to incomplete oxygen saturation because of the relatively low temperatures used. Efforts to improve the superconducting behavior led to heat-treatments at higher temperatures in O_2. Heating schedules of 0.2°C/min to 400°C in air, 1°C/min to 930 or 950°C in O_2 were examined. Samples heated in O_2 either to 930 °C or 950 °C for 2 hours followed by tempering in O_2 at 450 °C for 5 h showed slight increases in T_c. However, the ΔT_cs were still broad, despite a sharper drop in the exclusion curve between 92K-90K . Thus, higher temperature pyrolyses in O_2 do not significantly increase the amount the superconducting phase and also induce undesirable grain growth.

An improvement in superconductivity may be obtained by low temperature, long term curing in O_2 rather than heating to high temperatures. A SEM of a fiber treated in O_2 at 910 °C for 8 h is shown in Figure 20. Only minimum grain growth is observed. The above post-pyrolysis heat-treatments studies are only considered preliminary. More detailed efforts will be described at later date. The optimal final ceramic superconducting fiber will be thin (~10 μm in diameter) in diameter and fully dense in order to be flexible and strong. Our ability to consistently process high quality fibers requires considerable improvement. Only one in twenty of the precursor fibers survives intact through the final heat treatment and only one in forty fibers of lengths of the order of 5 cm will bend 90°.

Insert Figure 20

Summary

Working principles for the pyrolytic transformation of 123 precursor fibers to flexible (<20 μm in diameter), dense 123 superconducting ceramic fibers have been developed. By using carefully controlled heating schedules and atmospheres (typically 0.2°C/min to 400-500°C and °C/min to 900°C or above), dense (almost defect free) ceramic fibers can be obtained; although reproducibility is poor. At 900°C, conversion to the orthorhombic phase, as determined by XRD, was poor. Furthermore, flux exclusion studies indicated that the true superconducting phase is not formed using this simple heat treatment. Fibers heated ≥ 930°C exhibited high porosity and significant grain growth. Conversion to the orthorhombic phase was more complete according to XRD patterns as the pyrolysis temperature and/or time increased; however, flux exclusion measurements revealed very low contents of superconducting phase.

Flux exclusion measurements indicated that fibers heated to 900°C, when soaked in O_2 at 450°C, 900°C, and 910°C exhibited superconducting properties; although sharp T_cs and narrow ΔT_cs were never observed. Superconducting properties increased as the heating time in O_2 increased. However, higher temperature (≥930°C) did not give improvements in superconducting behavior. Low temperature, long term soaking appears to be necessary to obtain good superconducting properties while minimizing grain growth that might jeopardize fiber mechanical properties.

At the current stage of development, significant problems remain with respect to optimizing fiber integrity and microstructure. These problems are at least partly due to the need for very close control of the heating schedules. There are also problems remaining with regard to reproducibility of the superconducting properties. Studies designed to ameliorate these problems are ongoing. More complete descriptions of the fiber mechanical and conducting properties will be discussed in later papers.

Acknowledgments

We would like to thank the Defense Advanced Research Project Agency (DARPA Order No. 6499) for support of this work through AFOSR contract No. F49620-88-C-0413 and AFOSR contract No. F49620-89-C-0059.

References

1. First Paper in this series: a. M. L. Hoppe, K. A. Youngdahl, R. A. Kennish, and R. M. Laine. Fourth Internat. Conf. on Ultrastructure Processing of Glasses, Ceramics, Composites and Polymers, Symp. Proc., in Press. b. see also W. M. Carty, G. C. Stangle, R. M. Laine and K. A. Youngdahl, SAMPE 1988 Spring Meeting (Seattle) SAMPE Quart., Oct., (1988) p3.
2. Second Paper in this series: R. M. Laine, K. A. Youngdahl, R. A. Kennish, M. L. Hoppe, Z-F. Zhang, and D. J. Ray, J. Mat. Res., **6** [5], 895 (1991)
3. L. M. Shepard, Am. Cer. Soc. Bull., 666 (1990)
4. a. S. Jin, R. C. Sherwood, R. B. Van Dover, T. H. Tiefel, and D. W. Johoson, Jr., Appl. Phys. Lett., **51** [3], 203 (1987). b. Y. Yamada, N. Fukushima, S. Nakayama, H. Yoshino, and S. Murase, Jap. J. Appl. Phys., **26** [5], L865 (1987). c. M. A. Lusk, J. A. Lund, A. C. D. Chaklader, M. Burbank, A. A. Fife, S. Lee, F. Taylor and J. Vrba, Supercond. Sci. Technol., **1**, 137 (1988). d. N. Sadakata, Y. Ikeno, M. Nakagawa, K. Gotoh, and O. Kohno, Mat. Res. Soc. Symp. Proc., **99**, 293 (1988). e. S. Matsuda, M. Okada, T. Morimoto, T. Matsumoto, and K. Aihara, Mat. Res. Soc. Symp. Proc., **99**, 695 (1988).
5. a. S. Jin, T. H. Tiefel, R. C. Sherwood, G. W. Kammlott, and S. M. Zahurak, Appl.Phys. Lett., **51** [12], 943 (1987). b. M. Miljak, E. Babic, A. Hamzic, G. Bratina, and Z. Marohnic, Supercon. Sci. Technol., **1**, 141 (1988).
6. a. D. Gazit and R. S. Geigelson, J. Cryst. Growth, **91**, 318 (1988). b. R. S. Geigelson, D. Gazit, D. K. Fork, and G. H. Geballe, Science, **240**, 1642 (1988). c. G. T. Forrest, Laser Focus, **24**, 40 (1988).
7. a. J W. Halloran, J. D. Hodge, D. Chandler, L. J. Klemptner, M. Neal, M. Parish, H. Park, V. Pathare, G. Bakis and D. Eagles , J. Am. Ceram. Soc. **75**, 1992. b. T. Goto and M. Tsujihara, J. Mat. Sci. Lett., **7**, 283(1988). c. T. Goto and I. Horiba, Jap. J. Appl. Phys., **26** [12], L1970 (1987). d. J. C. W. Chien and B. M. Gong, Phys. Rev. B, **38** [16], 11.853 (1988). e. J. C. W. Chien, Polymer Bulletin, **21**, 1 (1989). f. S. E. Dorris, J. T. Dusek, M. T. Lanagan, J. J. Picciolo, J. P. Singh, J. E. Creech, and R. B. Poeppel, Ceramic Bull., **70**, No. 4, 1991.
8. a. F. Uchikawa, H. Zheng, K. C. Chen, and J. D. Mackenzie, High-Temperature Superconductors II, Extended abstracts, 89, MRS (1988). b. T. Umeda, H. Kozuka, and S. Sakka, Adv. Cer. Mat., **3** [5], 520 (1988). c. H. Zhuang, H. Kozuka, and S. Sakka, Jap. J. Appl. Phys., **28** [10], L1805 (1989). d. S. Katayama and M. Sekine, J. Mater. Res., **6**, No. 8, Aug 1991
9. T. Goto and T. Sugishita, J. Mater. Res., **7**, No.1, Jan 1992
10. T. Kumagai, H. Yokota, K. Kawaguchi, W. Kondo, and S. Mizuta, Chem.Lett., 1465 (1987).
11. H. Nasu, S. Makida, T. Kato, Y. Ibara, T. Imura, and Y. Osaka, Chem. Lett., 2403 (1987).
12. T. Kumagai, W. Kondo, H. Yokota, H. Minamiue, and S. Mizuta, Chem. Lett., 1465 (1987).
13. C. E. Rice, R. B. van Dover, and G. J. Fisanick, Appl. Phys. Lett., **51** [22], 1842 (1987)
14. A. H. Hamdi, J. V. Mantese, A. L. Micheli, R. C. O. Laugal and D. F. Dungan, Appl. Phys. Lett., **51** [25], 2152 (1987).

15. M. E. Gross, M. Hong, S. H. Liou, P. K. Gallagher, J. Kwo, Appl. Phys. Lett., **52**, 160 (1988).
16. A. Gupta, R. Jagannathan, E. I. Cooper, E. A. Giess, J. I. Landman, and B. W. Hussey, Appl. Phys. Lett., **52** [24], 2077 (1988).
17. D. F. Vaslow, G. H. Dieckmann, D. D. Elli, A. B. Ellis, D. S. Holmes, A. Lefkow, M. MacGregor, J. E. Nordman, M. F. Petras, and Y. Yang, Appl. Phys. Lett., **53** [4], 324 (1988).
18. W. W. Davison, S. G. Shyu, and R. C. Buchanan, Mat. Res. Soc. Symp. Proc., **99**, 289 (1988).
19. M. Klee, W. Brand, and J. W. C. de Vries, J. Cryst. Growth, **91**, 346 (1988).
20. M. Klee, G. M. Stollman, S. Stotz, and J. W. C. de Vries, Solid State Communications, **67** [6], 613 (1988).
21. H. Shimojima, K. Tsukamoto, and C. Yamagishi, Jap. J. Appl. Phys., **28** [2],L226 (1989).
22. Y. L. Chen, J. V. Mantese, A. H. Hamidi, and A. L. Micheli, J. Mat. Res., **4** [5], 1065 (1989).
23. a. H. M. O'Bryan, P. K. Gallagher, R. A. Laudise, A. J. Caporaso, and R. C. Sherwood, J. Am. Ceram. Soc., **72**, 1298-1300 (1989). b. T. B. Lindemer, J. F. Hunley, J. E. Gates, A. L. Sutton, Jr., J. Brynestad, C. R. Hubbard, P. K. Gallagher, J. Am. Ceram. Soc., 72, 1775-1788 (1989).
24. M. G. B. Drew, D. A. Edwards, and R. Richards, J. C. S. Chem. Comm., 124 (1973).
25. a. G. E. Legrow, T. F. Lim, J. Lipowitz, R. S. Reaoch, Mat. Res. Soc. Symp. Proc., **73**, 553 (1986). b. B. G. Penn, F. E. Ledbetter III, J. M. Clemons, and J. G. Daniels, J. Appl. Polym. Sci., **27**, 3751 (1982). c. D. Seyferth and G. H. Wiseman, Ultrastructure Processing of Ceramics, Glasses and Composites, p265 (1984). d. A. W. Chow, R. D. Hamlin, Y, Blum, and R. M. Laine, J. Polym. Sci. C, **26**, 103 (1988). e. K. B. Schwartz, D. J. Rowecliffe, Y. D. Blum, and R. M. Laine, Mat. Res. Soc. Symp. Proc., **73**, 407 (1986). f. K. A. Youngdahl, R. M. Laine, R. A. Kennish, T. R. Cronin, and G. A. Balavoine, Mat. Res. Soc. Symp. Proc., **121**, 489 (1988).
26. See for example, D. A. Edwards and R. Richard, J. C. S. Dalton, 2403 (1973).
27. D. A. Edwards and R. Richard, Inorg. Nucl. Chem. Letters, **8**, 783 (1972).
28. A. H. Hamdi, J. V. Mantese, A. L. Micheli, R. C. O. Laugal and D. F. Dungan, Appl. Phys. Lett., **51**, [25], 2152 (1987).
29. a. N. N. Sauer, E. Garcia, K. V. Salazar, R. R. Ryan, and J. A. Martin, J. Am. Chem. Soc., **112**, 1424 (1990). b. R. F. Baggio, P. K. de Perazzo, and G. Polla, J. Solid State Chem., **56**, 298 (1985). c. R. F. Baggio, M. A. R. de Benyacar, P. K. de Perazzo, and G. Polla, J. Solid State Chem., **56**, 298 (1985).

Figure Captions

Figure 1. TGA of $Y(O_2CCHMe)_3$, Heating Rate 5 °C/min to 900 °C in N_2, Air and O_2.

Figure 2. TGA of $Cu(O_2CCHMe)$. Heating Rate 5 °C/min to 900 °C in O_2.

Figure 3. TGA of $Cu(O_2CCHMe)_2$. Heating Rate 5 °C/min to 900 °C in Air.

Figure 4. DTA of $Cu(O_2CCHMe)_2$. Heating Rate 5 °C/min to 900 °C in Air.

Figure 5. TGA of System 2 Precursor. Heating Rate 5 °C/min to 900 °C in Air.

Figure 6. XRD Pattern of System 2. Precursor Pyrolyzed in N_2 to Various Temperatures.

Figure 7. DRIFT Spectra of Precursor Pyrolyzed in N_2 to Various Temperatures.

Figure 8.XRD Pattern of Precursor Pyrolyzed in Air to Various Temperatures.

Figure 9. DRIFT Spectra of Precursor Pyrolyzed in O_2 to Various Temperatures.

Figure 10. SEM of System 2 Precursor Fiber.

Figure 11.SEM of System 2 Precursor Fiber Cured in N_2 to 500°C.

Figure 12. SEM of System 2 Precursor Fiber Cured in N_2 to 500°C, and Then Pyrolyzed in Air to 900 °C.

Figure 13. SEM of Precursor Fiber Cured in Air to 500°C.

Figure 14. SEM of Precursor Fiber Pyrolyzed in Air to 900°C.

Figure 15.SEM of Precursor Fiber Pyrolyzed in Air to 930°C.

Figure 16. SEM of Precursor Fiber Pyrolyzed in Air to 950°C.

Figure 17. XRD of Precursor Powder Pyrolyzed in Air to 500°C for 0.5 h.

Figure 18.Flux Exclusion of Precursor Fiber Pyrolyzed in Air to 900°C and Then Soaked at 450°C in O_2 for 24 h.

Figure 19. Flux Exclusion of Precursor Fiber Pyrolyzed in air to 400°C, in O_2 to 910°C for 8 h, and Then Tempered at 450°C in O_2 for 24 h.

Figure 20. SEM of Fiber Pyrolyzed in air to 400°C, in O_2 to 910°C for 8 h, and then tempered at 450 °C in O_2 for 24 h.

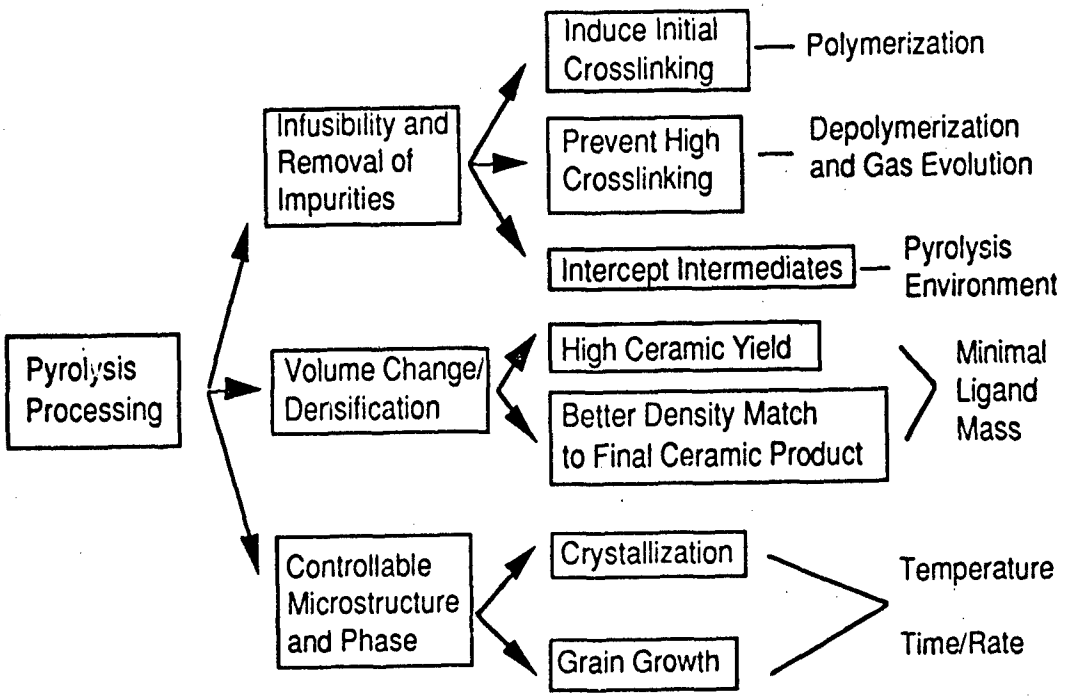

Scheme I. Problem Areas for Precursor Fiber Pyrolysis

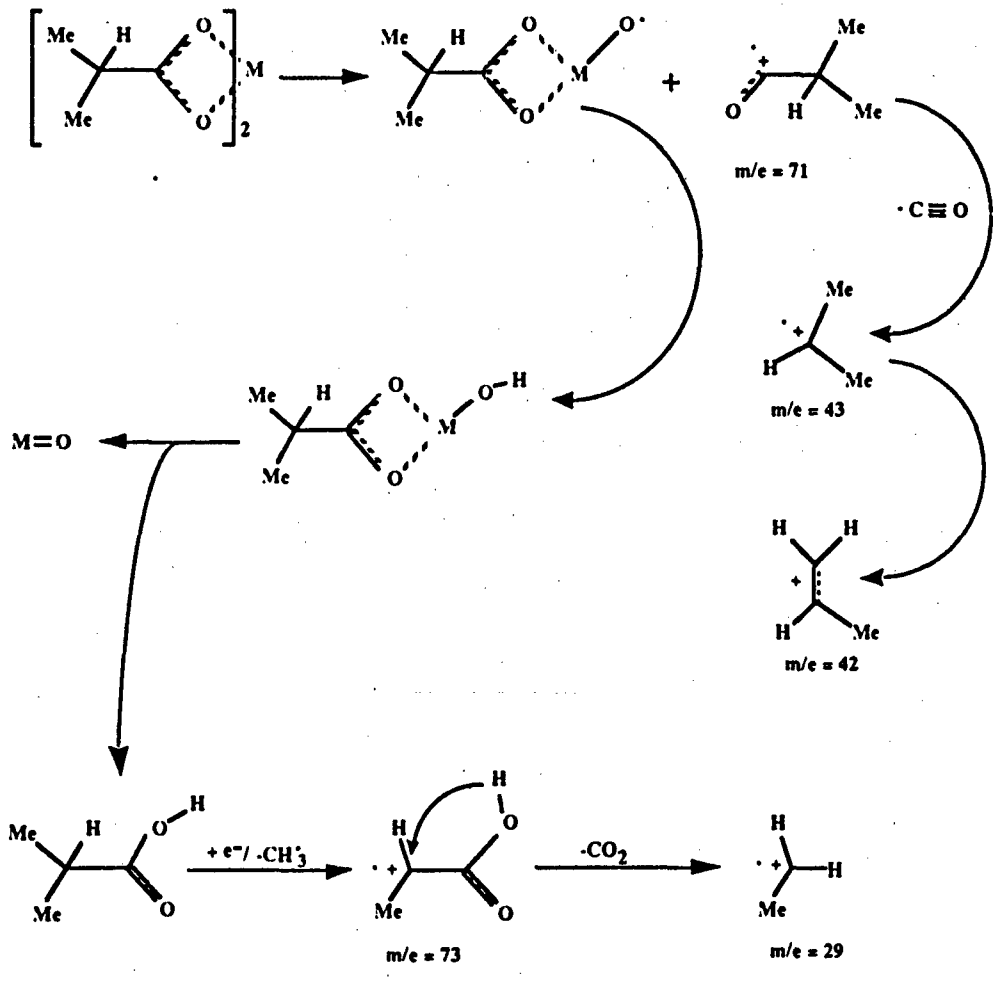

Scheme II. Decomposition Pathways Suggested for Ba and Y Isobutyrates.

Compound	Ceramic Yield Wt. % (Theory)	Decomp Product[a] % Metal (Theory)	Product
$Y(O_2CCHMe_2)_3$	32.2 (32.2)	78.8 (78.7)	Y_2O_3
$Ba(O_2CCHMe_2)_2$	61.4 (63.4)	70.6 (69.6)	$BaCO_3$
$Ba[O_2CCH(Et)(CH_2)_3CH_3]_2$	45.9 (46.6)	70.4 (69.6)	$BaCO_3$
$Cu(O_2CCHMe_2)_2$	29.5 (33.5)	78.5 (79.9)	CuO

Table I. TGA Results for Selected Metal Carboxylates. Heating rates used were 5°C/min in air to 900°C. a. Determined by chemical analysis (see experimental procedures).

Compound	O_2 (°C)	Air (°C)	N_2 (°C)
$Y(O2CCHMe_2)_3$	230-340	230-290	300-420
$Ba(O_2CCHMe_2)_2$	260-315	250-340	250-510
$Ba[O_2CCH(Et)(CH_2)_3CH_3]_2$	240-270	250-335	300-480
$Cu(O_2CCHMe_2)_2$	190-240	220-250	245-270

Table II. Decomposition Ranges Determined from TGA for Selected Metal Carboxylates. Heating rates were 5°C/min to a final temperature of 900°C. $Cu(O_2CCHMe_2)_2$ partially decomposes to Cu° in N_2.

Compounds	m/e (relative intensity)
Me_2CHCO_2H	43(100) 41(42) 27(40) 73(22) 39(15) 45(14) 42(11) 29(9)
$Ba(O_2CCHMe_2)_2$	28(100) 44(48) 32(27) 43(26) 49(24) 41(21) 18(21) 84(16) 31(14) 27(13) 29(12) 39(8) 73(7)
$Cu(O_2CCHMe_2)_2$	43(100) 41(51) 73(25) 27(23) 44(17) 41(15) 42(14) 18(13) 39(12)
$CH_3(CH_2)_3CH(Et)CO_2H$	88(100) 73(70) 57(29) 41(24) 79(18) 27(17) 43(16) 116(15)
$Ba[O_2CCH(Et)(CH_2)_3CH_3]_2$	28(100) 41(52) 73(50) 44(48) 88(34) 27(34) 42(33) 29(32) 43(32) 57(30) 55(24) 101(7) 116(7)
$Y[O_2CCH(Et)(CH_2)_3CH_3]_2$	73(100) 28(90) 88(79) 41(62) 44(55) 57(48) 43(40) 29(39) 27(38) 55(33) 87(21) 101(19) 116(12)
System 2	43(100) 73(86) 28(85) 41(77) 88(65) 44(50) 29(44) 55(44) 57(44) 27(40) 32(31) 87(19) 116(11)

Table III. Mass Spectral Fragmentation Patterns for Selected Metal Carboxylates. The insert probe was heated at a rate of 30 °C/min. No evidence was found for free acid in the unheated samples.

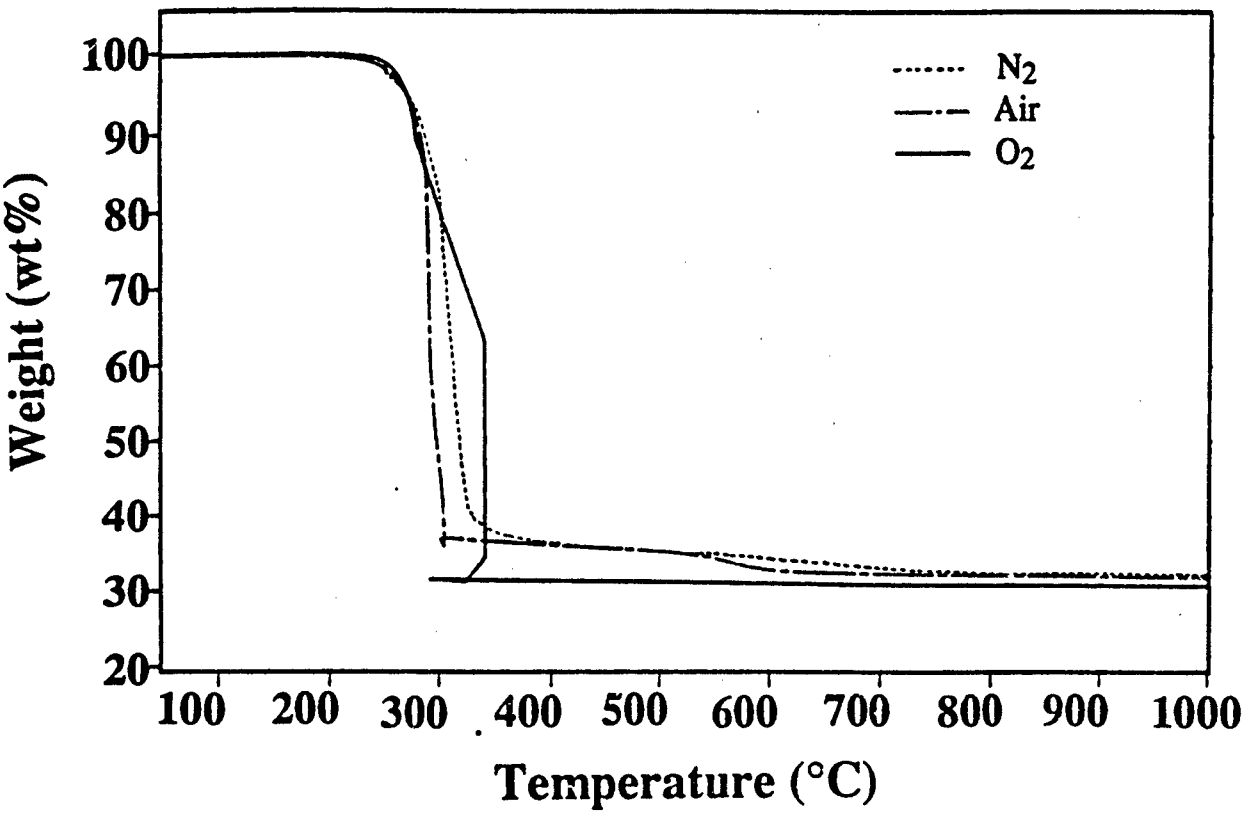
100
90
80
70
60
50
40
30
20
Weight (wt%)
100
200
300
400
500
600
700
800
900
1000
Temperature (°C)
N2
Air
O2

Figure 1

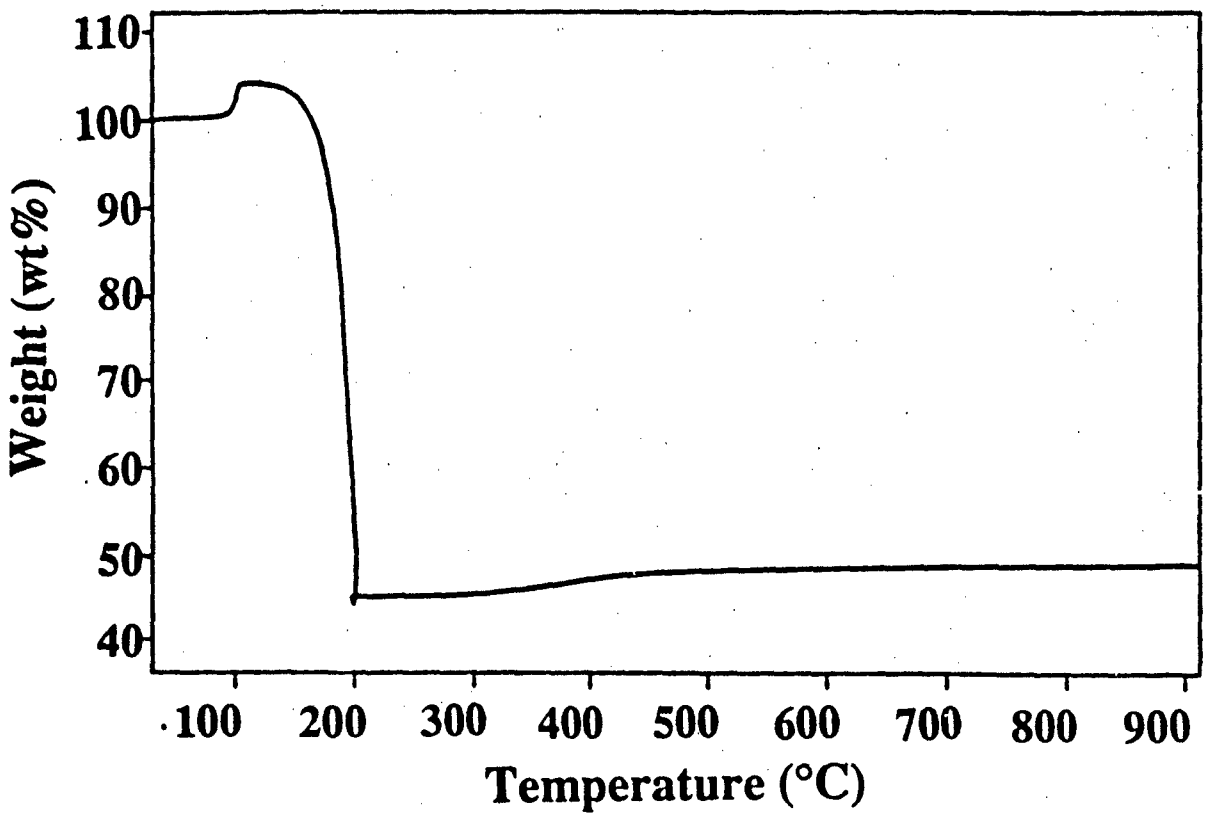
110
100
90
80
70
60
50
40
Weight (wt%)
100
200
300
400
500
600
700
800
900
Temperature (°C)

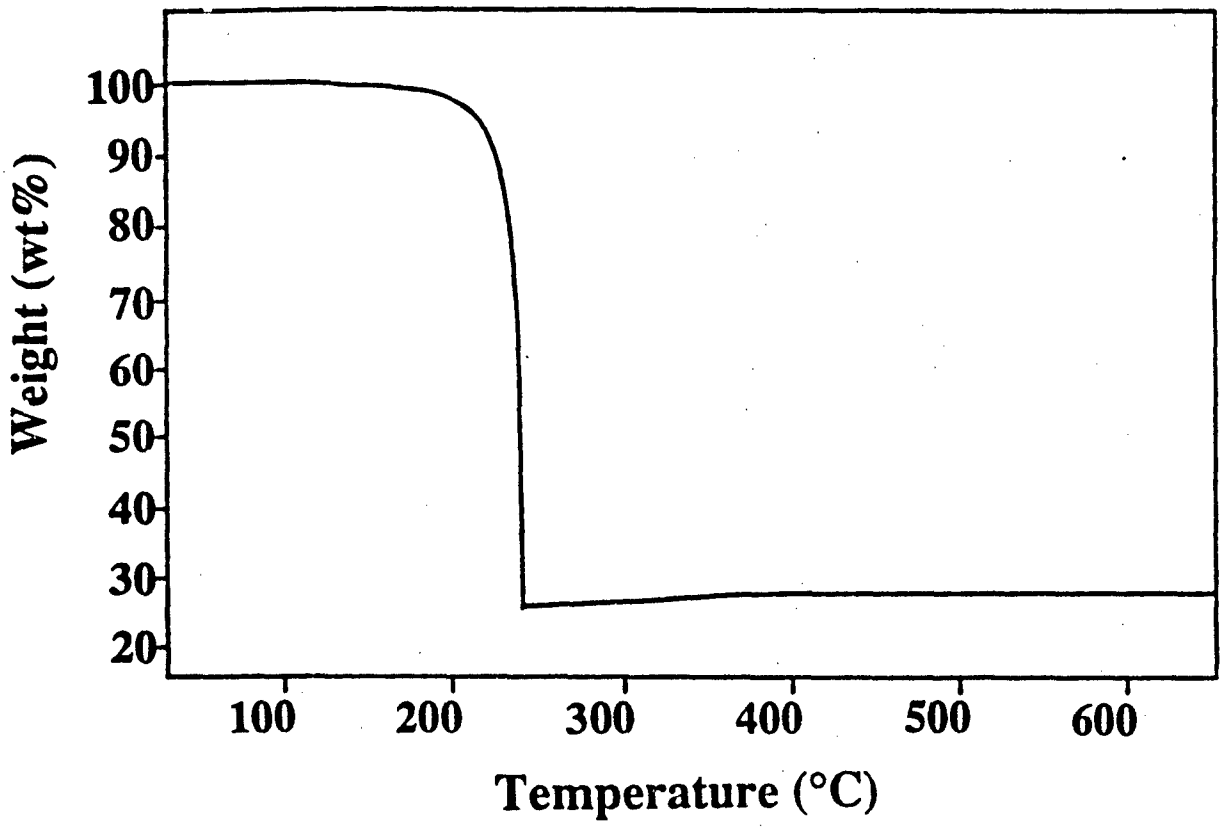
Weight (wt%)
100
90
80
70
60
50
40
30
20
100
200
300
400
500
600
Temperature (°C)

Figure 3

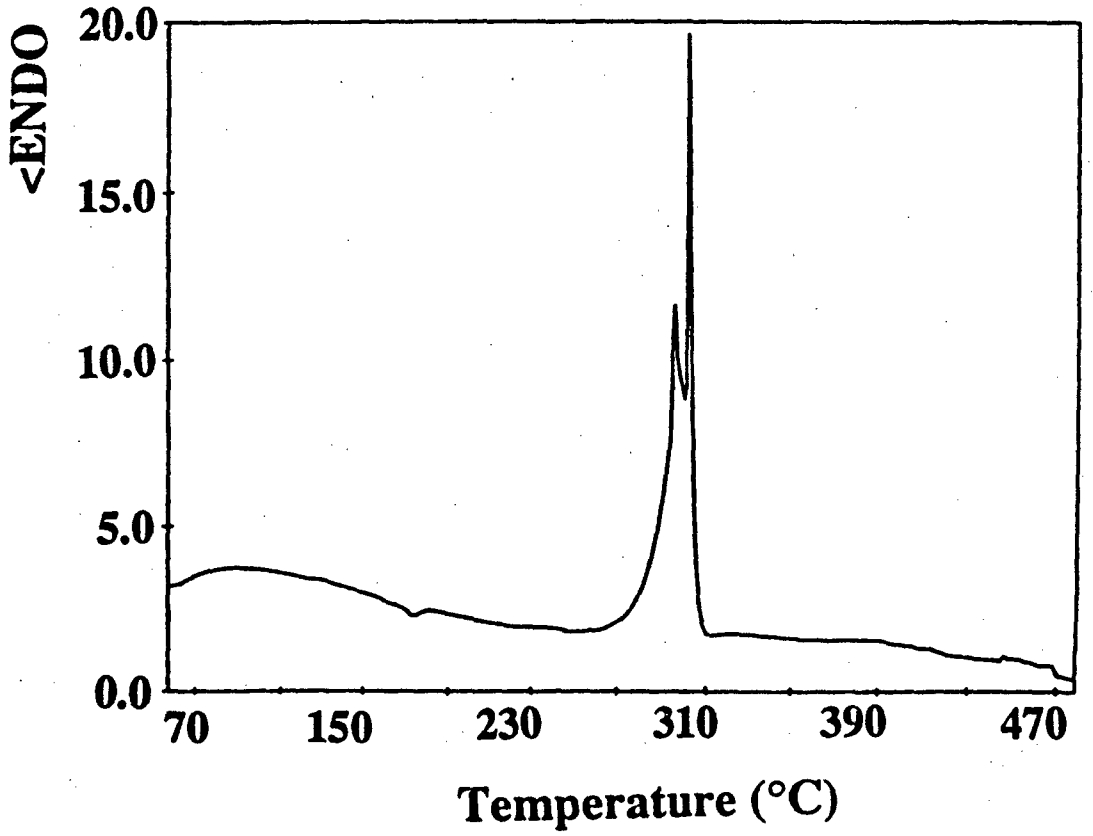

Figure 1

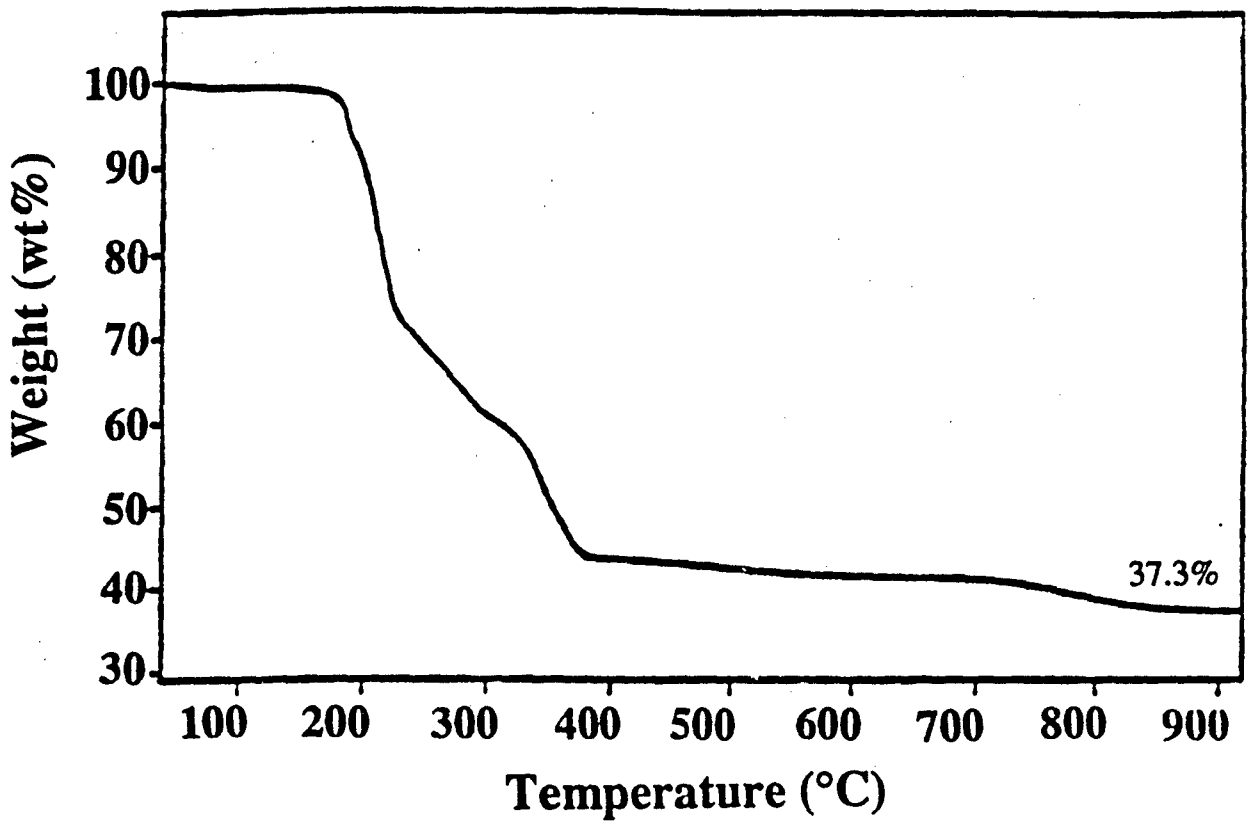
Weight (wt%)
100
90
80
70
60
50
40
30
37.3%
100
200
300
400
500
600
700
800
900
Temperature (°C)

Figure 5

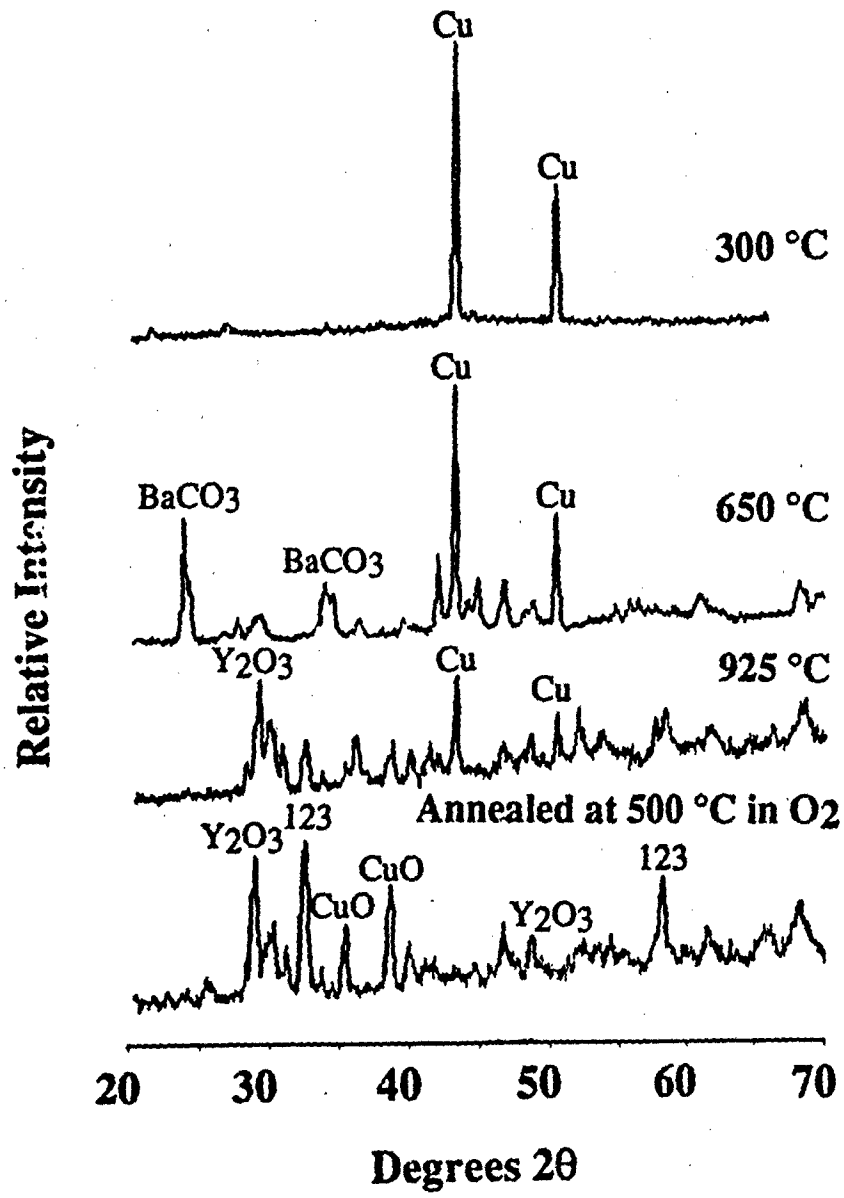
Cu
Cu
300 °C
Cu
BaCO3
Cu
650 °C
BaCO3
Y2O3
Cu
Cu
925 °C
Annealed at 500 °C in O2
Y2O3
123
CuO
CuO
Y2O3
123
Relative Intensity
20
30
40
50
60
70
Degrees 2θ

Figure 6

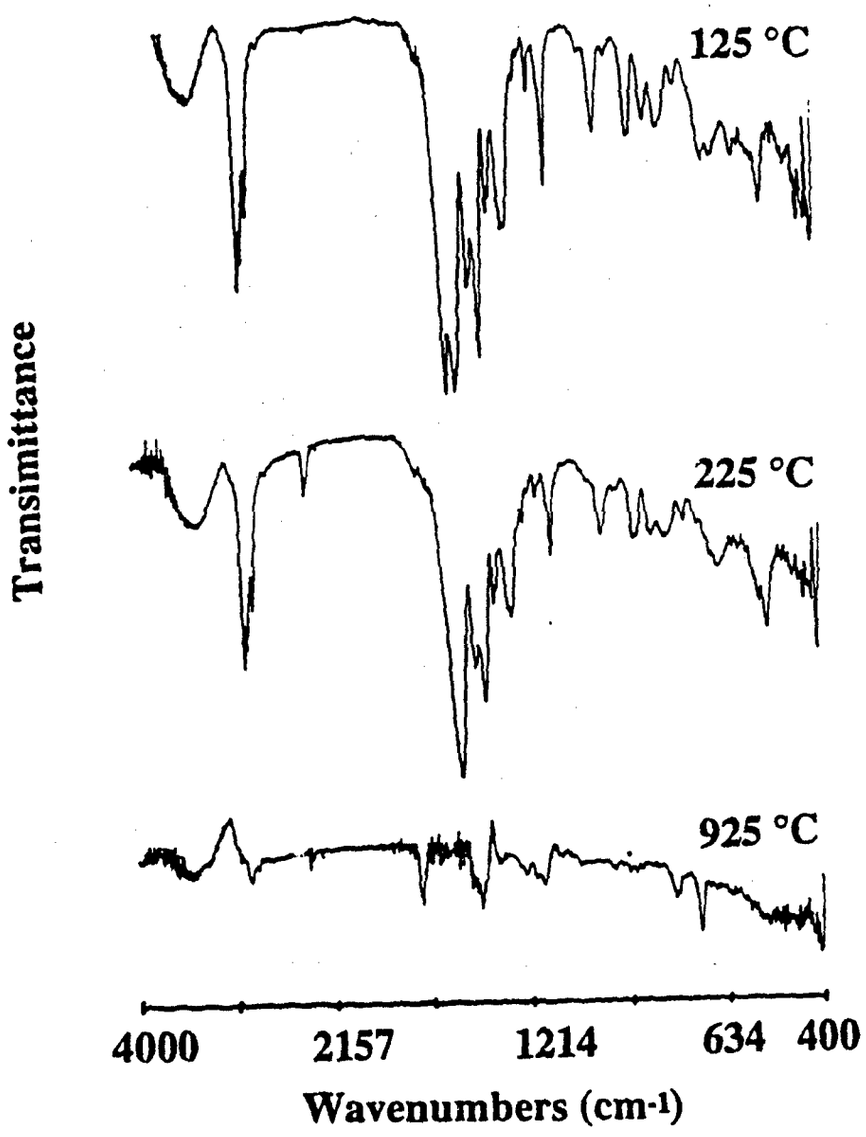
125 °C
225 °C
925 °C
Transimittance
4000
2157
1214
634
400
Wavenumbers (cm-1)

Figure 7

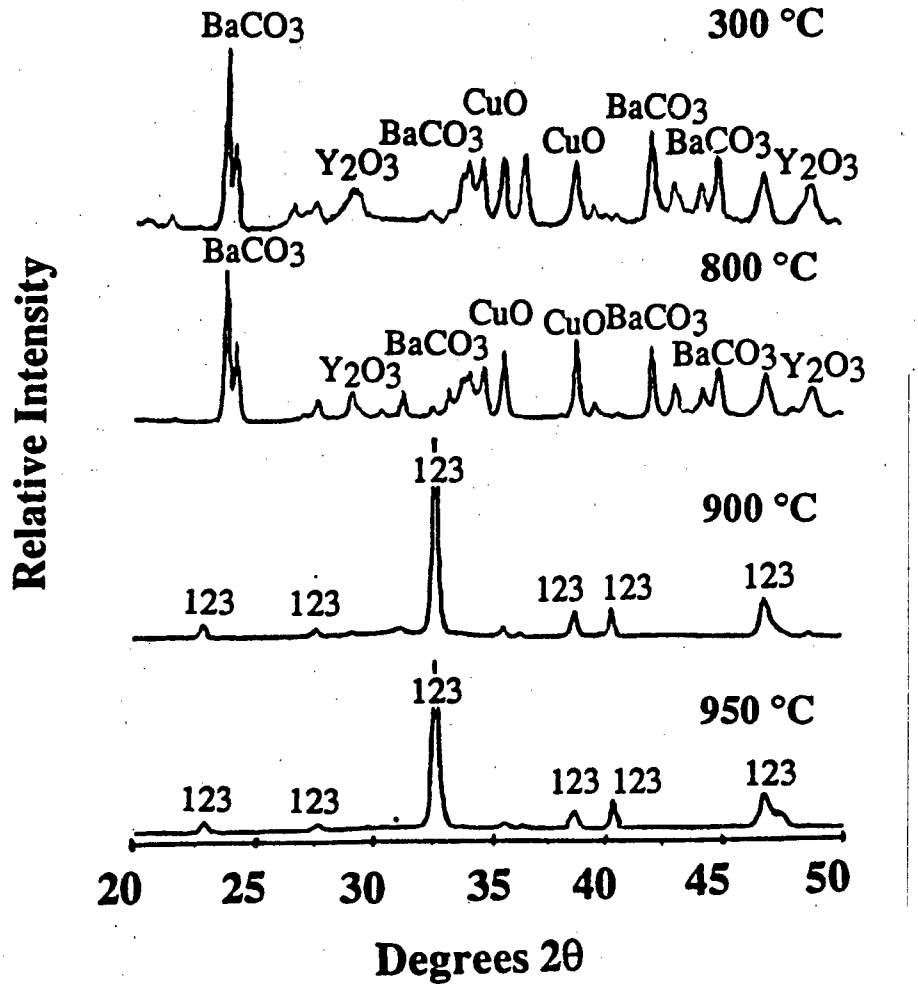
BaCO3
300 °C
CuO
BaCO3
BaCO3
CuO
BaCO3
Y2O3
BaCO3
Y2O3
800 °C
CuO
CuO
BaCO3
BaCO3
Y2O3
BaCO3
Y2O3
123
900 °C
123
123
123
123
123
123
950 °C
123
123
123
123
123
20
25
30
35
40
45
50
Relative Intensity
Degrees 2θ

FIGURE 6

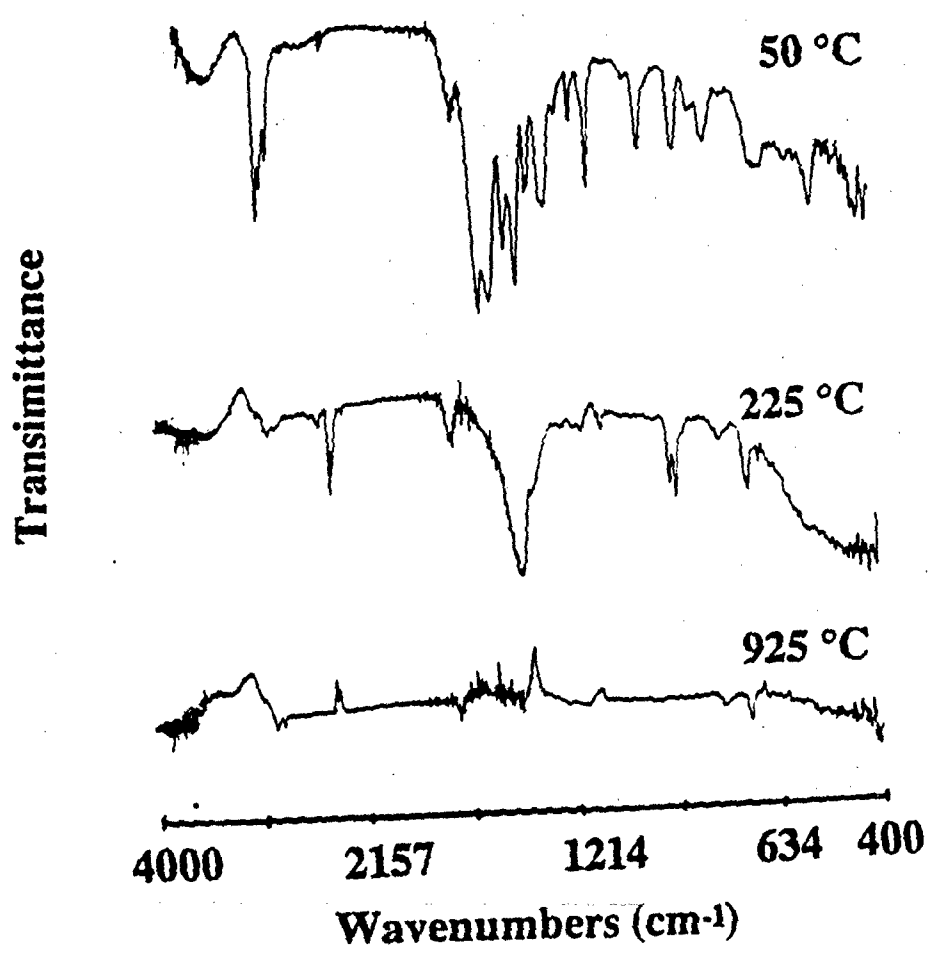
Transimittance
50 °C
225 °C
925 °C
4000
2157
1214
634
400
Wavenumbers (cm-1)

Figure 9

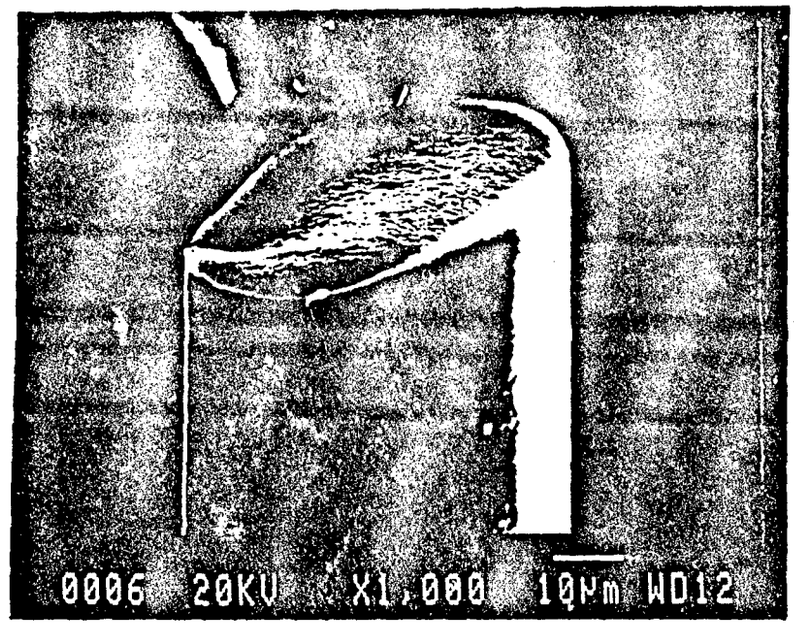

Figure 10

Figure 11

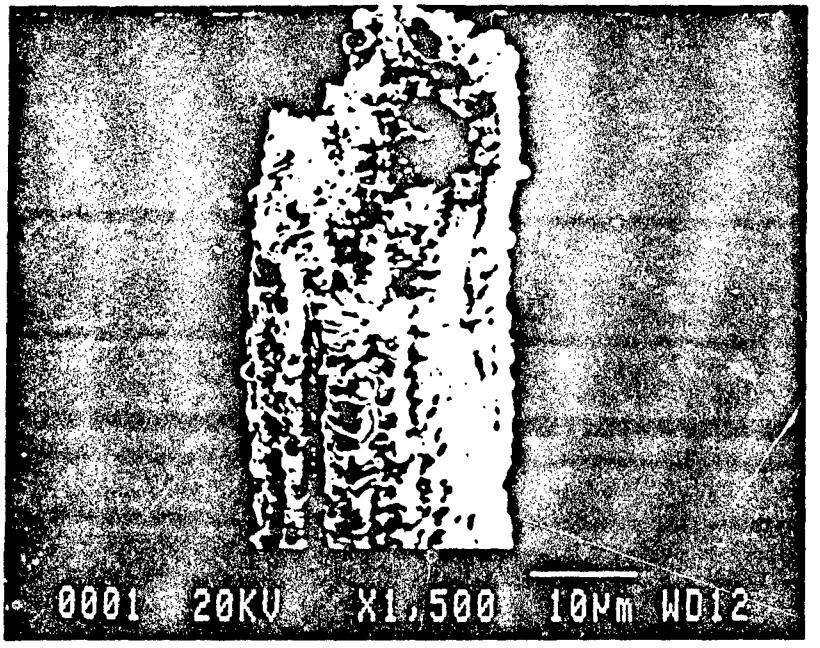

Figure 12

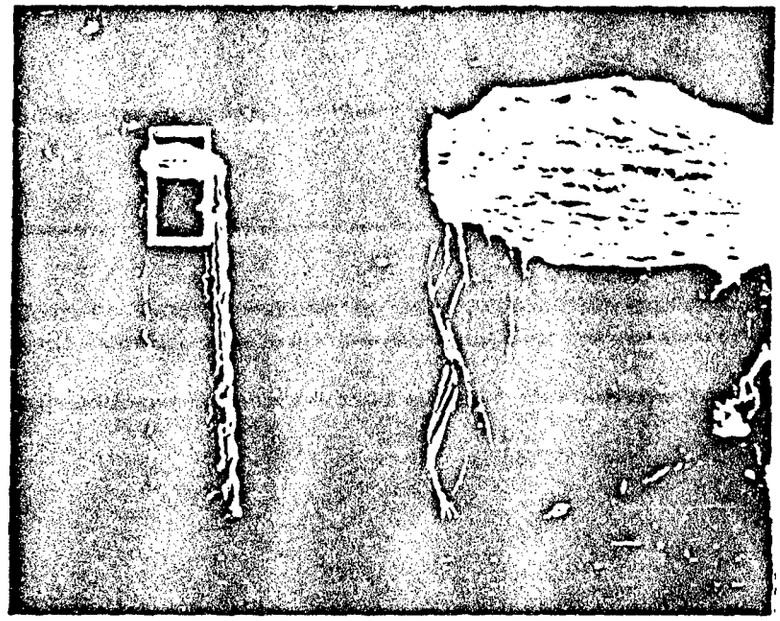

Figure 13

PAGES FIGURE 14

ARE

MISSING

IN

ORIGINAL

DOCUMENT

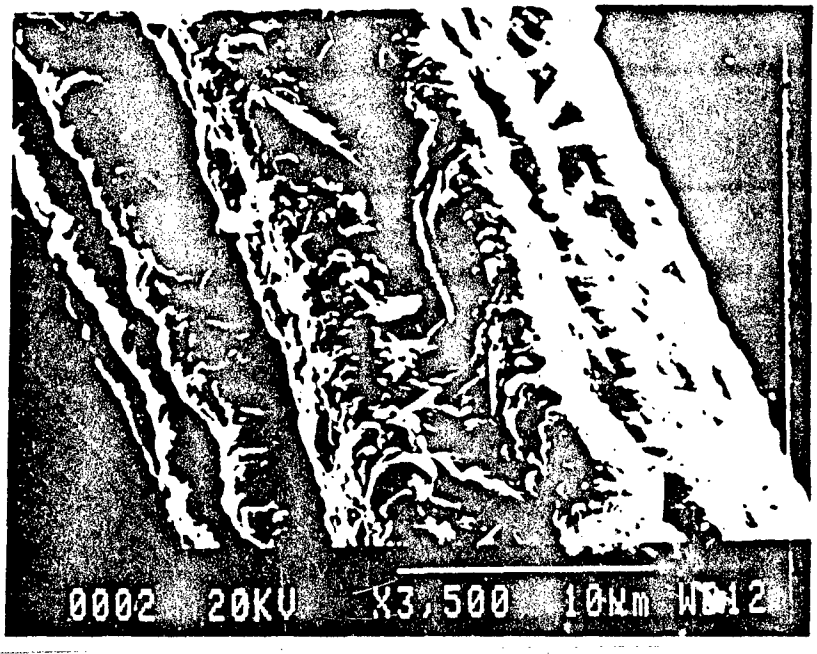

Figure 15

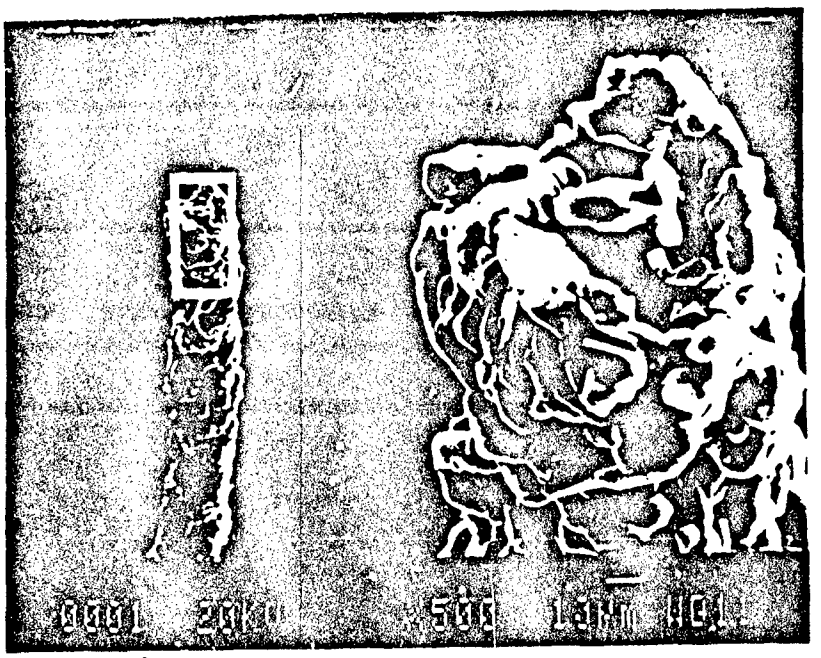

Figure 16

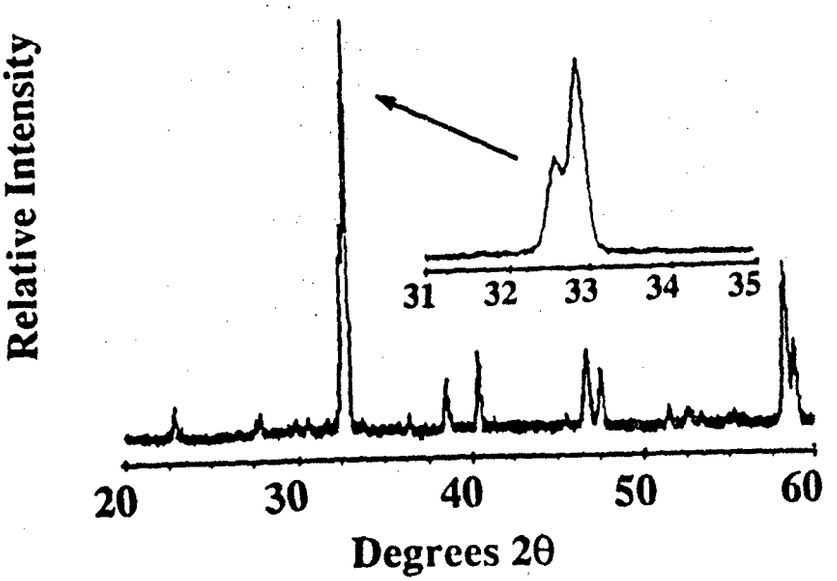

Figure 1

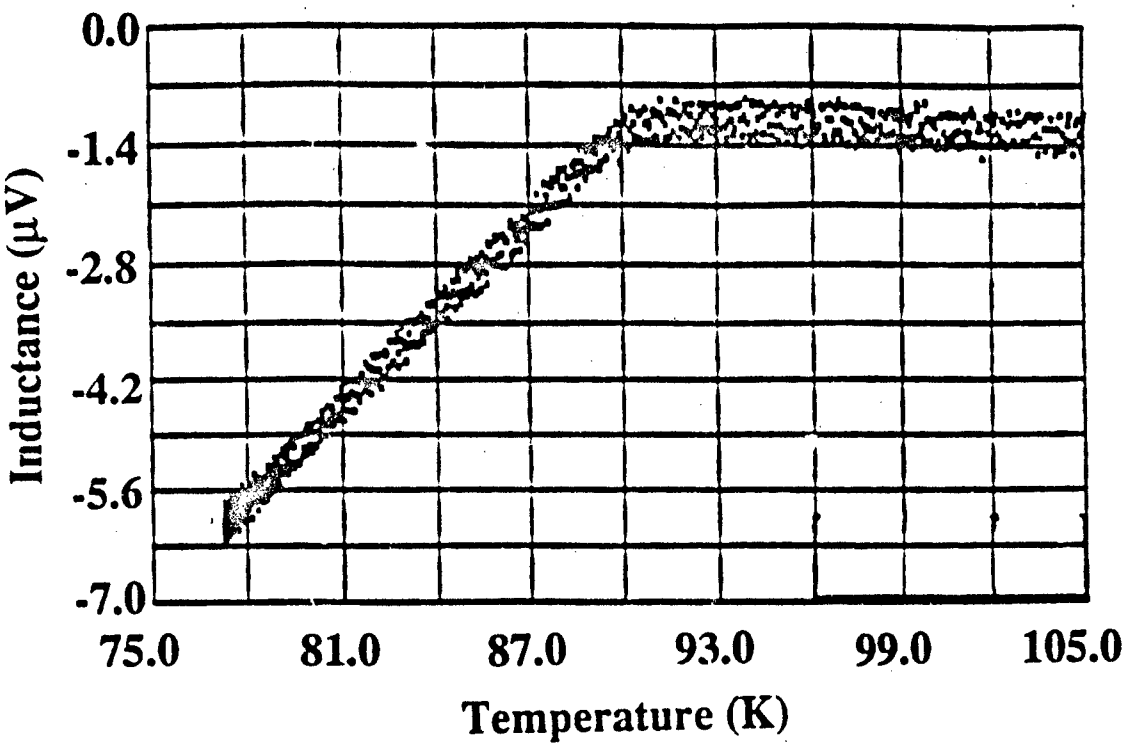
0.0
-1.4
-2.8
-4.2
-5.6
-7.0
Inductance (μV)
75.0
81.0
87.0
93.0
99.0
105.0
Temperature (K)

Figure 10

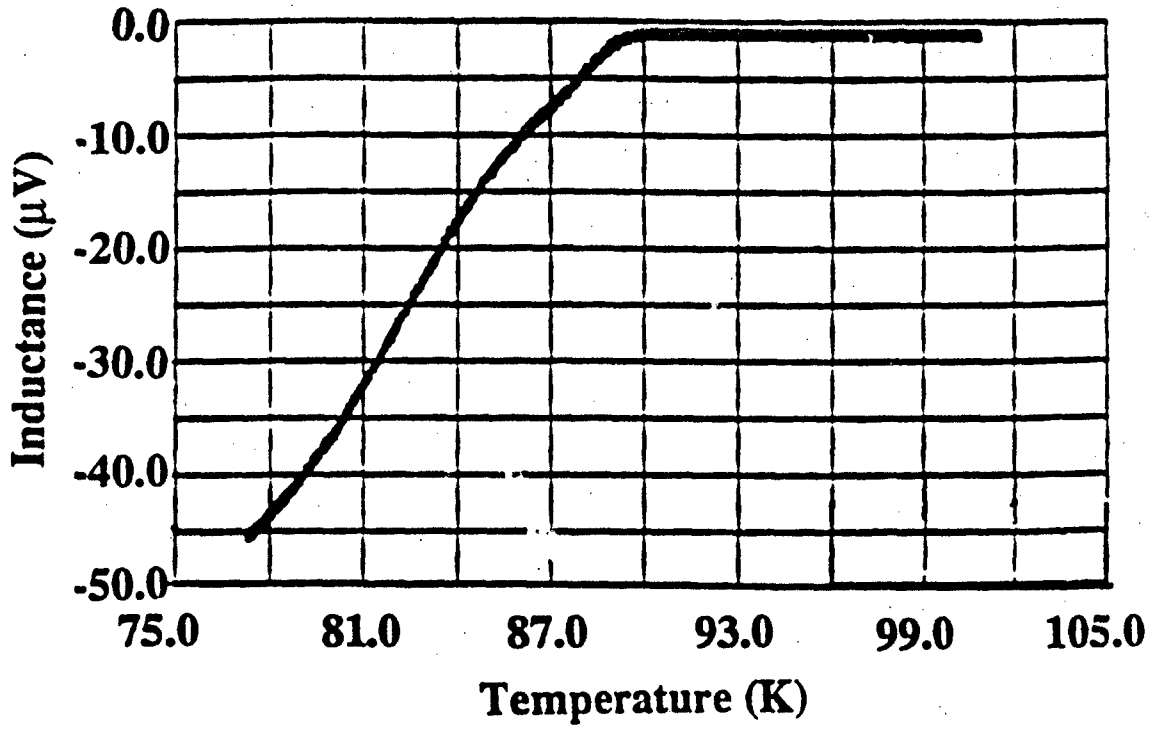
0.0
-10.0
-20.0
-30.0
-40.0
-50.0
Inductance (μV)
75.0
81.0
87.0
93.0
99.0
105.0
Temperature (K)

Figure 15

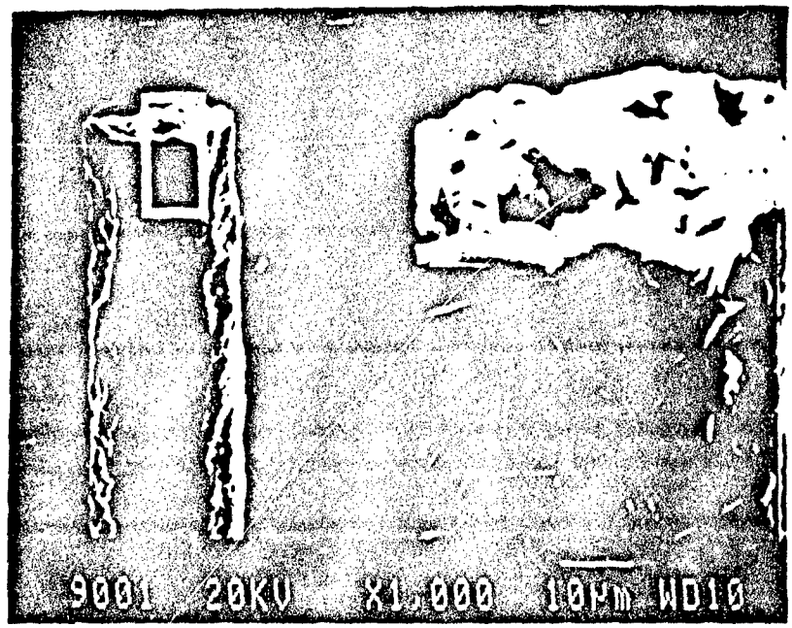

Figure 2J

APPENDIX 6

Mol. Cryst. Liq. Cryst., 1993, Vol. 225, pp. 153–165
Reprints available directly from the publisher
Photocopying permitted by license only

Printed in the United States of America

Thermotropic and Lyotropic Copolymers of Bis(Dioxyphenyl) Silanes

D. JEAN RAY,† RICHARD M. LAINE,†‡ TIMOTHY R. ROBINSON†

†Department of Materials Science and Engineering FB-10, University of Washington, Seattle, WA 98195, USA, ‡Department of Materials Science and Engineering, University of Michigan, Ann Arbor, MI 48109, USA

and

CHRISTOPHER VINEY§

Center for Bioengineering WD-12, University of Washington, Seattle, WA 98195, USA

(Received June 3, 1992)

Novel inorganic polymers are synthesized from two-component and three-component solutions of bis(1,2-dioxyphenyl) silane, bis(4-*t*-butyl-1,2-dioxyphenyl) silane and 1,4-dihydroxybenzene (hydroquinone). Molecular modeling predicts that these polymers have extended, linear conformations. Thermotropic nematic liquid crystalline phases are identified by transmitted polarized light microscopy. Additionally, lyotropic nematic phases are formed by polymers dissolved in xylene. Further characterization by diffuse reflectance infrared fourier transform (DRIFT) spectroscopy and differential scanning calorimetry is described.

Keywords: nematic, organometallic, silicon, polymer, thermotropic, lyotropic

INTRODUCTION

Almost all of the compounds known to form liquid crystalline phases are organic, with C, O, N and occasionally S acting as chain-building atoms in the mesogenic segments. Relatively few types of liquid crystalline materials contain organometallic or inorganic moieties, though the list continues to grow:

(a) Both WO_3 and V_2O_5 form anisotropic (also known as "tactoidal") gels[1]; in the latter case, the long range molecular order has been specifically identified as nematic.[2]
(b) Some small molecule liquid crystalline compounds containing a central tetrahedrally-coordinated Si-atom have been identified: di-*iso*-butylsilanediol, in which molecules are hydrogen-bonded as dimers that form a discotic

§To whom correspondence should be addressed.

arrangement,[3-5] and some tetrakis-siloxysilanes, that form thermotropic nematic and cholesteric phases.[6,7]

(c) Polysiloxane backbones[8] and polyphosphazene backbones (Reference 9, and citations therein) have been used in side-chain liquid crystalline polymers, where the side-chain mesogens are organic.

(d) Aromatic polyesters may be complexed with a metal center to yield smectic or other, unspecified, liquid crystalline phases.[10]

(e) Discotic mesophases may be formed by disk-like complexes that contain a central metal atom.[11-13] Lyotropic phases also form when such complexes are attached as pendant groups to a flexible organic backbone.[14]

(f) Lyotropic *main chain* polymers have been formed by extended chains consisting of acetylenes, phenyl groups, and palladium or nickel atoms.[15]

(g) Thermotropic nematic compounds containing square-planar coordinated Cu(II) atoms in the main chain have been synthesized.[16,17]

(h) Poly(di-*n*-alkyl silanes) thermotropically form columnar liquid crystalline phases.[18,19]

Only in cases (a), (g) and (h) do the inorganic components form a chain-building link in a *main chain thermotropic* polymer. In the present paper, we describe nematic phases formed by main chain random copolymers of biscatechol silane [i.e. bis(1,2-dioxyphenyl) silane] and bis(4-*t*-butyl-catechol) silane [i.e. bis(4-*t*-butyl-1,2-dioxyphenyl) silane]. In these compounds, the tetrahedrally coordinated Si-atoms are linked by pairs of 1,2-dioxyphenyl residues, some of which carry a 4-*t*-butyl group. We also describe the effect on nematic phase formation of replacing a minority of 1,2-dioxyphenyl residues with 1,4-dioxyphenyl groups, through reaction with hydroquinone.

There are several motives for seeking to incorporate a greater variety of elements in liquid crystalline polymers. In materials that are not conformationally rigid (including those discussed here), the formation of liquid crystalline phases depends on the stabilization of shape anisotropy by inter- and intramolecular forces. Our ability to model and predict this type of behavior is predicated on the careful characterization of as diverse a range of chemical compounds as possible. Also, exploration of organometallic and inorganic liquid crystalline polymers is expected to lead to new, processable materials that can be cross-linked for high temperature applications, and the presence of heteroelements in the polymer backbone will promote an extended variety of useful physical properties.

SYNTHESIS

Handling Procedures

Inert atmosphere procedures[20] were followed in all syntheses to avoid product hydrolysis to catechol and SiO_2. Schlenk glassware and a Vacuum Atmospheres (MO40-2) glovebox were used. All procedures were conducted under dry nitrogen.

Polymer Precursors

Catechol, 4-*t*-butyl-catechol and $SiCl_4$ were obtained from Aldrich Chemical Company. Preparation of biscatechol silane from $SiCl_4$ and catechol followed the Allcock synthesis[21] (Scheme I). The synthesis of bis(4-*t*-butyl-catechol) silane is analogous[22] (Scheme I). The ^1H NMR, ^{13}C NMR and IR spectra of these compounds are consistent with previously reported values.[22] Products were amorphous white powders.

Analysis for residual chlorine in the synthesized compounds was by a microchemical chloride test, using $AgNO_3$.[23] The results were negative, showing that only biscatechol compounds (no dichloro monocatecholato silanes) were produced in the above syntheses.

Preparation of Copolymers

Biscatechol silane and bis(4-t-butyl-catechol) silane. Polymerization was performed in solution, to facilitate mixing. Biscatechol silane and bis(4-*t*-butyl-catechol) silane (0.1–0.3 gm each in the range 93:7 to 33:67 mole%) were weighed in the drybox and placed in suitable Schlenkware. 15–25 ml of dry chloroform (distilled from $MgSO_4$) or dry xylene (distilled from Na) was cannulated into the flask containing the dry reactants under N_2. The reaction mixture was cycled between vacuum and N_2 several times before refluxing under N_2. After refluxing for 90 hours, the solvent was removed by vacuum distillation. Copolymers were yellow to light brown glassy to resinous solids. In order to observe lyotropic liquid crystalline behavior with solvent, these solutions were vacuum distilled only to the point where a gummy or soft residue remained.

Biscatechol silane and hydroquinone. Hydroquinone was obtained from Aldrich Chemical Company. Synthesis was as above, (range 50:50 to 91:9 mole%). Hydroquinone provides 1,4-dioxyphenyl groups that partially or wholly replace 1,2-dioxyphenyl groups (Scheme II). Solids precipitated rapidly from xylene solution and more slowly (one hour) from chloroform. The resulting white solids are easily isolated by filtration and vacuum drying.

Bis(4-t-butyl-catechol) silane and hydroquinone. Synthesis was as above (reac-

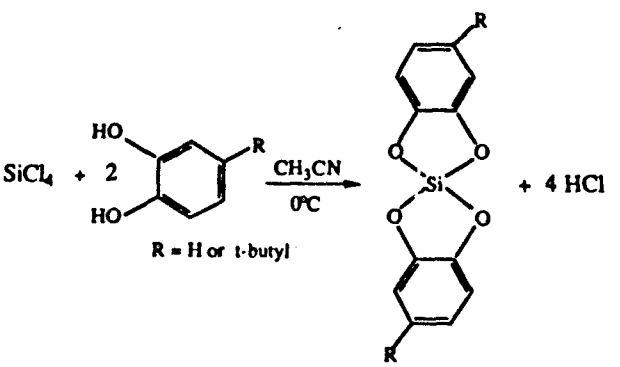

SCHEME I

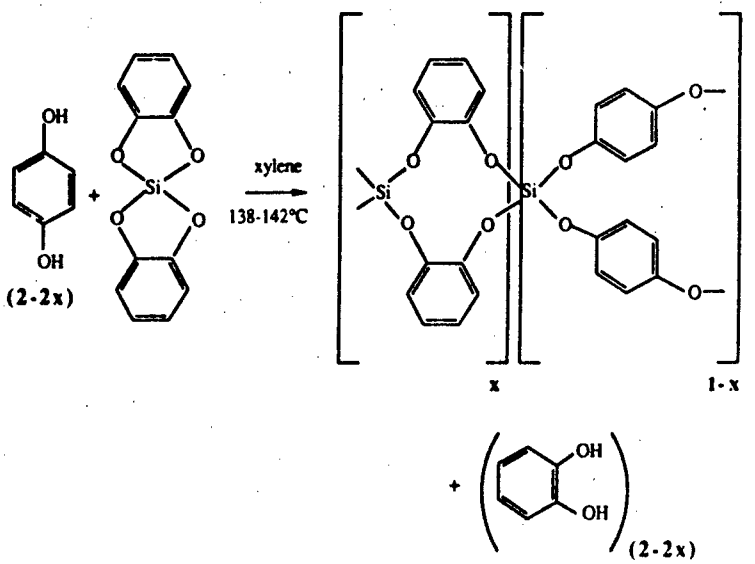

$$Si\,(1,2\ O\text{-}C_6H_4\text{-}O)_2 + (2\text{-}2x)\,(1,4\ HO\text{-}C_6H_4\text{-}OH) \longrightarrow$$

$$[Si\,(1,2\ O\text{-}C_6H_4\text{-}O)_2]_x\ [Si\,(1,4\ O\text{-}C_6H_4\text{-}O)_2]_{1-x} + (2\text{-}2x)\,(1,2\ HO\text{-}C_6H_4\text{-}OH)$$

SCHEME II

tant concentrations 52:48 and 91:9 mole%). White solids were precipitated slowly from solution after 48 hours refluxing in xylene.

Biscatechol silane, bis(4-t-butyl-catechol) silane and hydroquinone. Synthesis was as above, with the initial monomer concentrations in the ranges 29–67 mole% biscatechol silane, 20–67 mole% bis(4-*t*-butyl-catechol) silane and 4–33 mole% hydroquinone. At initial hydroquinone concentrations exceeding 9 mole%, solids precipitated during the polymerization in xylene. The solution becomes cloudy, then solids are formed that may be fibrous and adhere to the sides of the container or the stir bar. At 67 mole% biscatechol silane, the reaction solution becomes cloudy within 30 min. of refluxing (138–142°C). The cloudy solution begins to generate precipitate immediately. In contrast, with 67 mole% bis(4-*t*-butyl-catechol) silane, approx. 48 hours of reflux are required before the appearance of a cloudy solution and subsequent gelation. This observation, i.e. that the reaction proceeds more rapidly for higher starting concentrations of biscatechol silane relative to bis(4-*t*-butyl-catechol) silane, is consistent with 4-*t*-butyl-catechol residues providing a greater degree of steric hindrance to attack by hydroquinone.

After refluxing for 72–90 hours, solids present (melting at high temperatures >500°C) were recovered by filtration under N_2 and liquids were evaporated under vacuum. Yellow to brownish polymers and also 1,2 dihydroxybenzene (catechol) were recovered from the liquid phase (Scheme III).

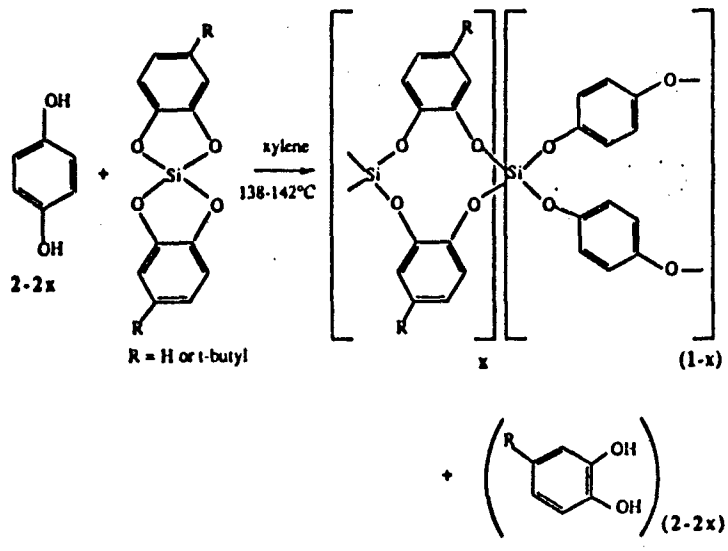

$$Si(1,2\ O\text{-}C_6H_4\text{-}O)_2 + Si[1,2\ O\text{-}C_6H_3(t\text{-}Bu)\text{-}O]_2 + (4-2x-2y)(1,4\ HO\text{-}C_6H_4\text{-}OH) \longrightarrow$$

$$[Si(1,2\ O\text{-}C_6H_4\text{-}O)_2]_x\ [Si[1,2\ O\text{-}C_6H_3(t\text{-}Bu)\text{-}O]_2]_y\ [Si(1,4\ O\text{-}C_6H_4\text{-}O)_2]_{2-x-y} + (4\text{-}2x\text{-}2y)(1,2\ HO\text{-}C_6H_4\text{-}OH)$$

SCHEME III

CHARACTERIZATION METHODS

^1H and ^{13}C nuclear magnetic resonance (NMR) spectroscopy were performed on a Varian XL 300 MHz spectrometer. Proton NMR spectra were obtained with the spectrometer operating at 300 MHz using a 4000 Hz sweep width, 1 sec. relaxation delay time, 82° pulse width, and 16K data points. Carbon NMR spectra were obtained with the spectrometer operating at 75 MHz using 16,000 Hz sweep rate, 0.5 sec. relaxation delay time, 60° pulse width, and 16 K data points. Samples were prepared in the drybox.

Diffuse reflectance infrared fourier transform (DRIFT) spectra were recorded on an IBM FTIR-44 spectrometer. Instrument resolution was 2.00 cm^{-1}, with 32 scans over the region 4000 cm^{-1} to 400 cm^{-1}. Sample pellets were prepared in the drybox by grinding the sample with KBr in an agate mortar and pestle, then pressing a pellet using a Spectra-Tech Econo-Press. The DRIFT sample chamber was purged with N_2 until CO_2 absorbances were no longer detected. The IR peak positions were identified using standard IBM FTIR 40 series software.

Models were built using Chem3D Plus software (version 3.0; Cambridge Sci-

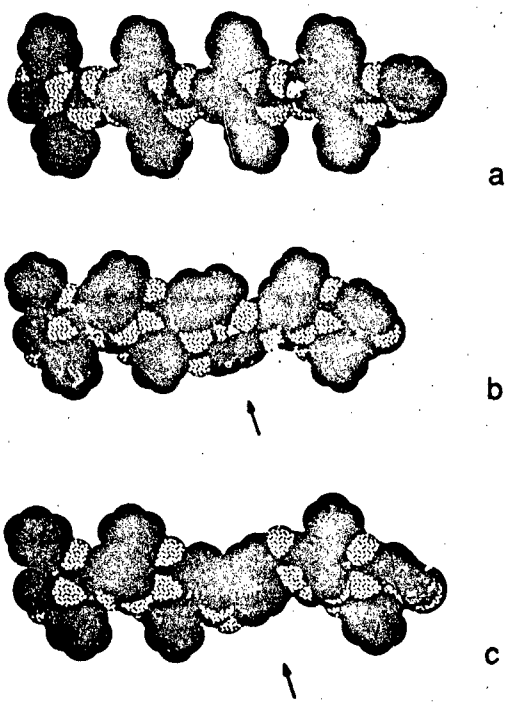

FIGURE 1 Conformation of molecules as predicted with Chem3D Plus software: (a) homopolymer of bis(1,2-dioxyphenyl) silane; (b) effect of replacing a single catechol residue with hydroquinone (arrow); (c) effect of substituting hydroquinone residues (arrow) for both catechol links between a pair of adjacent Si atoms.

entific Computing, Cambridge, MA) on a Macintosh IIci computer, to identify likely molecular conformations.

Light microscopy to identify and photograph liquid crystalline phases was performed on a Leitz Laborlux 12 POL polarizing microscope equipped with a Canon T90 camera. A Linkam 26-THM-600S heating/freezing stage with micromanipulator and 26-PR-600 controller were used to view microstructures at elevated temperatures (600°C maximum). Samples of the polymeric products were held between 18 mm diameter round coverslips, and were loaded into the heating stage in the drybox. The coverslips had previously been treated by a cleaning procedure similar to that recommended[24] as a general procedure for glass substrates used in liquid crystal microscopy. Coverslips were washed in 5% KOH/ethanol for one hour, rinsed in 5% H_2SO_4, followed by water and acetone rinses. They were then dried in a 120°C oven for one hour, and were stored in the drybox until used. All openings into the heating stage were sealed with rubber fittings, to retain the nitrogen atmosphere acquired in the drybox. Specimens on the heating stage were observed through a 32× (0.40 numerical aperture) objective lens, while specimens at ambient temperature could be observed at up to 100× (1.32 numerical aperture) with an oil immersion objective. Microstructures characteristic of elevated temperatures

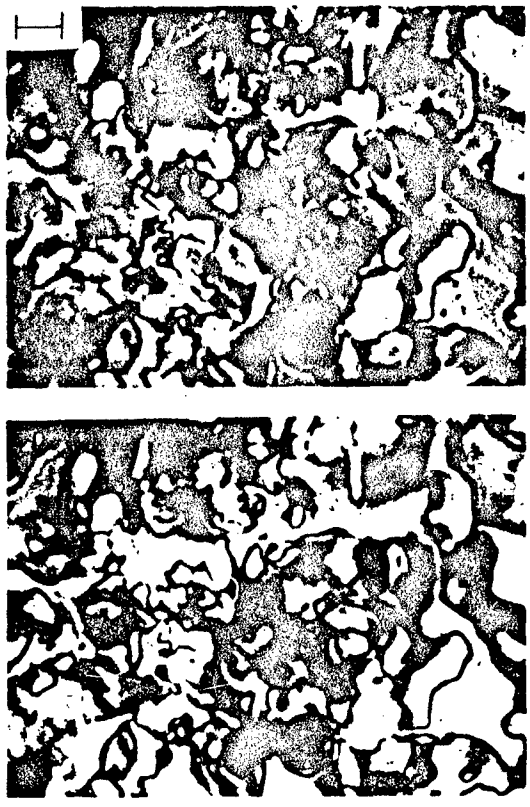

FIGURE 2 Thermotropic nematic schlieren texture of the soluble polymer obtained by reacting xylene solutions of biscatechol silane, bis(4-*t*-butyl-catechol) silane and hydroquinone in a 1:1:1 mole ratio. The specimen was quenched from 300°C. The scale bar represents 10 μm. Crossed polars rotated 15° between top and bottom micrographs.

were preserved to ambient temperature by quenching,[25] so that photomicrographs could be obtained at high resolution.

Thermal analysis was carried out with a Seiko Instrument Co. Differential Scanning Calorimeter DSC 100 (range 0°C–600°C) and SSC 5000 Series Thermal Analysis Disk Station. Specimens were 10 mg. (approximately) sealed samples scanned at 5°C/min or 10°C/min.

RESULTS AND DISCUSSION

Spectroscopic Characterization

The bis(1,2-dioxyphenyl) silane and bis(4-*t*-butyl-1,2-dioxyphenyl) silane polymer precursors were characterized by ^{1}H-NMR and DRIFT spectra. The NMR spectra

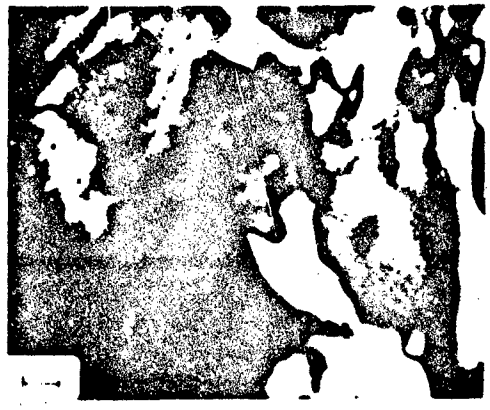

FIGURE 3 The microscopic mesomorphic texture of the soluble polymer obtained by reacting chloroform solutions of bis-catechol silane and bis-4-*t*-butyl-catechol silane in a 1:1 mole ratio. The specimen was quenched from 240°C. The scale bar represents 5 μm.

were compared to literature values[21] and the compounds were found to have no unreacted catechol and only minor solvent residue present. Samples stored in the drybox or in sealed vials were found to have an indefinite shelf life. This was confirmed by comparing the DRIFT spectra of both bis(1,2-dioxyphenyl) silane and bis(4-*t*-butyl-1,2-dioxyphenyl) silane with literature values.[21,22]

DRIFT spectra of the polymer products as recovered from both xylene and chloroform show that the polymers are susceptible to slow hydrolysis in air, but have an indefinite shelf life in the drybox. In all cases where hydroquinone was a reactant, DRIFT spectra of the polymer products confirm the participation of hydroquinone in the reaction: either the 1467 cm^{-1} component of the strong hydroquinone aromatic doublet at 1467–1515 cm^{-1} is missing or it is significantly reduced, and the 1515 cm^{-1} component is shifted slightly. Polymers retain the $\tilde{\nu}$ O—H (i.e., intermolecular O—H stretching) of hydroquinone at 3400–3600 cm^{-1}. More detailed polymer syntheses and spectroscopic characterization[26] will be published at a later date.

Molecular Modelling

The energy-minimized conformation predicted for the homopolymer of bis(1,2-dioxyphenyl) silane (Figure 1a) corresponds closely to the published x-ray structure.[27] The substitution of a single 1,2-dioxyphenyl group by a 1,4-dioxyphenyl group does not alter the linear, extended trajectory of the energy-minimized molecular conformation (Figure 1b). Even replacing both 1,2-dioxyphenyl bridges between adjacent Si atoms with 1,4-dioxyphenyl linkages does not change the overall rod-like aspect of the molecules (Figure 1c). Therefore, all the polymers described here are candidates for forming nematic phases, unless there is an overriding preference for crystallization. However, we expect that crystallization will be inhibited if there is no blockiness in the sequence of 1,2-dioxyphenyl and 1,4-dioxyphenyl linkages along the polymer chains.

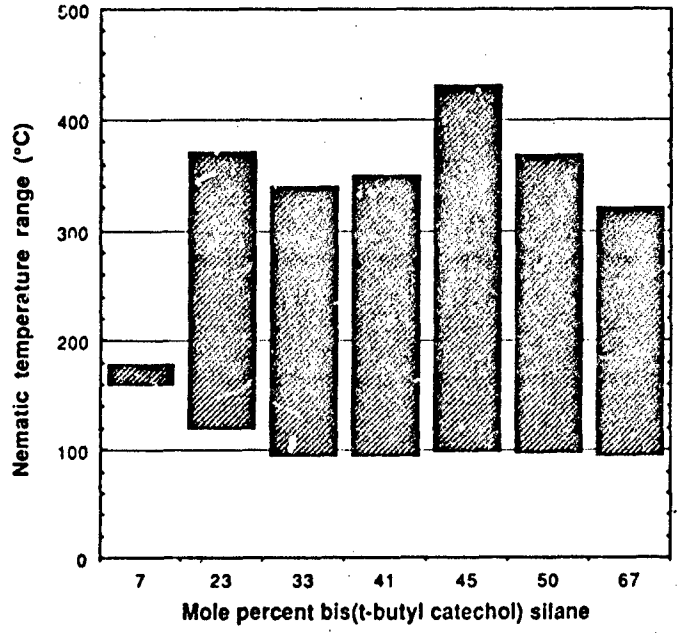

FIGURE 4 Nematic range of polymers prepared from xylene solutions of biscatechol silane and bis(4-*t*-butyl-catechol) silane. Data were obtained by transmitted polarized light microscopy of specimens on a sealed heating stage. The upper limit of the nematic range is masked by specimens tending to form homeotropic textures, and by the onset of degradation.

Transmitted Polarized Light Microscopy

No liquid crystalline phases were observed in samples of bis(1,2-dioxyphenyl) silane or bis(4-*t*-butyl-1,2-dioxyphenyl) silane when examined individually. This is consistent with the results of Eaborn and Hartshorne[3] that the dioxy silanes in general have not shown liquid crystalline behavior. Liquid crystalline phases also were not detected in homopolymers prepared from these individual monomers, or in co-polymers prepared from mixed solutions of bis(1,2-dioxyphenyl) silane and hydroquinone. In these cases, it appears that the molecular structure is sufficiently regular to promote crystallization relative to liquid crystallinity.

The remaining types of polymer formed thermotropic nematic phases, and additionally formed lyotropic nematic phases in xylene. The conditions giving rise to liquid crystallinity varied with (1) the ratio of monomers in the polymerization mixture; (2) the temperature at which the polymerization reaction occurred; and (3) the reaction (reflux) time.

All the nematic polymers demonstrated a strong tendency to form *homeotropic* textures, i.e. large areas of the microstructures are dark at all rotations of the crossed polars; the remaining areas of the microstructure exhibited either schlieren textures containing both integral-strength and half-integral-strength disclinations (Figure 2) or domain textures with inversion walls (Figure 3). Because samples were viewed in a sealed heating stage, we could not confirm the nematic nature

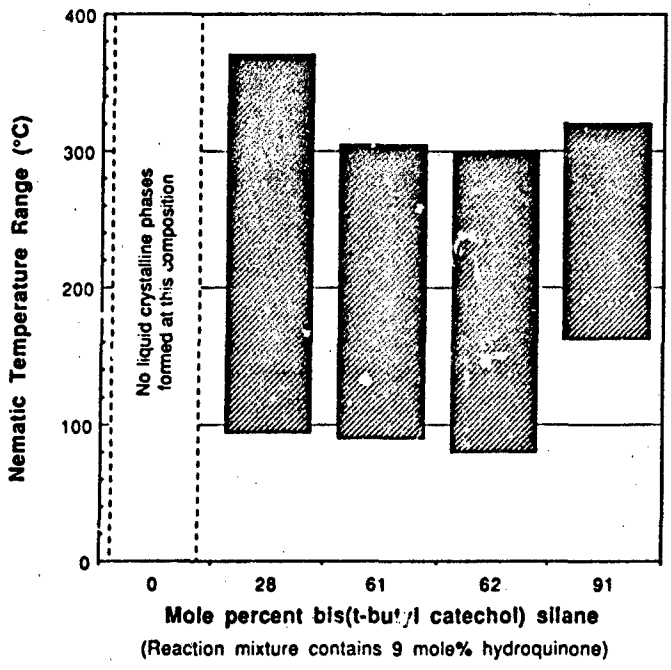

FIGURE 5 Nematic range of polymers prepared from xylene solutions of biscatechol silane, bis(4-*t*-butyl-catechol) silane and hydroquinone. The relative amount of hydroquinone was constant, at 9 mole% of dissolved reactants. Data were obtained by transmitted polarized light microscopy of specimens on a sealed heating stage. The upper limit of the nematic range is masked by specimens tending to form homeotropic textures, and by the onset of degradation.

of the entire sample by shearing the top cover slide. But, it is still possible to demonstrate that the dark regions coexisting with the schlieren or domain textures are in the nematic state: if there were an equilibrium between nematic and truly isotropic material, we would expect the regions of definitive texture to decrease continuously in size as a function of increasing temperature. Instead, we observe that regions of schlieren or domain texture remain unchanged from the temperature at which they first appear, up to the temperature at which they abruptly become isotropic. Not all regions of schlieren or domain texture in a given sample become isotropic at the same temperature, however. Our estimates of the nematic range of a material (Figures 4 and 5) are therefore obtained from microscopic observation of several samples at each composition: the solid-liquid crystal melting transition is identified at the temperature where areas of schlieren or domain texture first appear reversibly on heating, and the nematic-isotropic clearing transition is *at least* as high as the temperature where the last area of distinguishable texture reversibly disappears. In many samples, this temperature overlaps the onset of degradation.

The initial solids precipitated from the three-component polymerization reactions have high melting points (>500°C). Precipitation occurs when the amount of hydroquinone in the reaction mixture exceeds approximately 9 mole%. These con-

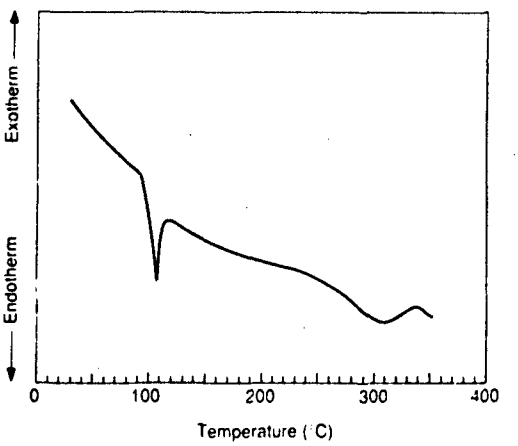

FIGURE 6 DSC heating trace of soluble polymer recovered from reaction of biscatechol silane and bis(4-*t*-butyl-catechol) silane (1:1 mole ratio) in xylene solution. A well-defined endotherm corresponding to the onset of liquid crystallinity at 94°C is seen. A broader endotherm centered at approximately 310°C may indicate the transition to the isotropic phase; its high-temperature side leads into the irregular oscillations that are characteristic of specimen degradation.

centrations of hydroquinone are apparently sufficient to promote a significant degree of cross-linking between the polymer chains,[28] rendering them insoluble.

Differential Scanning Calorimetry

A typical DSC trace of a sample being heated is shown in Figure 6. On initial inspection, the trace appears to exhibit a steeply tilting baseline. However, this feature is preserved at both higher and lower heating rates, and so cannot be a simple baseline artifact. Instead, we identify it as the low-temperature side of a broad "background" endotherm, extending over more than 200°C, and upon which more well-defined endotherms are superimposed. This type of behavior has been observed previously for organic thermotropic random copolymers,[25,29] where it has been interpreted as the melting of highly localized regions of order that arise from chance association between identical random monomer sequences on adjacent molecules.[30] Because a wide range of sequences and lengths are involved, they melt out over a wide range of temperatures. In the present case, we regard the broad DSC endotherms as supporting evidence that we have succeeded in preparing *random* copolymers. The sharp endotherm with an onset temperature of 94°C in Figure 6 corresponds to the temperature at which light microscopy first reveals liquid crystallinity in specimens of this composition. Light microscopy also suggests that the endotherm centered at approximately 310°C coincides with the nematic-to-isotropic transition in this material—though simultaneous specimen degradation at this temperature makes definitive textures difficult to obtain.

CONCLUSIONS

1. Copolymers synthesized from biscatechol silane and bis(4-*t*-butyl-catechol) silane consist of rod-like molecules that form nematic liquid crystalline phases.

The nematic phases form both thermotropically and lyotropically, in the latter case with xylene as the solvent.

2. Similar observations pertain to copolymers synthesized from biscatechol silane, bis(4-*t*-butyl-catechol) silane and hydroquinone.
3. Many of these liquid crystalline polymers are nematic over a wide temperature range, with the reversible clearing point for some compositions exceeding 400°C.

Acknowledgments

The authors are grateful to Dr. David Treadwell for helpful discussions, and to Susan Abrams and Dr. Paul Yager for access to and training on DSC equipment. Funding was provided by the Air Force Office of Scientific Research (AFOSR) through grant No. F49620-89-C-0059, and by the Washington Technology Centers.

References

1. H. Zocher and K. Jacobsohn, *Kolloidchemische Beihefte*, **28**, 167 (1929).
2. J. L. Watson, W. Heller and W. Wojtowicz, *Science*, **109**, 274 (1949).
3. C. Eaborn and N. H. Hartshorne, *Journal of the Chemical Society*, 549 (1955).
4. N. H. Hartshorne, *The Microscopy of Liquid Crystals*, (Microscope Publications, London, 1974), pp. 123–129.
5. J. D. Bunning, J. E. Lydon, C. Eaborn, P. M. Jackson, J. W. Goodby and G. W. Gray, *Journal of the Chemical Society, Faraday Transactions 1*, **78**, 713 (1982).
6. T. Imai and N. Koide, *Liquid Crystalline Organosilicon Compounds*, US Patent No. 4,774,028 (27 September 1988).
7. R. Eidenschink, paper presented at *The 13th International Liquid Crystal Conference*, Vancouver, B.C. (1990).
8. N. Koide, *Molecular Crystals and Liquid Crystals*, **139**, 47 (1986).
9. H. R. Allcock and C. Kim, *Macromolecules*, **24**, 2841 (1991).
10. K. Hanabusa, J.-i. Higashi, T. Koyama, H. Shirai, N. Hojo and A. Kurose, *Die Makromolekulare Chemie*, **190**, 1 (1989).
11. A. M. Giroud-Godquin and J. Billard, *Molecular Crystals and Liquid Crystals*, **66**, 147 (1981).
12. C. Piechocki, J. Simon, A. Skoulios, D. Guillon and P. Weber, *Journal of the American Chemical Society*, **104**, 5245 (1982).
13. H. Sakashita, A. Nishitani, Y. Sumiya, H. Terauchi, K. Ohta and I. Yamamoto, *Molecular Crystals and Liquid Crystals*, **163**, 211 (1988).
14. K. Hanabusa, C. Kobayashi, T. Koyama, E. Masuda, H. Shirai, Y. Kondo, K. Takemoto, E. Iizuka and N. Hojo, *Die Makromolekulare Chemie*, **187**, 753 (1986).
15. S. Takahashi, H. Morimoto, Y. Takai, K. Sonogashira and N. Hagihara, *Molecular Crystals and Liquid Crystals Letters*, **72**, 101 (1981).
16. C. Carfagna, U. Caruso, A. Roviello and A. Sirigu, *Die Makromolekulare Chemie, Rapid Communications*, **8**, 345 (1987).
17. U. Caruso, A. Roviello and A. Sirigu, *Macromolecules*, **24**, 2606 (1991).
18. R. Menescal, J. Eveland and R. West, *ACS Polymer Preprints*, **31**, 294 (1990).
19. P. Weber, D. Guillon, A. Skoulios and R. D. Miller, *ACS Polymer Preprints*, **31**, 296 (1990).
20. D. F. Shriver and M. A. Drezdzon, *The Manipulation of Air-Sensitive Compounds*, (John Wiley & Sons, New York, 1986), p. 30.
21. H. R. Allcock, T. A. Nugent and L. A. Smeltz, *Synthesis in Inorganic and Metal-Organic Chemistry*, **2**, 97 (1972).
22. T. R. Robinson, *Novel, Low Temperature Synthetic Routes to Tailored Soluble Silicates*, Masters Thesis, University of Washington, (1990).
23. E. M. Chamot and C. W. Mason, *Handbook of Chemical Microscopy, Vol. II. Chemical Methods in Inorganic Qualitative Analysis*, (John Wiley & Sons, New York, 1940), pp. 373–377.

24. W. H. de Jeu, *Physical Properties of Liquid Crystalline Materials*, (Gordon and Breach Science Publishers, New York, 1980), p. 23.
25. C. Viney and A. H. Windle, *Journal of Materials Science*, **17**, 2661 (1982).
26. R. M. Laine, N. Budrys, F. Babonneau and J. A. Rahn, unpublished results.
27. W. Hönle, U. Dettlaff-Weglikowska, L. Walz and H. G. von Schnering, *Angewandte Chemie International Edition in English*, **28**, 623 (1989).
28. R. Schwarz and W. Kuchen, *Zeitschrift für anorganische und allgemeine Chemie*, **266**, 185 (1951).
29. A. H. Windle, C. Viney, R. Golombok, A. M. Donald and G. R. Mitchell, *Faraday Discussions of the Chemical Society*, **79**, 55 (1985).
30. S. Hanna and A. H. Windle, *Polymer*, **29**, 207 (1988).

APPENDIX 7

Mol. Cryst. Liq. Cryst., 1991, Vol. 196, pp. 133–143
Reprints available directly from the publisher
Photocopying permitted by license only

Printed in the United States of America

Characterizing the Scale of Liquid Crystalline Textures: Rheinberg Differential Color Contrast

C. VINEY and C. M. DANNELS

Department of Materials Science and Engineering FB-10 and the Advanced Materials Technology Program, University of Washington, Seattle, WA 98195, USA

(Received May 19, 1990)

The limitations of referring to domain size as a unit of microstructural scale are discussed. A more practically useful measure of scale is given by the defect density. For this purpose, the distribution of defects in a texture can be highlighted with maximum contrast and resolution by using Rheinberg differential color illumination.

Keywords: domain, texture, scale, defects, Rheinberg, liquid crystal

INTRODUCTION

Characterizing and controlling microstructural scale, to optimize physical properties, is central to Materials Science. For example, a fine grain size in a metal translates to increased yield strength at room temperature, decreased high temperature creep resistance and increased electrical resistivity. The thermomechanical history required in order to obtain a particular grain (crystal) size and dislocation density in metals has been investigated exhaustively. Analogous studies have been performed on ceramics and polymers. However, although the physical properties of liquid crystalline materials must similarly be dependent on microstructural scale, the factors that determine domain size and defect (disclination) densities have received scant attention. It has been noted that some liquid crystalline polyesters have textures that are an order of magnitude finer than the textures of their oligomers[1-2]—but not even this observation has been explained. Theoretical studies of the liquid crystalline state have concentrated on the molecular parameters or environmental conditions that promote formation of liquid crystalline phases; they have not attempted to quantify the scale over which long range orientational order develops.

The impact of microstructural scale on physical properties is illustrated by the following examples:

- In conducting polymers and non-linear optical polymers, microstructures that promote extensive electronic or optical scattering must be avoided.
- Ways of increasing the compressive strength of liquid crystalline polymers are being sought actively. While several attempts have been made to enhance this property by tailoring the type of molecule and the type of order, the *dependence of strength on scale has been neglected*. If analogies are to be drawn with more traditional materials, one would expect a fine microstructure (i.e., a high density of orientational defects) to be beneficial.

DESCRIPTIONS OF MICROSTRUCTURAL SCALE

Attempts to identify a simple microstructural unit in liquid crystalline materials have led to the concept of a "domain". However, there is a lack of consensus about the physical nature of a domain. According to one view (Marrucci, quoted in Reference 3), a domain is a region in which the *net director orientation is zero*. While the director field surrounding a single disclination could meet this description in principle (Figure 1), the existence of such an idealized topology is unlikely. One would typically expect several line disclinations or even walls to be associated with each domain, to meet the requirement of no net director orientation. There is no *a priori* simple relationship between the size of a domain and the number of orientational defects that it contains. Yet, as we have seen, *it is the defect density that affects physical properties*, so the "domain size" as defined here does not necessarily help with property prediction.

An alternative definition[5-6] invokes the opposite extreme of director orientation in describing a domain: a region in which the *director orientation is essentially constant*, thus distinguishing it from a domain boundary where there is a rapid reorientation of the director over a relatively short distance. This description appeals to our familiarity with single crystals as the basis of metal and ceramic microstructures. A domain defined in this way need not contain any disclinations (Figure 2 and Reference 7), though they certainly can be accommodated (Figure 3 and Reference 7). Thus, as with Marrucci's definition, it again is not possible to

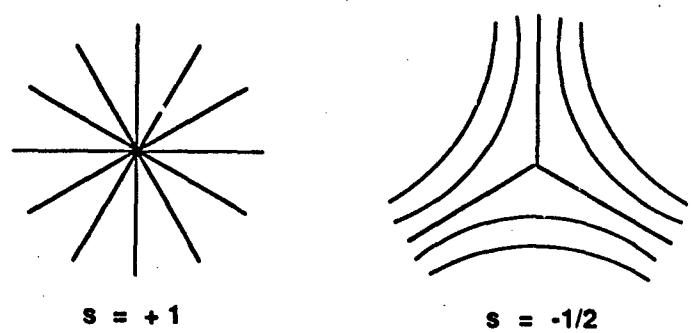

FIGURE 1 Schematic examples of undistorted director fields around an isolated disclination in a nematic.[4] The net director orientation in the vicinity of the disclination is zero in each case.

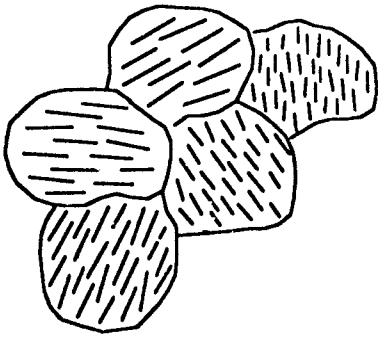

FIGURE 2 Schematic representation of a liquid crystalline microstructure in which regions of approximately constant director orientation are separated by abrupt boundaries. As a reminder that the directors have an out-of-plane component of orientation, their projections on the specimen plane have different lengths.

anticipate the number of disclinations that must be associated with any given domain. Also, there is an implication that a domain is a *discrete* area in the microstructure, clearly separated from its neighbors by a definite boundary or wall. This distinction can indeed be made—but only in some special cases:

- Nematic textures sometimes contain closed walls that may[7-8] or may not[7] contain disclinations. When a wall does contain disclinations, their distribution is analogous to the arrangement of dislocations in a low angle grain boundary in a metal.
- After liquid crystalline fluids are sheared, the molecular order typically relaxes to a pattern in which the director orientation varies periodically with position measured parallel to the shear direction.[9] A "divergence function" can be plotted,[10] showing how the angle between the director and the shear direction changes as a function of position along the shear direction. If the divergence function has a sawtooth profile, as in Kevlar,[11] the regions of approximately constant director orientation can be regarded as domains under the present definition.

More generally, it is possible to identify regions in which there is a rapid local change in director orientation, *without* these regions forming continuous (closed) boundaries around a domain. They can even exist within an otherwise constant director field, as already illustrated in Figure 3. The absence of experimental evidence for definitive domain walls in liquid crystalline polymers has been commented on previously.[12-13] This is taken into account by Noel's description of a domain[14] as a highly ordered region embedded in a matrix of less order.

An attempt has been made to define domains so that each is centered on a single disclination line.[15] While this is possible in the case of nematic schlieren textures, it is not satisfactory if other defects such as inversion walls are present. Also, the positioning of domain boundaries is arbitrary.

The difficulty of referring to domain size as the generalized unit of microstructural scale in liquid crystalline materials is apparent: there is some leeway in how we choose to define a domain, and there is no simple correlation between the domain

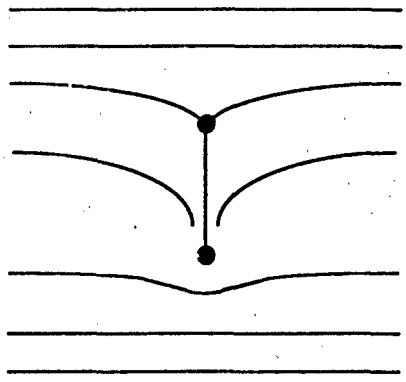

FIGURE 3 Schematic representation of an isolated orientational discontinuity that can exist entirely within an otherwise aligned director field.

size (however defined) and the concentration of orientational defects. It becomes expedient to dispense with dissecting the microstructure into domains, and, instead, to consider the distribution of orientational defects directly. We may think of the number density of these defects as being analogous to the dislocation density in a crystalline material. Practically, it is the *distribution of defects*, and not domain size, that most directly affects physical properties. We will therefore focus our attention on characterizing the distribution of orientationl uiscontinuities in liquid crystalline microstructures.

CHARACTERIZING ORIENTATIONAL DEFECT DENSITY BY LIGHT MICROSCOPY

Because orientational discontinuities are associated with abrupt changes in optical properties, they usually can be characterized by light microscopy. It is useful to distinguish between the following two approaches:

- The average separation of discontinuities can be quantified in terms of the average size of regions over which optical orientation is comparatively constant.
- The discontinuities themselves can be highlighted.

The first type of analysis can be achieved via the established microscopical method of observing thin specimens between crossed polars. The specimens may be in the fluid liquid crystalline state. Alternatively, in the case of polymeric liquid crystals, the mesophase in a small bulk sample may be preserved to room temperature by quenching, and a thin specimen is obtained by sectioning. (The latter preparation technique avoids the defect distribution being affected by interactions with the glass confining surfaces.) Specimens appear dark locally where the vibration directions (not necessarily the molecules)[16] are parallel to the transmission directions of the polars. The average size of ordered regions then corresponds to the average size of light regions as measured for a variety of crossed polar orientations. However,

the value of this approach is limited by the fact that, unless images are digitized, or are otherwise compared with calibrated reference values of optical density, determining the size of a "light" area involves subjective judgement. Furthermore, observations made with the specimen between crossed polars may not distinguish between regions that differ only in their out-of-plane molecular orientation (Figure 4).

Observations of texture between crossed polars do not highlight orientational defects explicitly. Instead, textures provide the preferred means of characterizing director orientations *between* the defects. Even a feature as "simple" as an inversion wall gives rise to a complex pattern of extinction (Figures 5a and 5b), which adds to the difficulty of interpreting fine microstructures. Orientational discontinuities in a schlieren texture are usually identified by looking at how the texture changes in a series of micrographs as the crossed polars are rotated:

- At point disclinations, and at disclination lines normal to the specimen surface, dark bands are seen to rotate about fixed points in the microstructure.
- Other abrupt discontinuities of in-plane molecular orientation are characterized by bands of extinction that move laterally over a very narrow range of positions during a 360° rotation of the crossed polars.

We have investigated a number of alternative contrast mechanisms available to the light microscopist, to specifically emphasize optical discontinuities. In conventional bright field illumination (both polars withdrawn, Figure 5c), optical discontinuities show up as a result of light scattering. The discontinuities cause light to deviate from its original path so that it cannot subsequently be collected by the objective; thus, the discontinuities are seen as locally darker features in the image. (The same scattering process is responsible for the turbid appearance of bulk liquid crystalline specimens.) Resolution is good, because the most effective scattering is achieved by discontinuities that have a scale comparable to the wavelength of light, and it is therefore the cores of disclinations that are darkest. Unfortunately, because only a small percentage of the light incident on the specimen is scattered, the *contrast* (visibility of detail) is poor: the fine detail is difficult to discern against the light that has *not* been affected by passage through the sample.

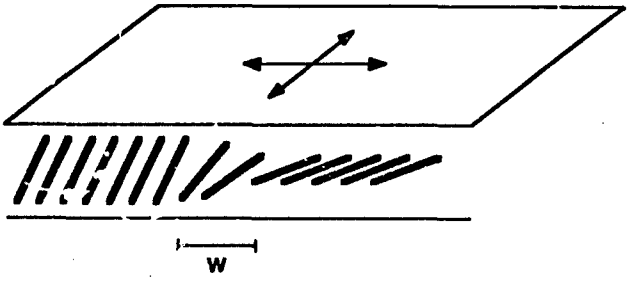

FIGURE 4 While molecular orientation varies abruptly over the distance w, observations of transmitted light intensity between crossed polars may not reveal the presence of two "domains", if all the molecules lie in the plane of the diagram. The crossed polar orientations that would make the entire specimen appear dark are marked on the top surface.

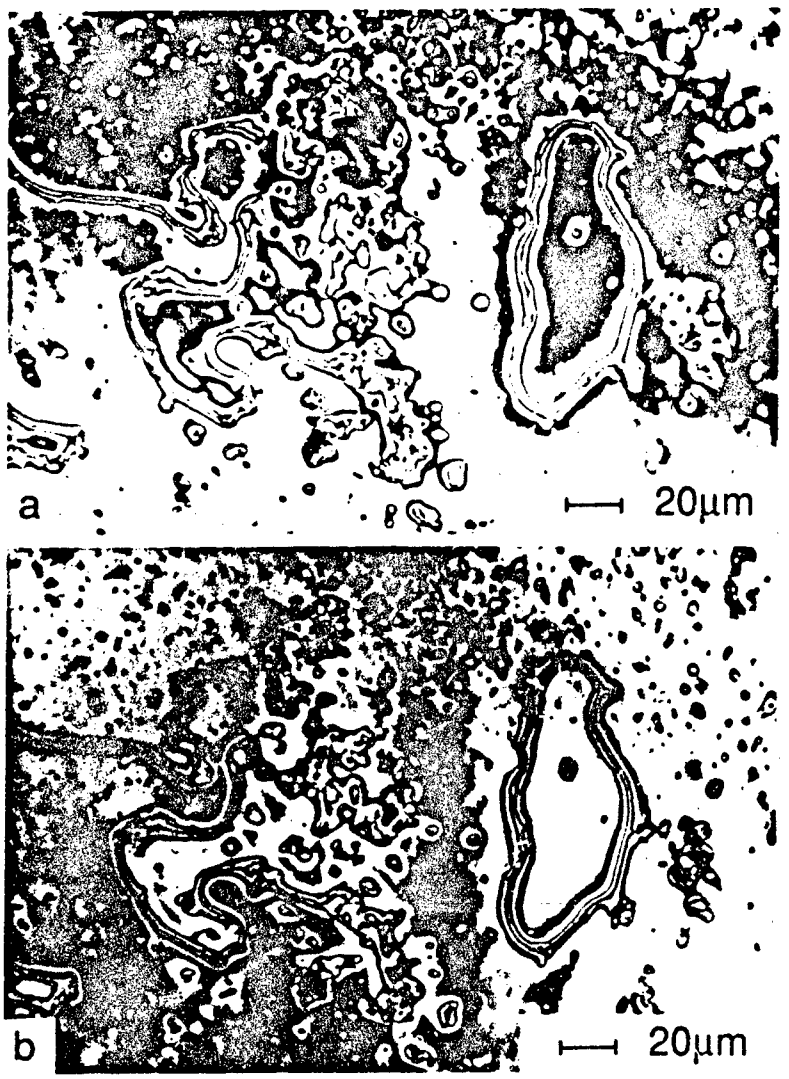

FIGURE 5 Nematic microstructure, including inversion walls, photographed under a variety of illumination conditions. The specimen was poly(*p*-hydroxybenzoic acid), quenched from 480°C; number average degree of polymerization = 15. (a) Crossed polars; polarizer vibration direction E–W; (b) Crossed polars rotated 45° from orientation in (a); (c) Bright field (no polars); (d) Phase contrast; (e) Dark field; (f) Rheinberg differential color illumination; blue central stop and green outer annulus; fine detail more visible than in the other cases. The phase contrast image was obtained with a ×40 objective; a ×32 objective was used for the others. See Color Plate V.

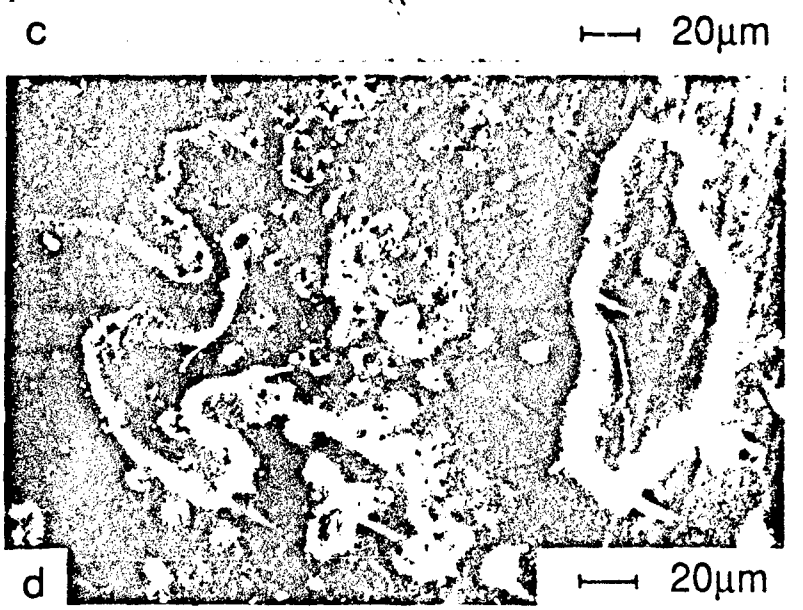

FIGURE 5 (*continued*) See Color Plate VI.

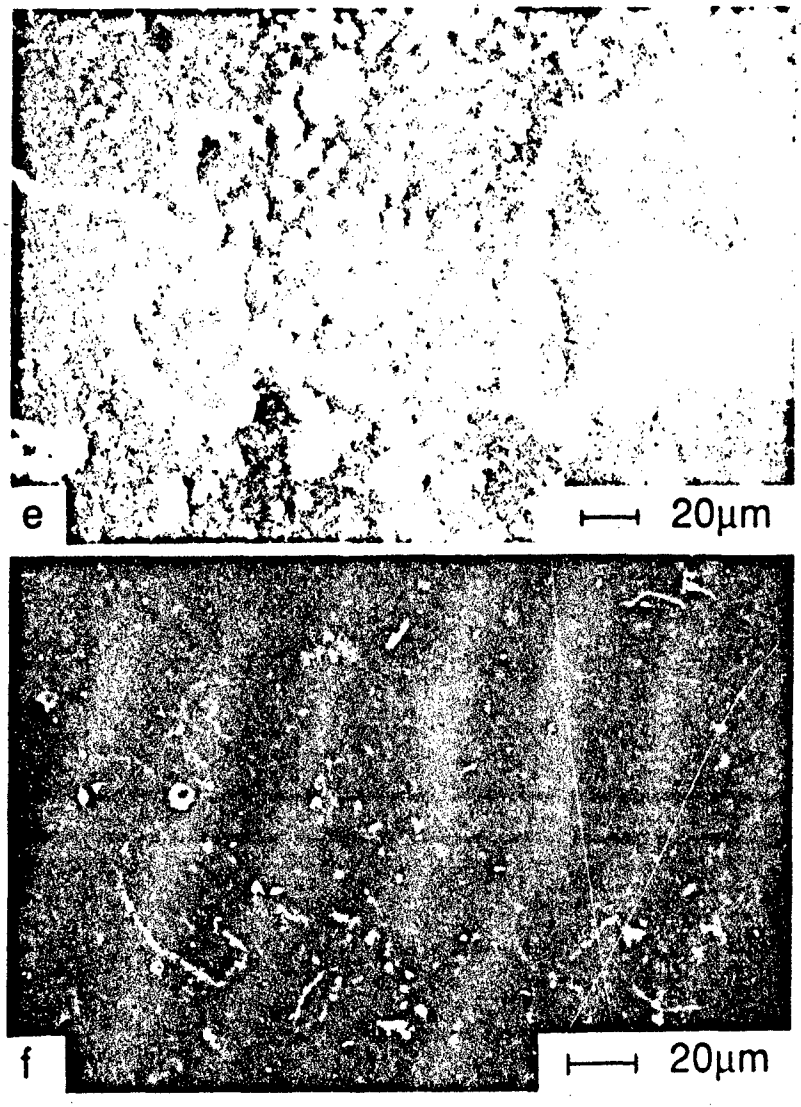

FIGURE 5 (*continued*) See Color Plate VII.

There are several techniques in light microscopy that enhance contrast relative to what can be achieved in bright field. Phase contrast[17,18] can be used to image point-to-point changes in refractive index. However, the gain in contrast is accompanied by a loss of resolution, because the refractive index change even at some distance from the core of abrupt discontinuities contributes to contrast. The discontinuities consequently are easier to see than under bright field conditions, but they also appear to be wider and more blurred (Figure 5d). It therefore is difficult to distinguish detail in regions that contain a large number of closely spaced disclinations.

Dark field microscopy (Figure 5e) essentially inverts the contrast observed in bright field—optical discontinuities appear as bright features on a dark background.[17] The contrast is excellent, because only the scattered light contributes to the image. The principal shortcoming of this technique is the loss in resolution that occurs if an objective with a high numerical aperture is needed to form images of the microstructure. It can be demonstrated theoretically[19] that the maximum resolution obtainable in bright field will always exceed that obtainable in dark field if the objective numerical aperature is greater than 0.43. In the case of liquid crystalline polymers, where microstructures can be an order of magnitude finer than in low molecular weight liquid crystals,[1-2] high objective numerical apertures are essential to resolving the microstructure adequately.

We have found that *Rheinberg differential color illumination* (Figure 5f) provides optimum contrast for imaging disclinations, without compromising the maximum resolution obtainable with a given objective. While the technique was invented almost a hundred years ago,[20] its use has been limited to biological specimens[21-26] and to textiles.[25,27] To obtain Rheinberg illumination, concentric color filters are placed below the substage condenser so that the axial and peripheral illuminating rays incident on the specimen have different colors (Figure 6). Because the peripheral illumination is responsible for resolving and reconstructing the finest detail in the image, this detail appears in the color of the outer filter, against a background color that is due to the inner filter. The resulting contrast is superior to that obtained by any mechanism that requires the viewer to differentiate between grey levels.[28-32] In addition to ensuring that both resolution and contrast are maximized, Rheinberg illumination offers control over the image in the following ways:

- Both coarse and fine microstructural detail can be included in the image.
- Both the color and intensity of the fine detail can be selected relative to that of the background.
- By varying the relative diameters of the two filters, one can control the scale of detail that appears as background or highlight respectively.

CONCLUSIONS

The microstructural scale of liquid crystalline materials can be characterized unambiguously in terms of the concentration of orientational defects. Attempts to quantify the scale in terms of "domain size" are limited by the difficulty of defining domains in most microstructures. Also, the defect concentration is associated di-

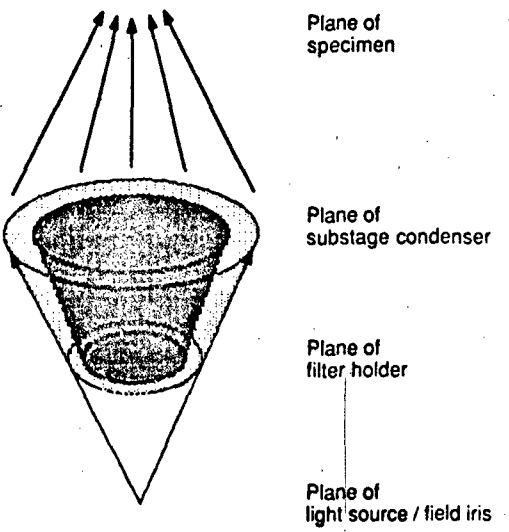

FIGURE 6 Schematic representation of Rheinberg illuminator.

rectly with physical properties, but is not a simple function of the size of arbitrarily described domains. While defects can be revealed by many light microscopical techniques, they are most usefully highlighted relative to the rest of the microstructure by using Rheinberg differential color contrast. This technique maximizes both contrast and resolution simultaneously.

Acknowledgments

We gratefully acknowledge the Donors of the Petroleum Research Fund, administered by the American Chemical Society, for partial support of this work. Support was also provided by AFOSR (No. 89620-89-C-0059), and by the IBM corporation.

REFERENCES

1. A. M. Donald, C. Viney and A. H. Windle, *Philosophical Magazine B*, **52**, 925 (1985).
2. J. Economy, W. Volksen, C. Viney, R. Geiss, R. Siemens and T. Karis, *Macromolecules*, **21**, 2777 (1988).
3. K. F. Wissbrun, *Faraday Discussions of the Chemical Society*, **79**, 161 (1985).
4. F. C. Frank, *Discussions of the Faraday Society*, **25**, 19 (1958).
5. A. H. Windle, *Faraday Discussions of the Chemical Society*, **79**, 186 (1985).
6. L. L. Chapoy, B. Marcher and K. H. Rasmussen, *Liquid Crystals*, **3**, 1611 (1988).
7. D. Demus and L. Richter, *Textures of Liquid Crystals*, Verlag Chemie, Weinheim, 1978, pg. 39.
8. J. Nehring and A. Saupe, *Journal of the Chemical Society, Faraday Transactions II*, **68**, 1 (1972).
9. B. J. A. Zielinska and A. Ten Bosch, *Liquid Crystals*, **6**, 553 (1989), and references cited therein.
10. C. Viney and A. H. Windle, *Polymer*, **27**, 1325 (1986).
11. S. C. Simmens and J. W. S. Hearle, *Journal of Polymer Scierce (Physics)*, **18**, 871 (1980).
12. M. R. Mackley, *Faraday Discussions of the Chemical Society*, **79**, 187 (1985).

13. E. L. Thomas, *Faraday Discussions of the Chemical Society*, **79**, 188 (1985).
14. C. Noel, *Makromolekulare Chemie, Makromolekulare Symposia*, **22**, 95 (1988).
15. T. Shiwaku, A. Nakai, H. Hasegawa and T. Hashimoto, *Macromolecules*, **23**, 1590 (1990).
16. C. Viney, G. R. Mitchell and A. H. Windle, *Molecular Crystals and Liquid Crystals*, **129**, 75 (1985).
17. S. G. Lipson and H. Lipson, *Optical Physics* (CUP, Cambridge UK, 1981), Ch. 9.
18. M. Pluta, in *Advances in Optical and Electron Microscopy*, edited by R. Barer and V. E. Cosslett (Academic Press, London, 1975), pp. 49–133.
19. C. Viney and W. S. Putnam, in *Proceedings of the 47th Annual Meeting of the Electron Microscopy Society of America*, edited by G. W. Bailey (San Francisco Press, San Francisco, 1989), pp. 364-365.
20. J. Rheinberg, *Journal of the Royal Microscopical Society*, **19**, 373 (1896).
21. J. R. Meyer-Arendt, *Applied Optics*, **4**, 1 (1965).
22. S. D. Wilson, *Applied Optics*, **5**, 1683 (1966).
23. D. M. Woolley, *Journal of Microscopy*, **121**, 241 (1981).
24. J. Forget and P. Couillard, *Canadian Journal of Zoology*, **61**, 518 (1983).
25. M. Abramowitz, *American Laboratory*, **15**, 38 (1983).
26. J. G. Delly, *Photography through the Microscope* (Eastman Kodak Company, Rochester, N.Y., 1988).
27. G. H. Needham, *The Microscope: A Practical Guide* (Charles Thomas, Springfield, Ill., 1968), pp. 72–73.
28. J. Bescos and T. C. Strand, *Applied Optics*, **17**, 2524 (1978).
29. F. T. S. Yu, A. Tai and H. Chen, *Journal of Optics*, **9**, 269 (1978).
30. J. Santamaria, M. Gea and J. Bescos, *Journal of Optics*, **10**, 151 (1979).
31. F. T. S. Yu, S. L. Zhuang, T. H. Chao and M. S. Dymek, *Applied Optics*, **19**, 2986 (1980).
32. L. Liu, *Applied Optics*, **22**, 3016 (1983).

APPENDIX 8

Mol. Cryst. Liq. Cryst., 1991, Vol. 198, pp. 341–350
Reprints available directly from the publisher
Photocopying permitted by license only

Printed in the United States of America

Factors Affecting Microstructural Scale in Liquid Crystalline Materials

CHRISTINE M. DANNELS,† CHRISTOPHER VINEY,† ROBERT J. TWIEG,‡ and MARTINA Y. CHANG†

† *Department of Materials Science and Engineering FB-10 and the Advanced Materials Technology Center, University of Washington, Seattle, WA 98195, USA*

and

‡ *IBM Almaden Research Center, 650 Harry Road, San Jose, CA 95120, USA*

(Received July 26, 1990)

Light microscopy was used to study the effects of molecular weight and chain flexibility on microstructural scale in liquid crystalline materials. Studies of poly(*p*-hydroxybenzoic acid) oligomers show that the scale exhibited by a semiflexible molecule is not sensitive to increasing molecular weight when the contour length exceeds the persistence length. For contour lengths shorter than the persistence length, the microstructural scale is significantly coarser and depends on molecular weight. In the case of linear rigid polytolan oligomers, increasing the molecular axial ratio results in coarser microstructures. Rheinberg differential color contrast is shown to provide an optimum combination of contrast and resolution for highlighting fine-scale orientational defects.

Keywords: axial ratio, domain size, flexibility, microstructural scale, molecular weight, Rheinberg

INTRODUCTION

The relationship between chemical structure and a wide range of physical properties in liquid crystalline materials has been studied in great detail. Thus, much is known about balancing the type, sequence and connectivity of rigid and flexible moieties to obtain a particular liquid crystalline phase.[1] One can predict how to tailor the temperature range over which the phase is stable, or how to ensure that the material exhibits particular optical properties. However, bulk physical properties cannot depend only on the chemical nature and conformation of individual molecules, but must also be affected by the microstructure—i.e., the scale on which different levels of molecular order occur—a fact clearly recognized in the traditional areas of materials science. For example, although polymer extruded in the liquid crystalline state may exhibit exceptionally high modulus and tensile strength, the compressive strength is generally still comparable to that of conventionally processed polymers; we expect that enhanced compressive strength would result from an

increased disclination (or orientational defect) density in the microstructure. Conversely, undesirable optical scattering by a film of liquid crystalline material may be avoided if the density of microstructural defects is reduced.

There are indications that high molecular weight liquid crystalline polymers exhibit finer scale microstructures compared to lower molecular weight liquid crystalline materials. This behavior was noted for poly(*p*-hydroxybenzoic acid)[2] and for poly(*p*-phenylene terephthalamide).[3] Monte Carlo models[4] predict that a coarser microstructural scale results from higher molecular axial ratios if molecules are perfectly rigid and experience only steric interactions.

MATERIALS

Poly(*p*-hydroxybenzoic acid) (PHBA) exhibits a thermotropic nematic phase. Also known commercially as Ekonol, it is useful for high modulus fibers.[2,5] The ester linkages in the backbone render the molecules semiflexible. Oligomers of PHBA[6] studied in this work are designated by their degrees of polymerization: DP4, DP15, DP18, DP23 and DP28. (The molecular weights range from ~500 to ~3400.)

Three oligomers based on a tolan unit were also studied. They are designated by their axial ratios: T4.3, T4.7 and T5.7 (Figure 1). These molecules are rigid and exhibit thermotropic nematic phases.[7]

EXPERIMENTAL: LIGHT MICROSCOPY

Transmitted Polarized Light Microscopy

Each polymer sample was held between two glass cover slips. No special steps were taken to modify the glass surfaces. Microstructural comparisons were always made between samples of similar thickness. Specimens were observed with a Leitz Laborlux 12 Pol microscope equipped with a Linkam 26-THM-600S heating/freezing stage and 26-PR-600 controller.

Samples of PHBA (DP15-DP28) were placed on the heating stage preheated to 1.1 times the crystalline→nematic transition, on an absolute scale. Pressure was applied by hand to the hot sample to promote formation of a thin specimen. The samples were then quenched to room temperature by transferring them onto an aluminum block. It has been previously demonstrated that microstructures typical

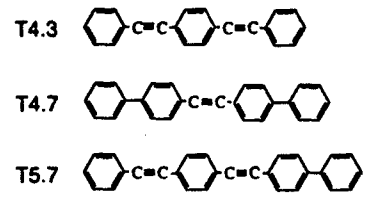

FIGURE 1 Molecular structures of linear oligomeric polytolans.

of elevated temperatures can be "quenched-in" by this technique.[2] In each case, the heating and cooling cycle was performed within 15 seconds to avoid sample polymerization or degradation. The quenched samples were examined at high resolution with a 100X oil-immersion lens.

The tetramer of PHBA (DP4) was placed on a heating stage preheated to 288°C and observed at temperature with a 32X long working distance objective.

The polytolans also were studied under the long working distance lens while on the heating stage. Each oligomer was placed on a heating stage preheated to 50°C above the nematic→isotropic transition. The isotropic droplets coalesced and spread to form one thin drop, wetting both glass surfaces. This thin specimen was then cooled at 10°C/min into the nematic temperature range (5°C below the isotropic→nematic transition).

Rheinberg Differential Color Contrast

In the context of liquid crystals, there are advantages to considering microstructural scale as the density of orientational defects, thus avoiding the ambiguities in the definition of a "domain size".[8] Microstructures observed between crossed polars contain extinction bands that are related to molecular order between defects, and thus detract from the defects themselves. As such, this contrast cannot easily be interpreted in terms of microstructural scale.[8] To highlight the orientational defects themselves, we turn to Rheinberg differential color contrast.[9-11]

The technique is similar to dark field microscopy, which utilizes an opaque stop in the light path to block the lower diffracted orders from reaching the center of the objective back focal plane (see Figure 2). In dark field microscopy, fine detail in the specimen appears light. Coarse structure and background are not observed. Rheinberg's technique uses a filter that is comprised of a central stop and an annulus that have different colors. The coarse information is not obliterated by an opaque stop; it merely appears in a color different from that of the detail. Also, while dark field microscopy will compromise high resolution,[12] Rheinberg does not.

Rheinberg filters were cut from colored gelatin films according to descriptions

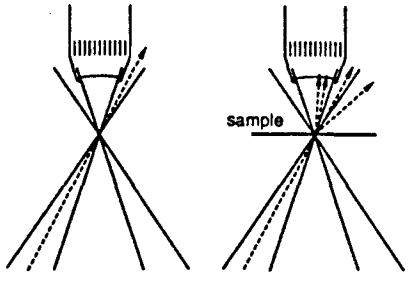

FIGURE 2 For both dark field and Rheinberg microscopy, a wide cone of light is used to illuminate the sample. The rays of light forming the outer part of the cone (unshaded) do not reach the objective except in the case that they are sufficiently scattered by the sample structure. For dark field conditions, the central part of the cone (shaded) is blocked by placing an opaque stop in or below the substage condenser. For Rheinberg conditions, the central and outer parts of the illuminating cone are given two different colors by using a colored stop and a colored annulus.

in the literature.[10-11] Blue was chosen for the annulus to obtain the highest resolution of detail. The filters were mounted onto microscope slides so that they would rest easily in the substage assembly, between the two condenser lenses. By observing the objective back focal plane, the filter could be centered accurately. The Rheinberg illumination technique was used with a 60X objective to examine the quenched PHBA samples. Images were recorded in color on slide film; black-and-white prints for this paper were made directly from the slides, so that fine detail appears dark.

RESULTS AND DISCUSSION

Molecular Weight Effects in Semiflexible PHBA

The quenched microstructures of DP15 and DP18 are shown in Figure 3. There is a marked decrease in scale between the two microstructures. The microstructures for DP23 and DP28 were not significantly different in scale from DP18. Rheinberg differential color contrast provided the same results about the relative microstructural scale of the PHBA oligomers (Figure 4). Note that, although an objective of lower numerical aperture was used in obtaining these microstructures, the degree of fine detail is comparable to that seen in Figure 3.

The tetramer (DP4) polymerized while on the heating stage. With increasing time, the microstructural scale initially coarsened, quickly became much finer (Figure 5), and then continued to decrease slowly.

The concentration of microstructural defects depends on the availability of defects in the *local* packing of molecules. For example, splay deformation, and therefore the disclinations that involve splay, cannot be constructed without the use of chain ends. So the number of defects at a micron scale will be related to the segregation of defects present at the Ångstrom scale. The disclination density can also be related to the elastic constants of the liquid crystalline material; higher elastic constants will result in coarser microstructures. We consider that, with increased polymerization of the material, there are three factors at a molecular level which might influence the microstructural scale.

Firstly, the increasing axial ratio of the molecules implies a decreasing *concentration of chain ends*. The fewer chain ends to be accommodated, the fewer defects will be present in the microstructure. More simply, the longer building blocks more readily form larger ordered regions. Also, the elastic constants increase.[13] Thus the scale of the tetramer initially coarsens as it polymerizes.

Secondly, because PHBA is *semiflexible*, the molecular conformation need not be linear. The molecule is only considered straight over segmental lengths corresponding to the persistence length. According to data in Reference 14 the persistence length of PHBA at 300°C is close to the contour length of the DP15 oligomer. At contour lengths greater than this, the semiflexibility of PHBA becomes apparent. These non-linear molecules cannot maintain their orientational order over as large a distance as molecules that are straight. Thus the scale is fine in Figures 3b and 4b. The increase in contour length between DP18 and DP28 does not lead to any further significant change in the conformation, so there is no significant change in the ability of these molecules to order. Because bend defor-

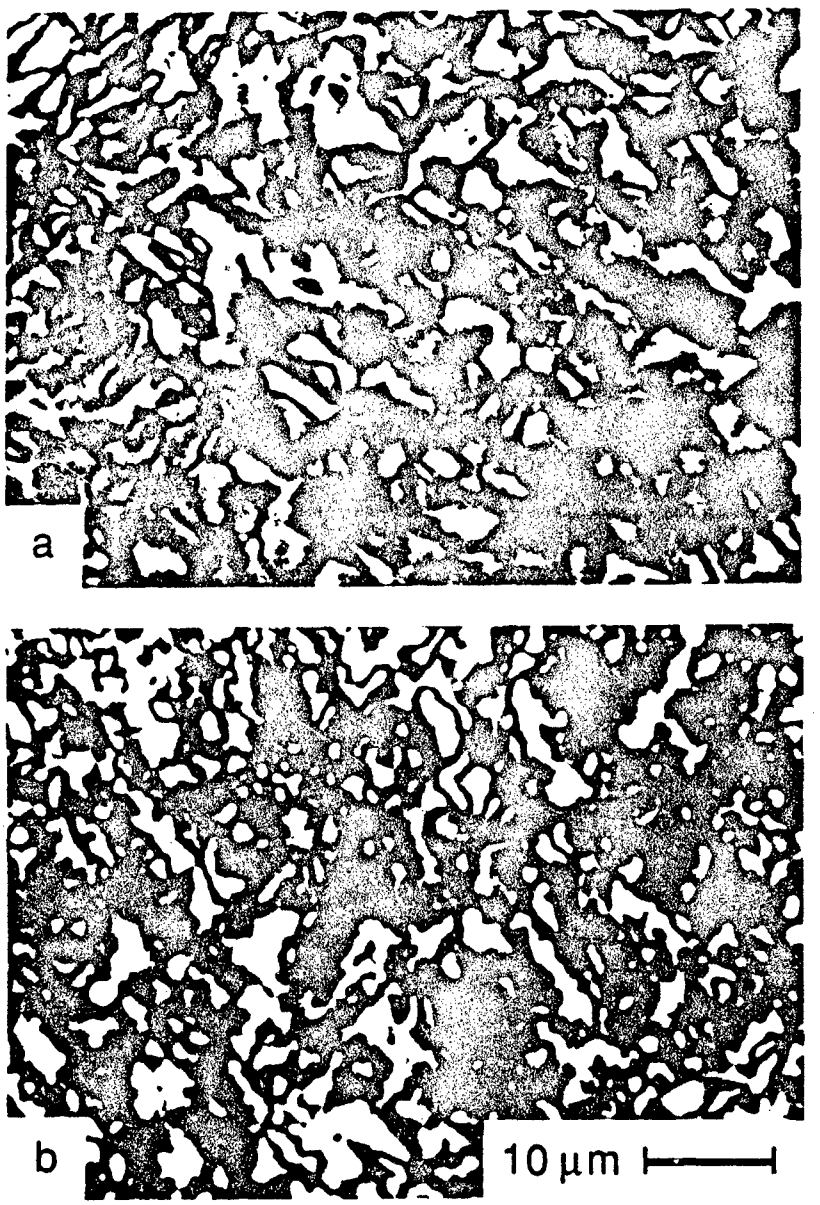

FIGURE 3 Schlieren textures observed between crossed polars for (a) DP15 quenched from 328°C and (b) DP18 quenched from 335°C. The scale of the DP15 microstructure is distinctly coarser.

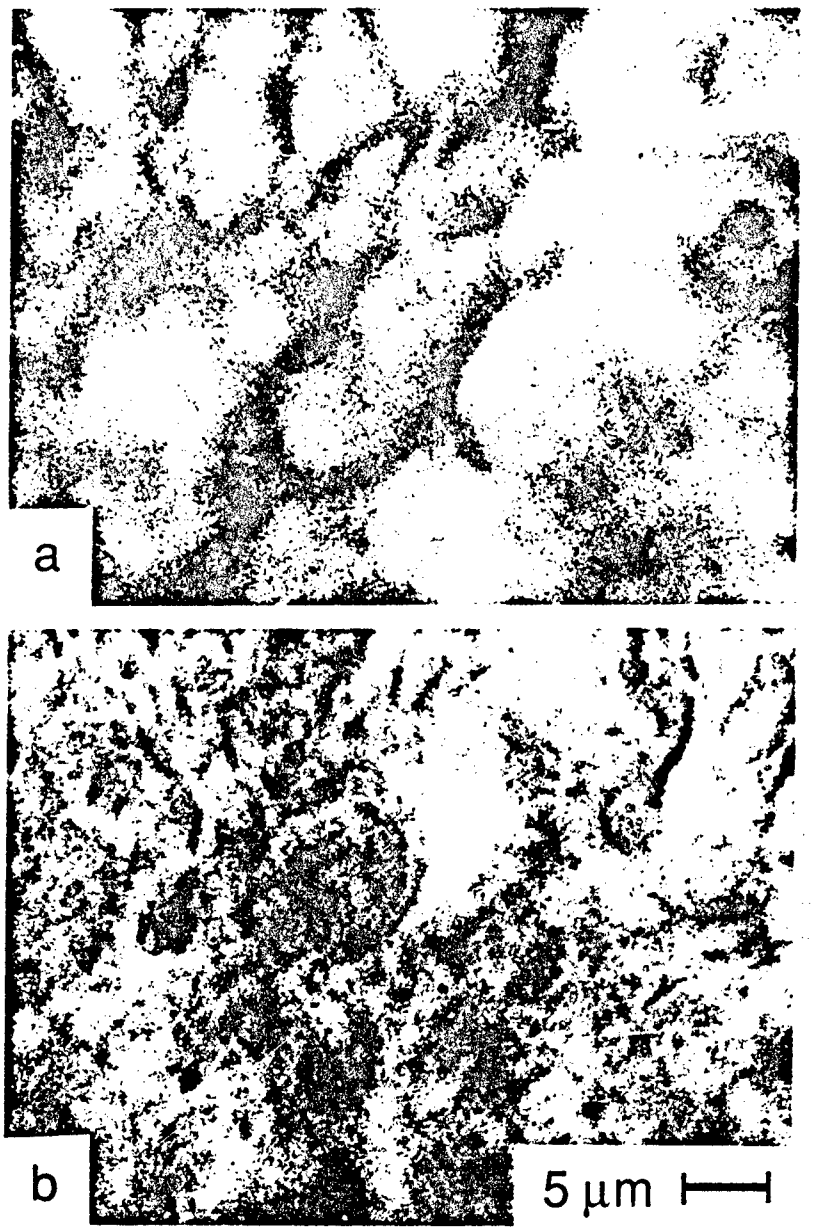

FIGURE 4 Quenched samples of (a) DP15 and (b) DP23 viewed under Rheinberg illumination conditions. Fine discontinuities in optical orientation appeared blue and coarse detail appeared red when viewed in the microscope. The black-and-white micrographs shown here were printed directly from color slides of the Rheinberg images; the fine detail therefore appears dark.

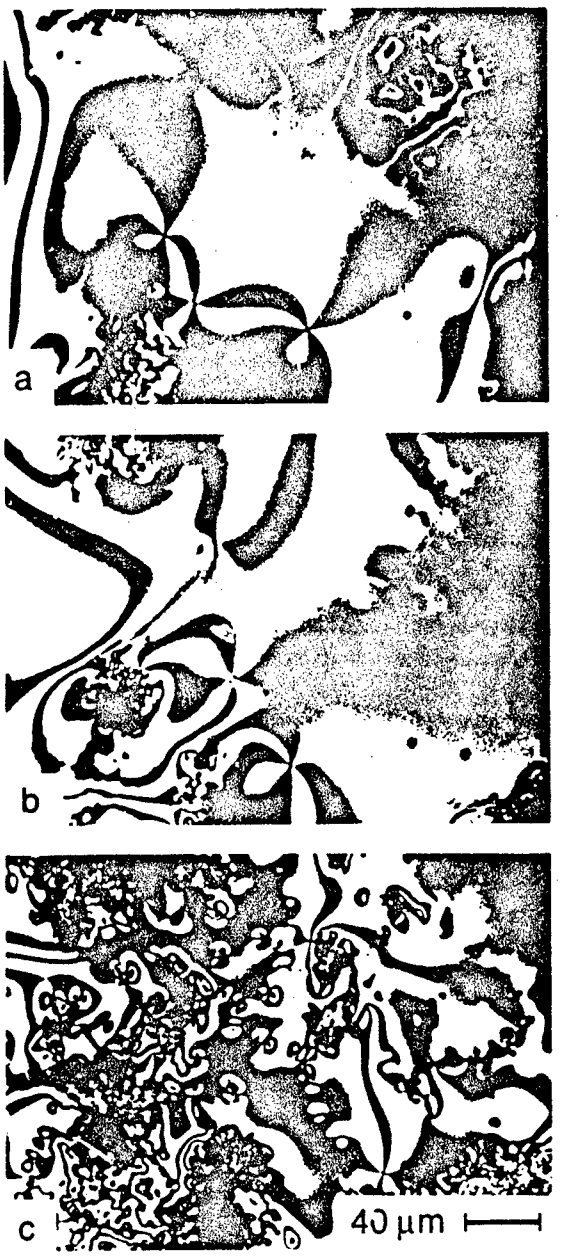

FIGURE 5 (a) Placed on the heating stage at 288°C, the tetramer of PHBA (DP4) melts and forms a schlieren texture which is initially coarse. The micrograph shows the texture after 1 minute on the stage. (b) After a further 1/2 minute, polymerization has caused the microstructure to become coarser. (c) After another 1/2 minute, further polymerization has led to an abrupt increase in the concentration of defects.

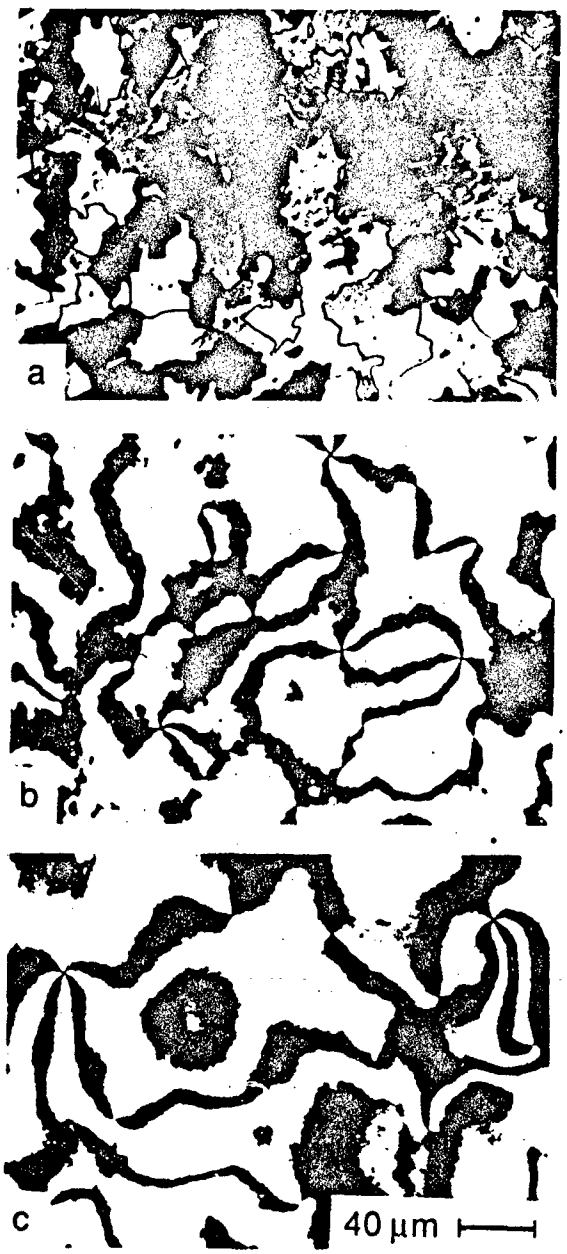

FIGURE 6 (a) Nematic marbled texture of T4.3 at 167°C. (b) Schlieren texture of T4.7 at 238°C. (c) Schlieren texture of T5.7 at 242°C. The scale of the polytolan microstructures increases with increasing molecular axial ratio.

mation is easier with flexible molecules, the bend elastic constants are lower. The fact that most disclinations in a nematic require some bend could account for the significant change in microstructural scale occurring in response to a relatively small increase in degree of polymerization.

The microstructure of the tetramer did continue to decrease in scale beyond the length at which the persistence length was exceeded. The third factor we recognize is the *polydispersity* of the sample. Polydispersity increases as polymerization proceeds. As the molecules become increasingly dissimilar their segregation patterns become more complex, leading to additional microstructural defects.

Molecular Weight Effects in Rigid Polytolans

The microstructure of T4.3 exhibited a nematic marbled texture between crossed polars (Figure 6a). Each domain varied in shade from light to dark as the polars were rotated through 90°. Samples T4.7 and T5.7 exhibited classic schlieren textures (Figure 6b, c). The scale of microstructure increases in the order T4.3 < T4.7 < T5.7. Of the three factors presented as relevant to the scale of PHBA textures, only the concentration of chain ends is relevant to the rigid, monodisperse polytolans. The observed increase in scale with increasing molecular weight is consistent with the initial behavior of the tetramer during polymerization.

CONCLUSIONS

We propose that:

1. Fine microstructures are promoted by semiflexible molecules of high molecular weights, by processing these molecules at temperatures where the contour length exceeds the persistence length, and by high polydispersity.
2. Coarse microstructures are promoted by high molecular weight rigid molecules, by processing semiflexible molecules at temperatures where persistence length exceeds contour length, and by low polydispersity.
3. Rheinberg differential color contrast provides high contrast and high resolution of orientational defects in liquid crystalline microstructures.

Acknowledgment

The authors benefitted from useful discussions with Dr. Rudolf Zentel. We gratefully acknowledge support from ACS-PRF (No. 21300-G7), AFOSR (No. 49620-89-C-0059) and the IBM Corporation.

References

1. D. Demus, *Liquid Crystals*, **5**, 75 (1989).
2. J. Economy, W. Volksen, C. Viney, R. Geiss, R. Siemens and T. Karis *Macromolecules*, **21**, 2777 (1981).
3. B. Millaud, A. Thierry and A. Skoulious, *J. de Physique*, **39**, 1109 (1978).
4. L. A. Chick, C. Viney and I. A. Aksay, in *Processing Science of Advanced Ceramics*, edited by I.

A. Aksay, G. L. McVay and D. R. Ulrich (Materials Research Society, Pittsburgh, 1989), pp. 331–342.
5. W. J. Jackson, Jr., *Mol. Cryst. Liq. Cryst.*, **169**, 23 (1989).
6. Compounds were provided by Dr. W. Volksen, IBM Almaden Research Center, San Jose; the synthesis is described in Reference 2.
7. C. Viney, R. J. Twieg, C. M. Dannels and M. Y. Chang, *Mol. Cryst. Liq. Cryst. Letters*, **7**, 147 (1990).
8. C. Viney and C. M. Dannels, *Molecular Crystals and Liquid Crystals*, in press.
9. J. Rheinberg, *J. Roy. Mic. Soc.*, **16**, 373 (1896).
10. G. H. Needham, *Practical Use of the Microscope* (Charles C. Thomas, Springfield IL, 1958)
11. J. G. Delly, *Photography Through the Microscope* (Eastman Kodak Company, Rochester NY, 1983), pg. 74.
12. W. S. Putnam and C. Viney, in *Proceedings of the 47th Annual Meeting of the Electron Microscopy Society of America*, edited by G. W. Bailey (San Francisco Press, San Francisco, 1989), pp. 364–365.
13. R. B. Meyer, in *Polymer Liquid Crystals*, edited by A. Ciferri, W. R. Krigbaum and R. B. Meyer (Academic Press, New York, 1982), Ch. 6.
14. R. L. Jaffe, D. Y. Yoon and A. D. McLean, in *Computer Simulations of Polymers*, edited by R. J. Roe (Prentice Hall, NY), in press.

APPENDIX 9

LIQUID CRYSTALS, 1993, VOL. 13, NO. 1, 95–100

High strength disclinations in a rigid rod nematic polytolane

by CHRISTOPHER VINEY*
Molecular Bioengineering Program, Center for Bioengineering WD-12,
University of Washington, Seattle, Washington 98195, U.S.A.

DANIEL J. BROWN and CHRISTINE M. DANNELS
Department of Materials Science and Engineering FB-10,
University of Washington, Seattle, Washington 98195, U.S.A.

and ROBERT J. TWIEG
IBM Almaden Research Center, San Jose, California 95120, U.S.A.

(*Received 28 April 1992; accepted 6 August 1992*)

Transient disclinations of strength $\pm 3/2$ were observed in the nematic phase of a single-component, thermotropic, rigid rod polytolane. These disclinations were characterized by 6 extinction brushes in textures observed by hot stage transmitted polarized light microscopy. The small number and short lifetime of these disclinations is discussed in terms of their energy per unit line length, and in terms of the force that causes them to be attracted to and annihilated at other disclinations.

1. Introduction

According to the textbook literature on liquid crystals, the only experimentally observed disclinations in nematics have been those with strengths $\pm\frac{1}{2}$ and ± 1. The research literature contains some isolated references to observations of higher strength disclinations in two-component materials: in a lyotropic liquid crystal [1–3], in mixtures of a lyotropic and a thermotropic liquid crystal [4], and in nematogens mixed with plate-like non-mesogenic molecules [5, 6]. A solvent or diluent is present in all these cases; it has been suggested that the high strength singularities are stabilized by the surface tension gradient at the interface with submicroscopic droplets [4], or by concentration gradients [5, 6].

This paper presents evidence that disclinations of strength $\pm\frac{3}{2}$ can exist in a single-component nematic material.

2. Experimental

2.1. *Material*

Microstructural studies were conducted on 1,4-bis(4-biphenylethynyl)benzene, a polytolane:

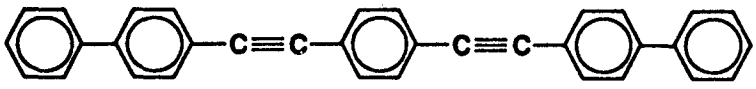

* Author for correspondence.

The bonds linking the phenyl and acetylene units are collinear. Therefore, each molecule of this compound resembles a rigid rod. The axial (length-to-width) ratio of the rods is 6·3, as determined by using Chem3D Plus software (version 3.0; Cambridge Scientific Computing, Cambridge, MA) to construct an energy-minimized model of the molecule. Similar (though shorter) polytolanes have been shown to form nematic liquid-crystalline phases [7].

2.2. *Synthesis*

In a 250 ml round bottom flask equipped with stirbar, reflux condenser and nitrogen inlet was placed 4-ethynylbiphenyl (5·35 g, 30 mmol), 1,4-diiodobenzene (3·30 g, 10 mmol), morpholine (75 ml) and triphenylphosphine (400 mg). The solution was warmed and degassed with nitrogen, and then palladium chloride (35 mg) and cupric acetate monohydrate (20 mg) was added. The resulting solution was heated in a 125°C oil bath for 5 hours and then cooled to room temperature. The resulting slurry was filtered and the solid washed first with morpholine and then ethanol and finally air dried to give the crude product (4·35 g). This material was taken up in hot *N*-methyl pyrrolidinone (100 ml) and allowed to cool and crystallize. The solid was isolated by suction filtration and washed with ethanol and then recrystallized again in the same fashion to give the pure product (3·72 g, 86 per cent).

Analysis: calculated for $C_{34}H_{22}$: C, 94·85 per cent, H, 5·15 per cent; found: C, 95·20 per cent, H, 5·21 per cent.

2.3. *Characterization*

Phase transitions were initially detected by differential scanning calorimetry (DSC), on a DuPont 1090 system. Specimens with an approximate mass of 10 mg were scanned at 10°C min^{-1} in an atomosphere of dry nitrogen. Phases were identified by transmitted polarized light microscopy. A Leitz Laborlux 12 POL microscope equipped with a Linkam THM 600 heating/freezing stage and PR 600 controller was used to examine the textures of samples confined between two glass cover slides. Microstructures were recorded on Fuji Neopan 1600 Professional black and white film, using a Canon T90 camera.

3. Results

The material exhibits the following phase transitions on heating

C 293·8°C S_A 299·1°C N 343·5°C I.

Undisturbed nematic samples exhibit disclinations of strength $\pm\frac{1}{2}$ and ± 1, characterized by either 2 or 4 extinction brushes between crossed polars. However, if nematic samples are stirred by vigorously agitating the top cover slide for a few seconds, occasional transient singularities of strength $\pm\frac{3}{2}$, characterized by 6 extinction brushes, can subsequently be found in the textures (see the figure). These disclinations are more frequently found at temperatures close to the clearing point, and they have only a short lifetime. In experiments on 50 samples, these disclinations were never seen for more than 34 s after samples were stirred. The disclinations do not remain stationary in the field of view. They move erratically towards another disclination or a sample/air interface, where they are annihilated. It was necessary to use high speed film (1600 ASA) to freeze this motion sufficiently to record textures with minimal blurring. However, use of such high speed film introduces significant 'grain' into the recorded images. Because

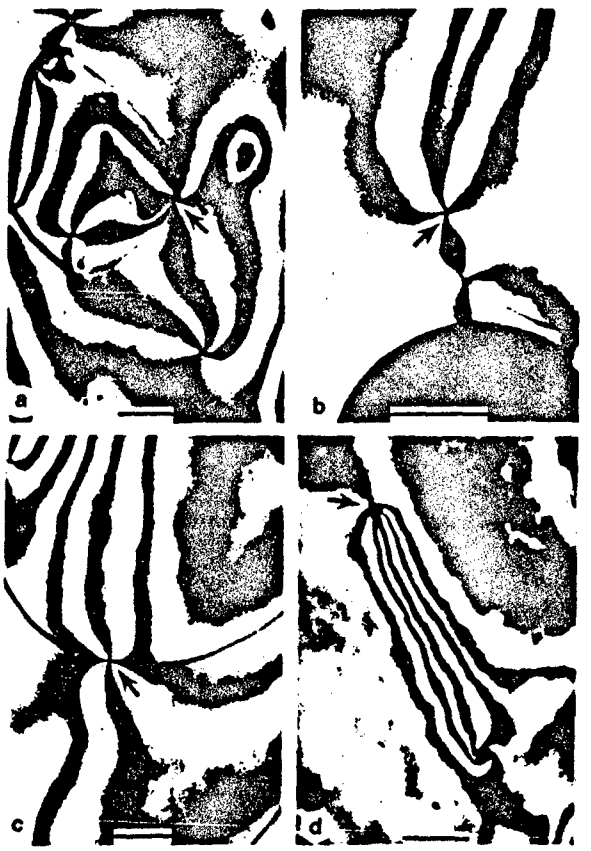

Sample microstructures at 340°C observed between crossed polars. The scale bar represents 10 μm in each case. Views (*a*)–(*c*) each contain a singularity of strength $\pm\frac{1}{2}$, characterized by 6 extinction brushes. View (*d*) shows a strength $\pm\frac{1}{2}$ singularity with a wider, isotropic core; observations with the analyser removed confirmed that isotropy was not due to the presence of air bubbles. A sharp line discontinuity passing through the singularity is clearly visible in (*a*) and (*c*), and faintly visible in (*b*).

of the mobility and short lifetime of the microstructure, it was not possible to rotate the crossed polars and reliably distinguish between disclinations of strength $+\frac{1}{2}$ and $-\frac{1}{2}$.

4. Discussion

For disclinations that have a distinct core, i.e. those with half-integral strength, the energy per unit line length is [8]

$$W = W_c + \pi K s^2 \ln \frac{R}{r_c}. \tag{1}$$

(The simplifying assumption is made that the elastic properties of the nematic can be described by the single elastic constant K, s is the strength of the disclination, R is its radius, r_c is the radius of the core, and W_c is the core energy.)

The core energy can be approximated by [9]

$$W_c = k_B \Delta T \pi r_c^2 \frac{\rho N}{M}. \tag{2}$$

(Here k_B is Boltzmann's constant, ΔT is the difference between the specimen temperature and the clearing point, ρ is the density of the nematic, N is Avogadro's number, and M is the molar mass.)

If m is the mass of a single molecule, this simplifies to

$$W_c = k_B \Delta T \pi r_c^2 \frac{\rho}{m}. \tag{3}$$

Therefore

$$W = k_B \Delta T \pi r_c^2 \frac{\rho}{m} + \pi K s^2 \ln \frac{R}{r_c}. \tag{4}$$

By differentiating, the value of r_c that minimizes the overall energy of the disclination can be found

$$r_c^2 = \frac{mKs^2}{2\rho k_B \Delta T}. \tag{5}$$

By substituting in equation (4) we obtain

$$W = \pi K s^2 \left[\frac{1}{2} + \ln\left(\frac{R}{s}\sqrt{\left(\frac{2\rho k_B \Delta T}{mK}\right)}\right)\right]. \tag{6}$$

Thus, for disclinations with half-integral strength:

> The overall energy increases with increasing strength, consistent with the fact that higher strength is accompanied by more complex director field distortions. Therefore, the number of $s = \pm\frac{1}{2}$ disclinations should always exceed the number of $s = \pm\frac{3}{2}$ disclinations.
>
> The energy of a disclination of given strength is decreased by a combination of high molecular weight and small undercooling, though the dependence is not a sensitive one. This is qualitatively consistent with our observation that the $\pm\frac{3}{2}$ strength disclinations are more common at temperatures close to the clearing point of the nematic, and may also help to account for the fact that we have not found these disclinations in the textures of shorter polytolanes.

If we substitute equation (5) into only the first term of equation (4) we obtain another useful expression for the energy of disclinations with half-integral strength:

$$W = \pi K s^2 \left[\frac{1}{2} + \ln \frac{R}{r_c}\right]. \tag{7}$$

This shows that the overall energy is higher for disclinations with narrow cores, which is consistent with the fact that narrow cores require more severe director field distortions.

If a disclination has integral strength, its core is expected to be diffuse, i.e. there is no line singularity associated with the disclination. The energy is then simply given by [9]

$$W = 2\pi K|s|. \tag{8}$$

We are now in a position to estimate and compare the relative energies of different disclinations. Dimensionless data for this comparison can be obtained from rearrangements of equations (7) and (8):

$$\frac{W}{\pi K} = s^2\left[\frac{1}{2} + \ln\frac{R}{r_c}\right], \tag{9}$$

$$\frac{W}{\pi K} = 2|s|. \tag{10}$$

We assume a reference value of $R \sim 10\,\mu m$, based on the scale of typical microstructures. The calculation for $\pm\frac{1}{2}$ strength disclinations is performed for several values of R/r_c, ranging from 5000 to 10. These values correspond to a core radius that ranges from being 1 molecule long to 500 molecules long; the actual value will depend on the (unknown) elastic constants of the material, and on the specimen temperature, as expressed in equation (5). The R/r_c values used to obtain the corresponding reduced energies for $\pm\frac{3}{2}$ strength disclinations must be normalized to take account of the fact that r_c is proportional to s (if all other parameters remain constant), again as expressed in equation (5). Values of reduced energy $W/\pi K$ are shown in the table.

We can now point to two reasons why the $\pm\frac{3}{2}$ strength disclinations are seen so much less frequently than $\pm\frac{1}{2}$ strength disclinations:

If the relative probability of forming a disclination is assumed to follow a Boltzmann-type distribution (i.e. if probability is inversely proportional to the exponential of reduced energy), the data in the table imply that $\pm\frac{1}{2}$ strength disclinations are 200–2000 times more likely to occur than $\pm\frac{3}{2}$ strength disclinations.

Because the force between disclinations is proportional to the product of their strengths [9], the higher strength disclinations should anneal out of the microstructure more rapidly.

The latter consideration may also contribute to explaining why ± 2 strength disclinations were not observed. On the basis of the reduced energies in the table, and the assumption of a Boltzmann-type relationship between energy and probability, we might expect to observe more ± 2 strength disclinations than $\pm\frac{3}{2}$ strength disclinations—unless the latter have very wide cores. However, regardless of core size, any ± 2 strength disclinations would be attracted to other disclinations and annihilated more rapidly than disclinations of lower strength. In addition, observations

Dimensionless reduced energies $W/\pi K$ for disclinations in a nematic, calculated from equations (9) and (10).

	R/r_c for disclination with distinct core						Diffuse core
s	5000	1000	500	100	50	10	
0·5	2·3	1·9	1·7	1·3	1·1	0·7	
1							2·0
1·5	17·8	14·2	12·6	9·0	7·5	3·8	
2							4·0

of ± 2 strength disclinations in nematogens mixed with plate-like non-mesogenic molecules [6] suggest that the director does not necessarily collapse in the third dimension near ± 2 strength defects. These disclinations therefore can have finite cores, in which case equation (9) would predict a higher reduced energy and a lower probability of formation, compared to $\pm\frac{1}{2}$ strength disclinations.

5. Conclusions

Transient disclinations of strength $\pm\frac{1}{2}$ can be generated during deformation or flow of the nematic phase of a single-component liquid crystal consisting of rigid rod-like molecules. Formation of these high strength disclinations is promoted by a combination of mechanical agitation, smaller undercooling below the clearing point, and higher molecular weight.

C.V. would like to acknowledge support from The Washington Technology Center, the donors of the American Chemical Society Petroleum Research Fund (Grant No. 21300-G7) and AFOSR (Grant No. 49620-89-C-0059).

References

[1] FRANK, F. C., 1958, *Discuss. Faraday Soc.*, **25**, 19.
[2] ROBINSON, C., WARD, J. C., and BEEVERS, R. B., 1958, *Discuss. Faraday Soc.*, **25**, 29.
[3] MADHUSUDANA, N. V., and PRATIBHA, R., 1989, *Liq. Crystals*, **5**, 1827.
[4] LEE, H., and LABES, M. M., 1982, *Molec. Crystals liq. Crystals*, **82**, 199.
[5] MADHUSUDANA, N. V., and PRATIBHA, R., 1982, *Curr. Sci.*, **51**, 877.
[6] MADHUSUDANA, N. V., and PRATIBHA, R., 1983, *Molec. Crystals liq. Crystals*, **103**, 31.
[7] VINEY, C., TWIEG, R. J., DANNELS, C. M., and CHANG, M. Y., 1990, *Molec. Crystals liq. Crystals Lett.*, **7**, 147.
[8] NEHRING, J., and SAUPE, A., 1972, *J. chem. Soc. Faraday Trans. II*, **68**, 1.
[9] KLÉMAN, M., 1983, *Points, Lines and Walls* (John Wiley & Sons), Chap. 3.